

Editor-in-Chief B.E. Paton

Editorial Board:

D.M. Dyachenko,
exec. secr. (Ukraine),
J. Foct (France),
T. El Gammal (Germany),
M.I. Gasik (Ukraine),
G.M. Grigorenko,
vice-chief ed. (Ukraine),
V.I. Kashin (Russia),
B. Koroushich (Slovenia),
V.I. Lakomsky (Ukraine),
V.K. Lebedev (Ukraine),
S.F. Medina (Spain),
L.B. Medovar (Ukraine),
A. Mitchel (Canada),
B.A. Movchan (Ukraine),
A.N. Petrunko (Ukraine),
V. Ramakrishna Rao (India),
Ts.V. Rashev (Bulgaria),
N.P. Trigub (Ukraine),
A.A. Troyansky (Ukraine),
M.L. Zhadkevich (Ukraine)

Executive director
A.T. Zelnichenko

Translator
S.A. Fomina

Editor
N.A. Dmitrieva

Electron galley
I.V. Petushkov,
T.Yu. Snegiryova

*Editorial and advertising offices
are located at PWI,*
International Association «Welding»,
E.O. Paton Electric
Welding Institute
of the NAS of Ukraine,
11, Bozhenko str., 03680,
Kyiv, Ukraine
Tel.: (38044) 227 67 57,
269 26 23,
Fax: (38044) 268 04 86
E-mail: journal@paton.kiev.ua
http://www.nas.gov.ua/pwj

Subscriptions:
\$184, 4 issue per year,
postage and packaging included.
Back issue available

CONTENTS

ELECTROSLAG TECHNOLOGY

**Shevtsov V.L., Zhadkevich M.L., Majdannik V.Ya.,
Puzrin L.G. and Bogachenko A.G.** Electroslag casting
instead of forging in the production of high-pressure
Christmas tree 2

Medovar L.B. About mill rolls of future and electroslag
technologies of their production 7

ELECTRON BEAM PROCESSES

**Trigub N.P., Zhuk G.V., Pikulin A.N., Kalinyuk A.N.
and Kornijchuk V.D.** Electron beam installation UE-185
for fusion of surface layer of ingots 10

Ivanchenko N.V., Ustinov A.I. and Mokhort V.A.
Thermodynamic analysis of evaporation of titanium and
nickel from Ti-Ni melt in vacuum 13

Lesnoj A.B. and Demchenko V.F. Modelling of
hydrodynamics and mass exchange in electron beam
remelting of titanium alloys 17

PLASMA-ARC TECHNOLOGY

Shapovalov V.A., Yakusha V.V. and Gnizdylo A.N.
Thermal field of large-sized refractory single crystals at
combined plasma-induction heating 22

VACUUM-ARC REMELTING

**Lisienko V.G., Nasyrov Ya.A., Klimov M.I., Altman
P.S., Tashkinov A.Yu. and Goncharov A.E.** Effect of
ionization on voltage drop and frequency of droplet
short-circuits in vacuum-arc remelting of high-alloy steels 25

GENERAL PROBLEMS OF METALLURGY

**Antonyuk S.L., Korol V.N., Molyar A.G., Romashko
I.M., Zamkov V.N. and Topolsky V.F.** Investigation of
mechanical properties of forged semi-products of
experimental titanium alloy T-110 27

Burylyov B.P. and Mojsov L.P. Distribution of nitrogen
between metal and slag 31

ELECTROMETALLURGY OF STEEL AND FERROALLOYS

Gasik M.I., Gasik M.M., Polyakov O.I. and Zubov V.L.
Thermodynamic model of process of melting ferrosilicium
in high-capacity ore thermal electric furnaces 34

ENERGY AND RESOURCE SAVING

Lakomsky V.I. Mathematical model of calculation of
specific electrical resistance of grained thermoanthracite
depending on its fractional composition 44

ELECTROSLAG CASTING INSTEAD OF FORGING IN THE PRODUCTION OF HIGH-PRESSURE CHRISTMAS TREE

V.L. SHEVTSOV², M.L. ZHADKEVICH¹, V.Ya. MAJDANNIK², L.G. PUZRIN² and A.G. BOGACHENKO¹

¹E.O. Paton Electric Welding Institute, NASU, Kyiv, Ukraine

²Innovation company «Elterm», Kyiv, Ukraine

It is shown that billets of strong bodies of Christmas tree (CT), produced by ESC method, are superior by characteristics of ductility and toughness to the forged metal of CT bodies, which are manufactured by advanced foreign companies. It is established that ESC metal is also superior to the forged metal by the capability to undergo the plastic deformation in the conditions of a complex stressed state. The manufacture of high-pressure CT using ESC provides at minimum cost the highest its reliability during long-time service.

Keywords: Christmas tree, strong bodies, high pressure, forged metal, electroslag cast metal, mechanical properties, brittle fracture resistance, reliability

The Christmas tree (CT) is used for oil and gas production using a fountain method. It is mounted on a well mouth and used for its operation during service and control of flow of the products produced. The CT, which is mounted on wells of a large depth (about 4000 m), operates under pressure up to 70 MPa. The increased fire hazard of oil and natural gas and their toxicity require especially high reliability of operation of the CT during a long period of its service [1]. It concerns, first of all, the capability of metal of bodies

of separate CT elements to resist brittle fracture in operation under the high pressure.

The CT set includes a massive head for suspension of a column of pumping-compressor pipes, shaft valves, valves on branch pipes, throttles and other components. The as-assembled CT complete set for 70 MPa has 3.6 m height and 3.5 t mass (Figure 1). In the process of manufacture the body of each component of this CT is subjected to testing at 105 MPa pressure. Until recently this CT was not manufactured in Ukraine. The demand for it was realized by import.

The E.O. Paton Electric Welding Institute of the NAS of Ukraine in collaboration with innovation company «Elterm» has mastered for the first time in Ukraine the manufacture of a reliable CT, operating under 70 MPa pressure [2, 3]. In the development of technology of production of this CT the major attention was paid to the increase in reliability in its operation during the long-time service. In this article we shall describe the solution of only one, but in our opinion, most important problem of ensuring a reliable operation of strong valve bodies of CT under the high pressure.

Bodies of CT components, especially of valves, have a rather intricate shape. Mass of billets, from which these bodies are manufactured, may amount to more than 500 kg. These billets are often produced by the method of a conventional casting. Castings in manufacture of these components require only minimum mechanical treatment. However, due to low heat conductivity of the mould material, the crystallization of metal during casting occurs slowly and with a small overcooling. Due to this, a coarse-grain structure is formed in the casting metal and a significant zonal liquation of alloying elements and impurities takes place. The surface layers of casting are firstly solidified and the further its crystallization occurs without an additional hot topping with a molten metal. As a result of this, pores and shrinkage porosity are formed,

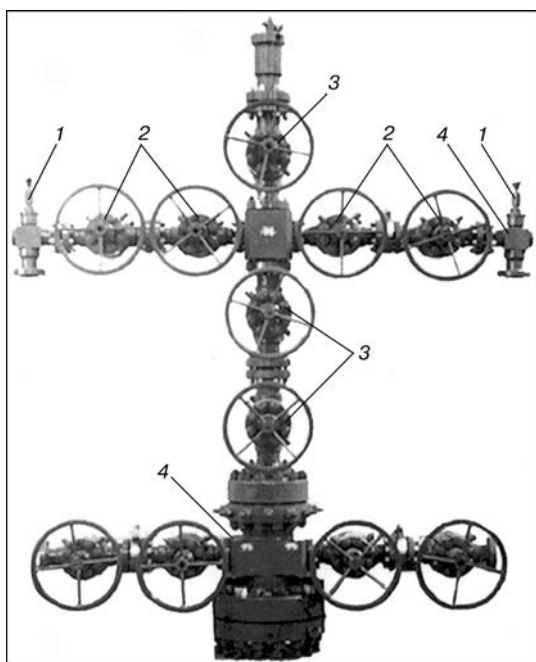


Figure 1. Christmas tree AFK6-80/50X70: 1 — throttles; 2 — valves at branch pipes with 50 mm diameter passing section; 3 — shaft valves with 80 mm diameter passing section; 4 — heads of pumping-compressor pipe

**Table 1.** Mechanical properties of billets of CT bodies produced by different methods

Method of producing	$\sigma_{0.2}$, MPa	σ_t , MPa	$\sigma_{0.2}/\sigma_t$, %	δ , %	ψ , %	KCU , J/cm ²
Casting* (steel 34CrMo4)	363–396 376	651–729 695	51.1–55.8 54.2	6.0–20.0 11.1	10.0–27.1 17.7	16.3–25.8 21.1
Forging* (steel 34CrMo4)	466–496 483	704–782 735	62.6–69.1 65.8	18.0–25.0 22.3	31.1–62.0 48.8	28.5–131.6 95.6
ESC** (steel 35KhM)	548–588 568	700–746 721	78.2–78.8 78.5	17.7–23.3 20.0	63.4–69.5 66.4	146.0–206.0 179.3

Note. Above the line the minimum and maximum values are given, under the line the mean values are given.

*Data of company «Cameron» [4].

**Data of company «Elterm» obtained in testing of 24 specimens.

thus reducing the metal density and leading to the comparatively low and instable mechanical properties of cast billets. Data about mechanical properties of billets of CT bodies, obtained by different methods using steel 34CrMo4 and single-type steel 35KhM, are given in Table 1. Chemical composition of these steels is given in Table 2.

As is seen from Table 1, the values of ductility (δ , ψ) and toughness (KCU) in billets of CT bodies produced by a conventional casting occurred to be the lowest. These are the values that define the capability of metal to resist brittle fracture under the conditions of three-dimensional stressed state, which can occur under the action of high operating pressure in those places of bodies where stress concentrators, for example, shrinkage porosity, are present. Therefore, it is profitable to manufacture the bodies by the traditional casting from the economical point of view only in production of CT operating under the pressure of not more than 35 MPa. This pressure does not cause a hazardous level of stresses in cast billets of CT bodies.

All the foreign companies, which produce CT for operation under the pressure above 35 MPa, manufacture bodies of its components from forged billets. The forged metal, unlike the metal of conventional castings, has higher density, increased strength properties and higher and stable ductility and toughness that is especially important to prevent hazard of brittle fracture. However, the production of CT bodies by the methods of forging increases greatly the cost of their manufacture, due to need in use of expensive equipment, and also to increase tolerances for sizes of billets, i.e. to increase the volumes of mechanical treatment.

The German company «Cameron», the leading manufacturer of CT, has developed the technology of manufacture of billets of its bodies, which includes melting steel in electrical furnaces, its pouring into metallic moulds, repeated heating of ingots and their cogging in presses. Then the surface of the produced forgings is machined and cut into billets of strictly

definite mass. These measured pieces are pressed in closed dies and billets of intricate shape with a degree of cogging are produced from them [4]. Company «Cameron» produces billets of CT bodies with high mechanical properties using this labour-intensive technology (see Table 1). External configuration of these billets, the same as in conventional casting, is close to the shape of ready valve bodies. However, this advantage is attained by using unique forge and stamping presses of force up to 35000 t. Outlining the high quality and reliability of its products, the company «Cameron» recognizes that the price of its CT and valves is occurred to be higher than that of their competitors, due to use of the complex equipment and expensive technologies [4].

At the same time, the decreased ductile properties of flange metal and, in particular of metal of branch pipe, connecting flange to the valve body attract attention in data given by the company «Cameron». In parallel with high values of reduction in area (ψ_{long}) and impact strength (KCU_{long}) of longitudinal specimens of branch pipe the radial specimens have rather low properties: $\psi_{\text{rad}} = 31.1$ %, while $KCU_{\text{rad}} = 28.5$ J/cm² [4]. Characteristic of anisotropy N calculated by formula

$$N = 0.5(\psi_{\text{long}}/\psi_{\text{rad}} + KCU_{\text{long}}/KCU_{\text{rad}}), \quad (1)$$

for metal of this branch pipe is equal to 3.22. This value of characteristic N proves high anisotropy of mechanical properties of metal of billets of CT bodies manufactured from forgings.

The E.O. Paton Electric Welding Institute and innovation company «Elterm» selected another way in production of high-quality and reliable high-pressure CT and used, for the first time in the world, the method of electrosag casting for manufacture of its bodies [5]. The high quality of electrosag metal ranks it beyond the competition with the metal of open melting. This fact is confirmed by numerous investigations carried out both in our country and abroad [6–8].

Table 2. Grade chemical composition of steels used for manufacture of strong bodies of CT components

Steel grade	Element content, wt. %								
	C	Si	Mn	Cr	Mo	Ni	V	S	P
34CrMo4	0.30–0.37	0.17–0.37	0.50–0.80	0.80–1.20	0.15–0.30	≤ 0.30	≤ 0.06	≤ 0.035	≤ 0.035
35KhM	0.32–0.40	0.17–0.37	0.40–0.70	0.80–1.10	0.15–0.25	≤ 0.30	≤ 0.06	≤ 0.035	≤ 0.035

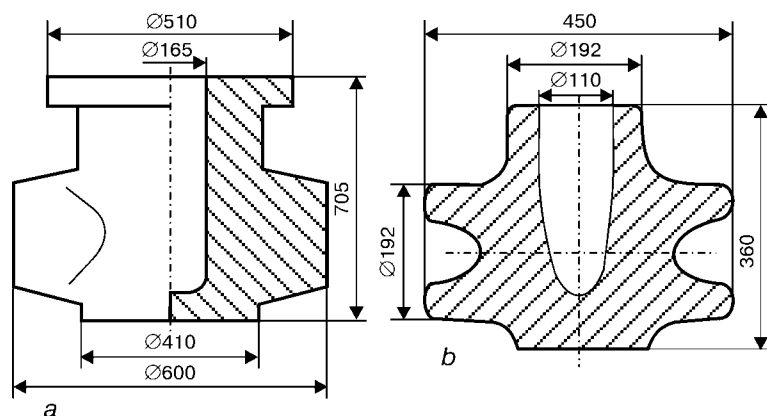


Figure 2. Scheme of ESC billets: *a* — bodies of power stop valves; *b* — T-joint piece

The premises for the creation of technology of ESC of billets for CT bodies were the technologies, developed at PWI for ESC of power stop valve bodies designed for operation in heat and nuclear power stations [5], and also for centrifugal casting of T-joint bodies used at gas-condensate deposits of the Extreme North at pressure up to 35 MPa [9]. In assembly of this equipment these valves and T-joint pieces are joined to pipelines by welding. For this purpose, their bodies have branch pipes (Figure 2) which do not hinder shrinkage of metal in mould during the billet casting.

The CT valves have flanges at the ends of branch pipes (Figure 3), designed for joining separate CT sub-assemblies with pins. These junctions are necessary to replace valves, coming out of order during service, directly on operating well. Due to high fire hazard the welding jobs there are not admissible [1]. It is more difficult to manufacture the bodies of valves with flanges using ESC method, as the flanges hinder metal shrinkage in mould and promote the formation of hot cracks in cast billet.

In the creation of the technology of manufacture of CT bodies from electroslag metal, we have over-

come these difficulties and developed two variants of ESC technology. One of them is the remelting of consumable electrode in special composite water-cooled moulds capable to compensate the longitudinal temperature shrinkage of billet during ESC. Configuration of the inner surface of these moulds corresponds to the external surface of billets melted [10]. The second variant is the centrifugal casting using electroslag crucible melting of metal [11]. Electroslag billets of CT bodies produced by these methods have shape and sizes close to ready bodies (Figure 3). The ESC billets, similar to billets produced by conventional casting or stamping in closed dies, require only minimum mechanical treatment of external surface. Here, the quality of cast electroslag billets is not only inferior to the quality of forge billets, but even superior to it by many characteristics (see Table 1).

In electroslag remelting the content of such harmful impurities as sulphur, gases and non-metallic inclusions is decreased. Table 3 shows the change in composition of steel 35KhM in the process of manufacture of CT bodies from it using the method of ESC of billets. Owing to directed heat removal the crys-

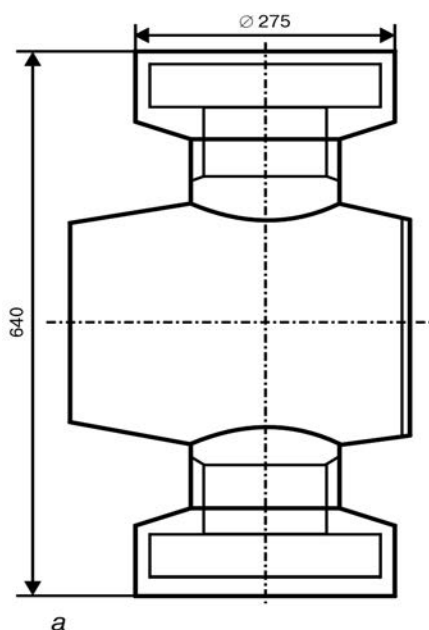


Figure 3. Scheme (*a*) and appearance (*b*) of billet of CT shaft valve with 80 mm diameter passing section produced by the method of electroslag casting (thin lines show the external contour of a ready component)

**Table 3.** Chemical composition of steel 35KhM before and after electroslag casting

Object of analysis	Element content, wt. %							Non-metallic inclusions, vol. % · 10 ⁻⁴
	C	Si	Mn	Cr	P	S	O, % · 10 ⁻⁴	
Electrode	0.35–0.37	0.21–0.31	0.45–0.60	0.93–1.15	0.014–0.019	0.015–0.020	0.21–0.24	175–185
ESC body	0.35–0.37	0.19–0.29	0.43–0.51	0.93–1.05	0.014–0.017	0.006–0.009	0.20–0.23	98–122

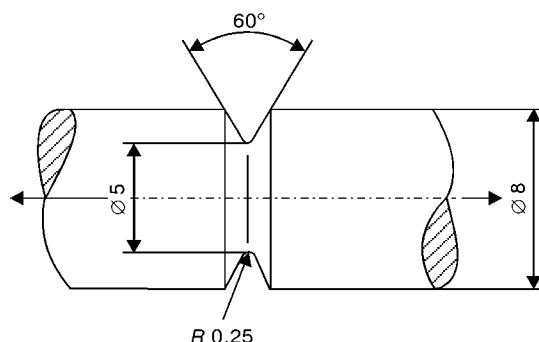
Note. Data are given from 29 meltings.

tallization of electroslag billets occurs with a noticeably higher rate and overcooling than in conventional casting that promotes the producing of dense fine-grain structure of metal and decrease in microscopic and zonal liquation in the cast billet body. All this leads to the increase in density of the electroslag metal. For example, the density of cast electroslag steel of 35KhM grade, from which the CT bodies are manufactured, is equal to 7.8201 g/cm³. At the same time the density of rolled stock from this steel is only 7.7811 g/cm³, i.e. by 0.5 % lower [6]. Owing to all these positive factors the electroslag metal acquires higher ductility and toughness than the forged metal (see Table 1). This promotes the increase in resistance of metal to brittle fractures that should lead to the growth of reliability of structure made from cast electroslag billets.

To confirm this statement we have carried out comparative mechanical tests of cast electroslag metal and wrought metal of conventional casting to determine the capability of these metals to resist fracture under the action of high stresses in the conditions of three-dimensional stressed state near the stress concentrator and to be strengthened during deformation without fracture. This state is typical of body of CT components in service.

The strong high-pressure CT bodies are manufactured from structural steels of 40Kh, 38KhM, 35KhM grades and some other. We used the least alloyed steel 40Kh for testing, which has the lowest level of ductility among the above-mentioned grades. Mechanical tests were performed on round specimens with a notch (Figure 4). These specimens were cut in different directions from the billet of cast electroslag body of valve and rolled consumable electrode which were used for melting this billet.

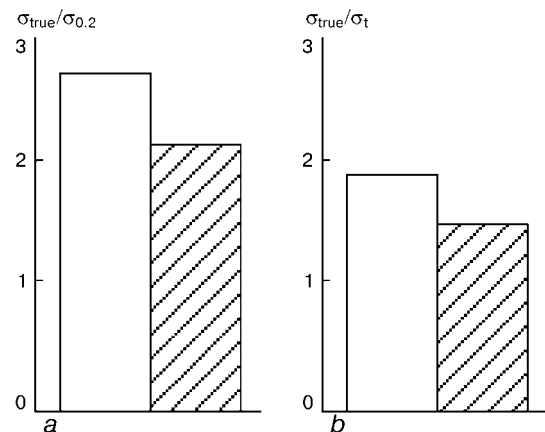
At uniaxial tension of these specimens a three-dimensional stressed state is occurred in a place of notch, that hinders the plastic deformation of the metal. Moreover, the value of stresses near the concentrator

**Figure 4.** Scheme of notch on specimen for tensile test

(notch) several times increases the level of stresses at some distance from it [12, 13]. This three-dimensional state takes place also in massive CT bodies both near the possible defects of structure and also in place of mating separate design elements of the body. The capability of metal in these condition to undergo the plastic deformation without fracture in places of maximum stresses and, thus, to redistribute load to lower-stressed regions, defines the reliability of structure during service.

In tensile test of notched specimens the estimation of metal brittle fracture resistance is performed by a value of true stresses in fracture (σ_{true}), relation of this value to yield strength ($\sigma_{\text{true}}/\sigma_{0.2}$) and tensile strength ($\sigma_{\text{true}}/\sigma_t$) and reduction in area of metal in notch area after fracture (ψ_n). Here, the values $\sigma_{0.2}$ and σ_t are determined on standard flat specimens without notch. The true stresses in fracture of notched specimens are determined as a quotient from division of fracture force by specimen area in place of fracture, measured after tests.

Table 4 gives mechanical properties of cast electroslag billet from steel 40Kh and rolled consumable electrode in the form of 110 mm diameter rod after oil quenching from 860 °C temperature and tempering at 680 °C, obtained during standard tests of cylindrical 5-fold specimens without notch. In this Table the higher values of strength of rolled metal, especially along rolling, as compared with that of cast metal, attract attention. However, the lower values of its ductility and toughness, and also anisotropy of properties, typical of wrought metal, are also seen. Characteristic of anisotropy for a rolled electrode, calculated by formula (1), is 1.76. It should be noted here, that the metal of cast electroslag billet of valve body

**Figure 5.** Ratio $\sigma_{\text{true}}/\sigma_{0.2}$ (a) and $\sigma_{\text{true}}/\sigma_t$ (b) for steel 40Kh, obtained in comparative tests of smooth specimens and specimens with a sharp notch: □ — cast electroslag metal; ▨ — wrought metal of open melting

**Table 4.** Mechanical properties of smooth specimens of steel 40Kh

Place of specimen cutting out	$\sigma_{0.2}$, MPa	σ_t , MPa	$\sigma_{0.2}/\sigma_t$, %	δ , %	ψ , %	KCU, J/cm ²
ESC body:						
longitudinal	482–505	701–713	68.7–70.8	23.0–23.3	61.9–65.9	93.5–119.9
	494	707	69.7	23.1	63.9	106.7
radial	496–518	699–741	69.9–71.0	15.7–22.0	59.8–63.9	142.1–142.3
	507	720	70.5	18.9	61.9	142.2
Electrode (rolled metal):						
longitudinal	564–583	876–876	64.4–66.45	17.0–18.7	57.8–61.9	89.9–103.5
	573	876	65.4	17.8	59.8	96.7
radial	513–517	728–745	68.9–69.4	15.7–18.7	41.0–41.2	43.8–50.14
	515	736	69.2	17.2	41.1	47.0

Note. Above the line the minimum and maximum values are given, under the line the mean values are given.

Table 5. Results of tensile tests of notched specimens

Characteristics of strength and ductility	Place of specimen cutting out			
	ESC body		Electrode (rolled metal)	
	Longitudinal	Radial	Longitudinal	Radial
σ_{true} , MPa	1405–1409 1407	1370–1394 1382	1263–1269 1266	1181–1206 1193
ψ_n , %	16.4–17.6 17.0	17.5–19.7 18.6	5.3–5.7 5.5	1.9–2.5 2.2

Note. Above the line the minimum and maximum values are given, under the line the mean values are given.

of steel 40Kh has no almost anisotropy of mechanical properties ($N = 1.12$).

Results of tensile tests of notched specimens are given in Table 5. These specimens were manufactured from the same billets as the flat specimens and passed heat treatment in the same furnace charge. Data of this Table show adequately that the cast electroslag metal is much superior to the wrought metal of open melting by the values of true stresses of fractures and, especially, by reduction in area under the conditions of plastic deformation in complex-stressed state. Thus, the values ψ_n obtained in testing longitudinal specimens from electroslag metal, are 3–4 times higher than the similar values in specimens from wrought metal. Values ψ_n obtained on radial specimens have much larger difference.

Advantage of cast electroslag metal is also confirmed by ratios $\sigma_{true}/\sigma_{0.2}$ and σ_{true}/σ_t , given in Figure 5. As is seen, the ratio $\sigma_{true}/\sigma_{0.2}$, obtained in testing specimens from cast electroslag metal, by 23 % higher of similar ratio in specimens from the wrought metal. In comparison of σ_{true}/σ_t ratios it is seen that this ratio in electroslag metal is by 27 % higher than that in rolled metal. The above results of tests make it possible to consider that structures made from cast electroslag metal have the higher margin of reliability in service than the similar structures made from wrought metal of open melting. Thus, the replacement of forgings in production of strong CT bodies by electroslag cast billets can increase the reliability of CT structure.

The application of electroslag casting for manufacture of billets of bodies allowed PWI and innovation company «Elterm» not only to establish the pro-

duction of CT for 70 MPa at small capital investments and minimum production expenses, but also to increase significantly the reliability of its operation during long-time service.

1. Vajsberg, G.L., Rimchuk, D.V. (2002) *Flowing safety*. Kharkiv.
2. Artyomov, V.I., Kanakov, V.V., Shevtsov, V.L. et al. (2001) Christmas tree for pressure of up to 70 MPa. *Naftova i Gazova Promyslovist*, **3**, 25–28.
3. Shevtsov, V.L., Majdannik, V.Ya., Khanenko, V.M. et al. (2001) Manufacturing of Christmas tree for deep oil and gas wells by methods of electroslag casting and plasma-powder surfacing. *Svarshchik*, **4**, 8–9.
4. *Steel forgings instead of steel castings*. Advertising of «Cameron» company for the Exhibition «Neftegaz-90».
5. Paton, B.E., Medovar, B.I., Bojko, G.A. (1980) *Electroslag casting*. Kyiv: Naukova Dumka.
6. (1981) *Electroslag metal*. Ed. by B.E. Paton, B.I. Medovar. Kyiv: Naukova Dumka.
7. Medovar, B.I., Shevtsov, V.L., Martyn, V.M. et al. (1988) *Electroslag crucible melting and pouring of metal*. Ed. by B.E. Paton, B.I. Medovar. Kyiv: Naukova Dumka.
8. Ujii, A., Sato, S., Nagata, J. (1973) Application of ESR for production of heavy thickness material of pressure vessel. In: *Proc. of Conf. on Electroslag Refining of Iron and Steel Inst., Sheffield Met. and Eng. Assoc.*, Sheffield, Jan. 10–11, 1973; London: Iron and Steel Inst.
9. Paton, B.E., Medovar, B.I., Shevtsov, V.L. et al. (1987) Centrifugal electroslag casting of billets of tee-joint pipes. *Problemy Spets. Elektrometallurgii*, **1**, 3–5.
10. Shevtsov, V.L., Majdannik, V.Ya., Zhadkevich, M.L. et al. (1998) Electroslag casting of billets of high-pressure Christmas tree bodies. *Ibid.*, **4**, 3–12.
11. Shevtsov, V.L., Majdannik, V.Ya., Zhadkevich, M.L. et al. (1999) Centrifugal electroslag casting of billets of high-pressure Christmas tree valve bodies. *Ibid.*, **4**, 12–22.
12. Gulyaev, A.P. (1986) *Physical metallurgy*. Moscow: Metallurgiya.
13. Lebedev, A.A., Kovalchuk, B.I., Giginyak, F.F. et al. (1983) *Mechanical properties of structural materials in complex stress state*. Refer. Book. Ed. by V.T. Troshchenko. Kyiv: Naukova Dumka.



ABOUT MILL ROLLS OF FUTURE AND ELECTROSLAG TECHNOLOGIES OF THEIR PRODUCTION

L.B. MEDOVAR

E.O. Paton Electric Welding Institute, NASU, Kyiv, Ukraine

State-of-the-art of production of mill rolls and tendency of its updating are discussed. It is shown that the mill rolls of the near future will be produced double-layered with a high-alloy working layer. Advantages of application of electroslag technologies in production of double-layer roll are considered.

Keywords: mill roll, electroslag remelting, electroslag cladding, centrifugal casting, CPC technology

State-of-the-art of production and application of mill rolls in Ukraine and CIS countries arouse anxiety. By some types of rolls the lag from world level is about 30 years. The most striking example is double-layer working rolls with a working layer of high-chromium cast iron for finishing stands of wide-strip mills of hot rolling. In foreign countries the rolls of this type began to be used as far back as the 1970s of last century and only several years ago in Ukraine and CIS countries.

During recent years in Ukraine and CIS countries the advanced rolls of different types of leading world companies appeared in many mills. Specialists in this field had an access to the newest information on rolls. Nevertheless the major tendencies in the development of «roll» industry, interrelation between market requirements, as is said now, and practice of production of mill rolls are not much evident. An attempt is made in this work to outline some major, in the author's opinion, problems in this field of metallurgy. Taking into account the discussion nature of presented considerations and conclusions, the references on numerous recent publications on the above-mentioned problems are not given purposefully.

So, what are the rolls of future, what is the future of rolls? These are two questions, one of them concerns the manufacturers of rolls, while another question is related to the ferrous metallurgy. Undoubtedly, the evolution of ferrous metallurgy defines completely the progress and selection of strategy of production of rolls. There are no doubts that radical changes will be expected in future, which will concern not only technology and quality of products, but also relations with consumers. Partially, these revolutionary changes without exaggeration, have been already started in the world, however in Europe this process delayed, also due to a slow progress in production of rolls of the new generation, including so-called «high-speed» rolls. Until now, almost all the manufacturers of rolls, who used technology of forging and/or cast-

ing, were living and working without problems as to rolls for strip mills of cold and hot rolling.

Today the situation has changed. The price of rolls of traditional quality was decreased drastically, some of manufacturers occurred to be incapable to follow the technical revolution and had to close business. Situation will aggravate in the most near future, because the rolls of the new generation will have 3–4 higher service life than the present-day rolls of the traditional quality. There are no doubts that this is not a single improvement, but a revolution. The consequences are evident:

- real scientific knowledge about rolls will become a decisive factor. However until now, the situation is observed when single-type rolls of different suppliers are differed significantly in operation in the same mill, in the same stand. Moreover, the rolls of the better quality have not always the higher price respectively;

- specialization of production only on rolls of a single type, for example, for flat rolled stock, will remain in the past. Each of manufacturers of rolls should be ready to the fact that it would be necessary to produce rolls both for sheet and for shaped metal of the wide assortment as much as possible. In particular, the manufacturers of rolls for flat rolled metal will have to produce not only the working rolls of finishing stands of hot rolling mills, but also the working rolls of cold rolling, rolls of roughing stands and rolls for plate mills;

- relations between the rolls manufacturers with metallurgists will also change in future. Globalization and internationalism in the world ferrous metallurgy have been already led to the next increase in a role of technical experts in the formation of politics of metallurgical companies and to the more often prevailing of quality over the price. The quality of rolled metal depends mainly on the quality of rolls. Therefore, the increase in the quality of rolls occurs sometimes to be more important than the balance «price–quality». This situation with rolls is observed in Japan and partially in Asia as a whole. Gradually, in the North America, the most quality and expensive Japanese «high-speed» rolls CPC also begin to force out the «high-speed» rolls of a centrifugal casting.



The major changes in metallurgy of rolls can be defined by two clear conceptions: increase in amount of MC carbides, i.e. carbides of superhigh hardness in a working layer of rolls; increase in hot hardness of a working layer of rolls by control of a secondary hardening. This means the application of high austenitizing temperatures (more than 1100 °C) and increased temperatures of tempering to eliminate completely the residual austenite.

These two strategic metals science conceptions mean the more and more wide application of such materials as high-speed and semi-high speed steels, and also a chilled cast iron strengthened with carbides. The application of the above-mentioned materials for the technology of production of rolls assumes the wider transition from monolithic rolls, manufactured from one material, to double-layer rolls with relatively inexpensive axle and a working layer differed from the axle material. Here, one important fact should be noted: for some types of rolls, for example of pilger mills and 20-roll mills of Sendzimir, the above-mentioned conceptions of selection of materials are used for a long time (steels of 3Kh2V8, Kh12M, R6M5 types).

At present three main technologies are used in production of bimetal rolls for flat rolled metal: centrifugal casting and cladding using Japanese technology of continuous pouring for cladding (CPC) or Ukrainian technology of electrosag cladding with a liquid metal (ESC LM). In [1] the expert comparison of these technologies and quality of rolls is given. To manufacture cast iron rolls with a chilled layer, strengthened with carbides, both centrifugal and also stationary casting, including two-layer casting, is used.

In continuous wide-strip mills of hot rolling the double-layer rolls with a working layer from a high-speed steel are almost everywhere used for first four-five stands of a finishing group in Japan and the North America. For the latter stands of a finishing group the rolls with a working layer from a chilled cast iron, strengthened with carbides, are used. It is notable that the standard cast iron rolls, including double-layer rolls with a working layer from high-chromium cast iron, are not almost used. At the same time in Europe the lag in use of «high-speed» rolls is remarkable. They are used mainly in those mills where the stainless steel is rolled.

In Asia the new types of rolls are used almost in all the modern mills. In CIS countries the «high-speed» rolls are at the stage of testing only in some mills. In spite of great differences in spreading new types of rolls by countries, the advantages of «high-speed» rolls are beyond the doubts at present, in particular, with allowance for a continuously growing requirements for the quality of surface and accuracy of the hot-rolled sheet.

In roughing stands of continuous wide-strip mills the double-layer rolls with a working layer from high-chromium, semi- and high-speed steels are more often

used. With allowance for sizes of these rolls they are manufactured now only by a centrifugal casting, however, in the nearest future the appearance of this type of rolls produced also by ESC LM is expected. Double-layer rolls with a working layer from a chilled cast iron, strengthened by carbides, produced by a centrifugal casting, are best now for plate mills.

For mills of cold rolling the forged working rolls from 5 % Cr steel have already become conventional. Gradually, the mastering of these rolls is beginning also in CIS countries. The new generation of working rolls of cold rolling mills is the double-layer rolls with a working layer from semi-high-speed steels providing the three-fold increase in service life of rolls at the highest quality of surface owing to absence of microporosity, typical of rolls with 3–5 % Cr.

So, the modern tendency in application of double-layer rolls with a highly-efficient working layer, 3–4 times increasing the service life of the roll in the mill, is quite evident. It is naturally that this increase in service life of rolls leads to a corresponding decrease in their total consumption, at least, 3 times. Today, in the world, as was above-mentioned, there are only three technologies of producing double-layer rolls of the mentioned types. These are centrifugal casting and technology of cladding CPC and ESC LM. It should be also noted that the earlier attempts of application of banding rolls, including also support rolls, which are made also now due to certain economical aspects, are not challenging. This is connected with the fact that the growth in requirements for accuracy of geometric sizes of rolled metal stipulates the need in preserving geometry of rolls in the process of rolling, that can be hardly provided for banding rolls. However, even in this case one important idea is noticeable, i.e. desire to have a multiple use of roll axle, because the mass of a roll working layer, minimizing in the process of service, exceeds seldom 15 % of the total roll mass.

The similar approaches are also seen for section rolls: recently, there appeared information about successful application of «high-speed» rolls in section mills. As a whole, when characterizing the state-of-the-art of production of mill rolls, it is necessary to note one more specifics, which was actually described above. We are speaking about the striking wide spectrum of technologies and materials. In this spectrum an electrosag remelting exists for a long time.

Traditionally, the ESR in roll production is used for melting superhigh quality forging ingots, i.e. billets of rolls of cold rolling. It is also important that ESR preserves its positions in the production of rolls of superhigh quality also today. In production of rolls with a level of hardness *HSC* 102, in particular for modern mills of cold rolling, ESR is remained to be the main technology in production of rolls even from steels with 3–5 % Cr. The reason is not only in some lower porosity, but also in additional margin of ESR metal ductility as compared with metal of open melting of the same chemical composition and the same level of contamination. Therefore, the ESR preserved



and strengthened its positions in this sector of the roll production. It is important also that it is impossible to produce a roll with a stable structure and consumer's properties taking into account the noted tendencies in complication of systems of rolls alloying without control of ingot solidifying and strict control of shape and constancy of depth of two-phase zone. It should be noted that only advanced automatic systems of ESR technological process control provide melting of sufficiently homogeneous ingots for subsequent forging and manufacture of ingot. But this application of ESR does not come beyond the scope of traditional.

Many times the attempts were made to produce ingots-billets of rolls with a variable chemical composition using ESR, because it is clear that rolls of sheet mills should have variable composition not only across section, but also in roll barrel length. Technology of electroslag cladding with a liquid metal, developed under the supervision of Prof. B.I. Medovar, makes it possible to solve both problems, i.e. producing roll billet with a preset heterogeneity of composition and properties across section and in length. This specifics of ESC LM and also the feasibility of restoration of worn-out rolls using the above-mentioned methods are described in detail in special publications. From the point of view of considering changes in roll market, we shall note major capabilities of ESC LM for present-day rolls. In Ukraine and, to a certain extent, in CIS countries, it becomes a quite real situation when rolls of the best quality operate in the larger and larger amount of rolling mills. These future prospects for the domestic manufacturers of rolls mean only that even today they entered the competitive struggle with the best world roll companies. The experience of recent years showed that in this path our roll manufacturers (and also neighbors in Russia) selected usual, but impassed way of repetition of all things that have been already created and operated in advanced roll and metallurgical companies. Taking into account the lag in time, and also the need in gaining experience of application of advanced rolls in various types of mills for rolling of different types of steels, it is possible to assume with confidence that only copying to obtain the low cost will not lead to the success. At the same time the domestic technology of ESC LM, mastered successfully at Novo-Kramatorsk Machine-Building Works for high-chromium double-layer rolls of hot rolling allow producing of double-layer roll of all the above-listed types.

In conclusion, we shall try to ground our vision in rational application of this ESC LM technology for production of double-layer rolls of the most complex composition, i.e. rolls of future. It is important to note that the centrifugal casting in its nature does not provide a sufficient homogeneity across thickness of a high-alloy casting, while in our case the homo-

geneity across thickness of the roll working layer is provided. The Japanese technology CPC, as was already mentioned, provides producing rolls of the best quality. However, as to nature of joining of axle metal with working layer metal, CPC is the process of brazing that specifies special requirements to the axle preparation for cladding. At the same time in ESC LM the dissimilar metal joining is occurred in the process of electroslag welding, that simplifies the surface layer preparation. In addition, in spite of name CPC (Continuous Pouring for Cladding), this is the process with a portion feeding of molten metal into the mould, the same as in ESC LM. In production of double-layer billets of rolls for hot rolling mills, which are rolling sheets of about 1 mm thickness, and for cold rolling mills using CPC technology, it is impossible to prevent the appearance of non-homogeneity in structure of the working layer being deposited. This caused the need in machining an additional layer from the surface of a double-layer billets of up to 10–15 mm thickness, up to 20 mm in total. At the same time the quality of surface of billets is such that it was enough to machine only 5–10 mm. It is possible to avoid these troubles in ESC LM and to use the same tolerances for mechanical treatment of surface as for the standard ESR ingots. Moreover, the known peculiarities of electroslag process are such that it is possible to realize the directed control of carbide formation in ESC LM that is important in principle for advanced materials of rolls. Coming from above-said, we suppose that ESC LM can become the basic technology for production of double-layer rolls for mills of hot and cold rolling of flat rolled metal. Moreover, if for working rolls of continuous mills the metallurgical quality of CPC and ESC LM rolls is comparable at undoubted advantage of ESC LM by economical aspect, then for support rolls of mills of these types the ESC LM can become, probably, the major technological process in the nearest future.

The author is grateful to his colleagues, because the appearance of this information became possible only due to continuous discussions with specialists of the E.O. Paton Electric Welding Institute, «Elmet-Roll, Ltd.», «NKMZ, Ltd.», namely B.B. Fedorovsky, A.K. Tsykulenko, V.Ya. Saenko, V.I. Us, A.V. Chernets, V.E. Shevchenko, I.A. Lantsman, G.M. Skudar, V.B. Shabanov, O.V. Sviridov, Yu.A. Grushko and J.-K. Werquin (France) and R. Bagley (UK).

The continuous discussions of the problem of production and application of mill roll with Prof. B.E. Paton were especially valuable.

1. Medovar, L.B., Granovsky, V.K. (2001) Problems and prospects of production of current mill rolls. *Problemy Spets. Elektrometallurgii*, 4, 44–47.



ELECTRON BEAM INSTALLATION UE-185 FOR FUSION OF SURFACE LAYER OF INGOTS

N.P. TRIGUB, G.V. ZHUK, A.N. PIKULIN, A.N. KALINYUK and V.D. KORNIJCHUK

E.O. Paton Electric Welding Institute, NASU, Kyiv, Ukraine

Equipment and elements of technology of fusion of a lateral surface of ingots of metals and alloys using electron beam are described. The offered design of the installation and mechanisms can realize fusion of both round and also slab ingots, the fusion of slab ingots being performed here for a single evacuation. Main technical parameters of the installation are given.

Keywords: *electron beam fusion, ingot, mechanism of displacement and rotation, electron beam gun*

By several reasons caused by metallurgical and technological specifics, the different types of defects, such as corrugations, cracks, films, ripples, etc., are formed on the surface of ingots from alloys on the base of iron, nickel, refractory metals, produced by vacuum-arc, plasma-arc and electron beam remeltings. The most widely spread methods of removing these defects are mechanical methods: trimming, abrasive cleaning, milling, gouging, etc. [1]. These methods are characterized by a low productivity and life of a tool, and also by the presence of waste in the form of chips or metal abrasive dust, that amounts finally to 6–15 % of mass of the ingot being treated.

In the 1980s the methods of treatment of surface of metallic materials began to be widely applied in industry using concentrated power sources, such as laser and electron beams, and also a plasma arc [2, 3]. The electron beam treatment of the surface layer of ingots and billets has certain advantages, such as presence of vacuum in a furnace space as protective and refining medium, high density of energy supplied, precision, simplicity of monitoring and control of technological parameters.

At the E.O. Paton Electric Welding Institute of the NAS of Ukraine, a pilot-industrial installation of the UE-185 type has been designed, manufactured and mounted for fusion of a surface layer of slab and round ingots (Figure 1). The installation operation is based on the principle of ingot fusion with an electron beam [4].

Technical characteristic of the installation

Dimensions of ingots for fusion, mm:

round	
diameter	100–1100
length	≤ 2000
slab	
width	≤ 970
height	≤ 165
length	≤ 2000
Speed of rotation of ingots, rpm:	
operating	0.1–0.3
travel	10
Maximum displacement of tailstock, mm	1200

Maximum displacement of mechanism

for ingot loading, mm	2150
Residual pressure, Pa:	
in cavity of electron guns	$1.3 \cdot 10^{-2}$ – $6.6 \cdot 10^{-2}$
in chamber of fusion	$1.3 \cdot 10^{-2}$ – $1.3 \cdot 10^{-1}$
Number of electron guns, pcs	3
Accelerating voltage, kV	30
Rated current of gun, A	4

Requirements specified to energy and heat suppliers, are as follows:

Rated voltage of mains of three-phase AC	
at 50 Hz frequency, V	380
Set power, kV·A	900
Pressure of cooling water, Pa	$(3-4) \cdot 10^5$
Consumption of cooling circulating water	
at temperature 15 °C, m ³ /h	50
Quality of cooling circulating water, class	6
Pressure of hot water, Pa	$(3-4) \cdot 10^5$
Consumption of hot water at temperature	
50 °C (supplied 30 min before evacuation	
of installation), m ³ /h	5
Quality of hot water, class	6
Air consumption at pressure $(2-6) \cdot 10^5$ Pa, m ³ /h	≤ 2
Quality of air, class	10

The installation represents a vacuum chamber with mechanisms, devices and systems, ensuring the proceeding of technological process of fusion (Figure 2). Vacuum chamber of fusion is a horizontally arranged cylindrical vessel with double walls, connected with flanges to each other, and manufactured from a low-carbon steel. A cooling water is circulating in a gap between the walls. Inner diameter of the chamber is 1800 mm and length is 3000 mm. Thickness of walls of the vacuum chamber provides rigidity and safe protection of the personnel from X-ray radiation. Observation systems are arranged over the entire length to observe the technological process.

A branch pipe is connected to the chamber to have connection to a system of vacuum pumps. The branch pipe has a stop valve for removing gases at emergency increase of pressure in the melting chamber.

The vacuum chamber is sealed with two vertical covers, on one of which the mechanisms of rotation and displacement of round or slab ingots are mounted. Two hatches are located beneath the chamber, on which the mechanisms of vertical displacement of slab

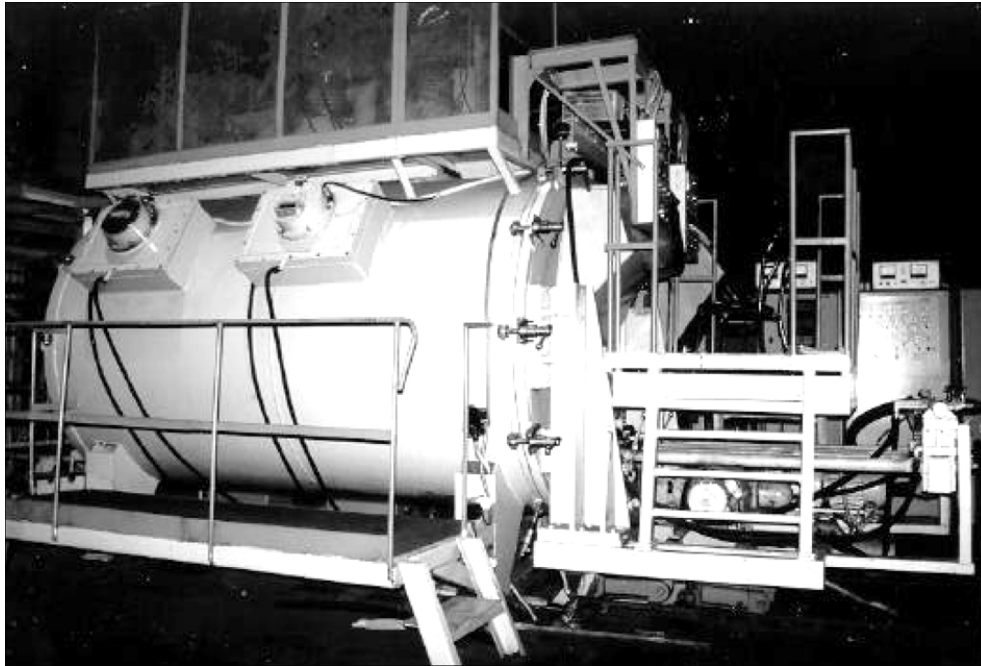


Figure 1. Appearance of electron beam installation UE-185

ingots and prevention of their bending during fusion process are mounted.

Mechanism of rotation and displacement of round ingots consists of a cover, which is adjacent by its lateral surface to the chamber and fastened to a frame of a wheeled-out carriage with brackets. On the frame are arranged four rolls for fusion of round ingots. The rolls are set into a rotational motion from a drive, having adjustment of the rotation speed. Mechanism wheeling-out is realized by a drive with a chain gear. The cover has an observation system to observe the technological process.

A chuck with movable and stationary water-cooled copper shoes and two beams, connected between themselves by a traverse, is fixed in the mechanism of

rotation and displacement of slab ingots at the axis of a cover lateral surface, which is abutted the chamber. Tailstock, having also a chuck mounted on the axis, is fixed and displaced longitudinally on the beams. Ingot of the rectangular section is fixed by shoes in chucks and set into rotation from a drive. In other respects, the design of mechanism of rotation and displacement of slab ingots repeats the mechanism for the round ingots.

As a heat source, three axial guns «Paton-300», designed at PWI, are used [5]. Guns are mounted on water-cooled flanges in the upper part of the chamber.

The vacuum system of the electron beam installation allows separate evacuation of the fusion chamber and electron beam guns. The preliminary evacuation

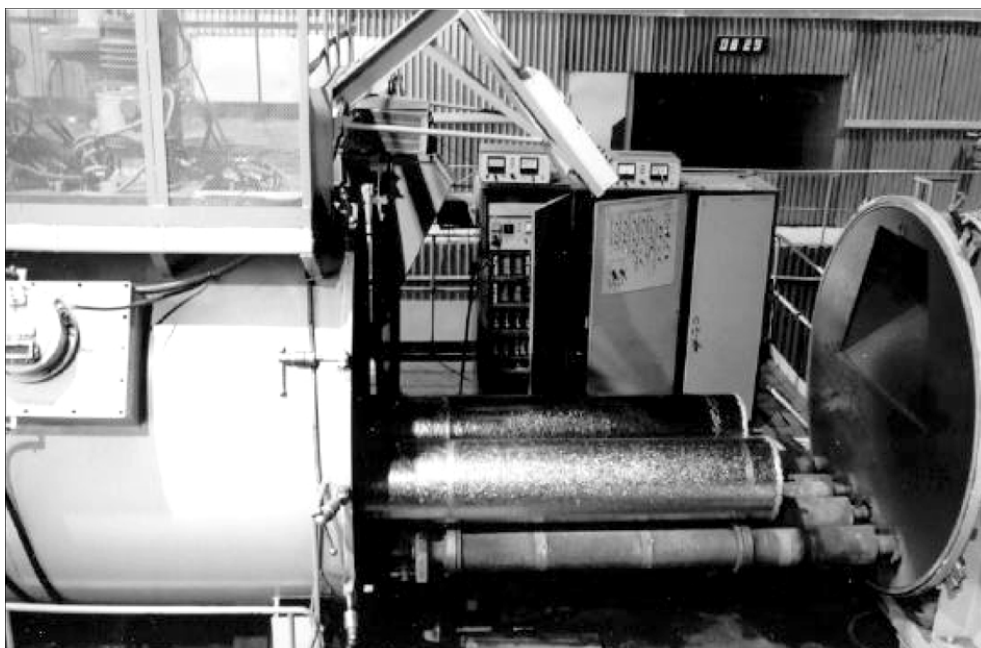


Figure 2. Mechanism of rotation of ingots



Figure 3. Process of fusion

in the vacuum chamber is created by a system of mechanical pumps NVZ-300 and 2DVN-1500. Evacuation of the fusion chamber is realized by two oil-vapour booster pumps 2NVBM630, and evacuation of cavities of electron beam guns is made by high-vacuum diffusion pumps N160/700.

Cooling system consists of a complex of hydraulic units and collectors providing supply and drain of water used for cooling chamber, mechanisms, pumps and heat-loaded units of the installation.

To provide fusion conditions (stabilization of beams of guns, rotation speed of ingots, operation of vacuum units, measurement of evacuation degree and so on), there is a system for monitoring and control of the technological process.

Technology of fusion of round ingots can be divided into three stages: preliminary (preparation), ingot fusion proper and final.

Preliminary stage. Operator of a shop crane (10 t capacity) is laying ingot to be fused on rolls of the mechanism of rotation and displacement of round ingots and checking the operation of the rotation drive. Then, the drive is energized and the operator aligns the mechanism cover with the chamber using clamps. Cover, locating from the opposite side of the chamber and moving along the beam on a suspension, is also aligned by the operator with the chamber using clamps. The installation is evacuated, and the cooling system is switched on.

Stage of ingot fusion. Operator switches on the high-voltage supply source and system of guns control. Drive of rotation of rolls, on which the ingot is arranged, is energized. Then, the filament current is gradually increased, focusing the beams of electron guns on the ingot, and then the guns are set for the operation condition. Fusion of the ingot is performed by a preset technological diagram. The process of fusion of ingots is shown in Figure 3, and their appearance is given in Figure 4.

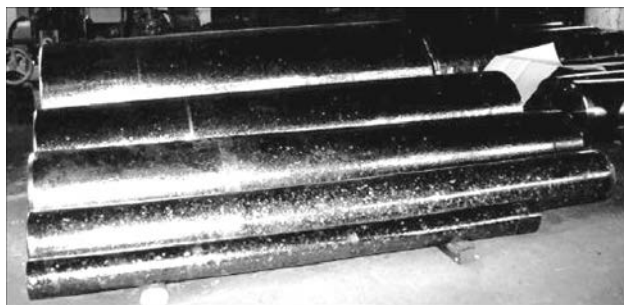


Figure 4. Ingots of 115–600 mm diameter after fusion

Final stage. After a required holding (cooling) of ingot in vacuum, the operator depressurizes the installation (cover is released from clamps). The cover of mechanism of rotation and displacement of round ingots is separated from the installation and the fused ingot is withdrawn by a shop crane.

To perform fusion of slab ingots, it is necessary to perform the similar complex of works, differing only from the previous ones by some technological features. During preliminary and final stages these features are due to the need in fixation of a slab ingot in a special device providing its rotation during fusion. This device is mounted on the mechanism of rotation and displacement of a slab ingot. The technology of fusion in this case can be divided into four stages (by the number of facets of the slab ingot). After fusion of each facet the process is interrupted, the ingot is returned by 90° and then the next facet is subjected to fusion. The operation of rotation is repeated until fusion of all the facets.

The electron beam installation UE-185 makes it possible to increase the efficient metal yield up to 15 % and to improve the ecology in the industrial shops.

1. Shuralev, M.V. (1953) *Methods of dressing of surface defects of metal*. Moscow: Metallurgizdat.
2. Latash, Yu.V., Torkhov, G.V., Modelkin, Yu.I. et al. (1983) On problem of plasma-arc remelting of surface layer of vacuum-arc remelting ingots. In: *Problems of special electrometallurgy*. Issue 18.
3. Schiller, Z., Gajzik, U., Panzer, Z. (1980) *Electron beam technology*. Moscow: Energiya.
4. Paton, B.E., Trigub, N.P., Kozlitsin, D.A. et al. (1997) *Electron beam melting*. Kyiv: Naukova Dumka.
5. Trigub, N.P., Zhuk, G.V., Pap, P.A. et al. (2003) Electron beam installation UE-121. *Advances in Electrometallurgy*, 2, 15–17.



THERMODYNAMIC ANALYSIS OF EVAPORATION OF TITANIUM AND NICKEL FROM Ti–Ni MELT IN VACUUM

N.V. IVANCHENKO², A.I. USTINOV¹ and V.A. MOKHORT²

¹International Center of Electron Beam Technologies of the E.O. Paton Electric Welding Institute, NASU, Kyiv, Ukraine

²National Technical University of Ukraine «KPI», Kyiv, Ukraine

Taking into account the real values of thermodynamic properties of titanium and nickel in melt Ti–Ni, the characteristics of evaporation of components in vacuum are analyzed depending on their characteristics in melt and its temperature. It is shown that with increase in melt temperature of alloys of Ti–Ni system the coefficient of evaporation of nickel is greatly decreased. Chemical composition of molten pool in the range of temperatures from 1600 to 2200 K, required for attaining equiatomic composition of vapour phase, is calculated.

Keywords: nitinol, electron beam evaporation, rate of evaporation, evaporation coefficient

Over the recent years a great attention is paid to the manufacture of devices on the base of alloy Ti–Ni (nitinol), close by the composition to equiatomic alloy. This is stipulated by the fact that these alloys possess stable characteristics of shape memory effect after multiple cycles of shape changing at the amplitude of deforming up to 10 % [1]. Miniature devices and implants on the base of nitinol are of a special interest [2]. To create these devices and implants, the nitinol is required in the form of a thin foil with preset characteristics of shape changing. The producing of a thin foil of nitinol by rolling is difficult due to high sensitivity of its mechanical properties to impurities and texture formation. Therefore, in some works [3, 4] the technologies of producing of a thin foil from the vapour phase are developed. From this point of view, it seems promising to use methods based on electron beam evaporation of ingots on Ti–Ni base of the preset composition and condensation of vapour in vacuum. In turn, the ingots (targets), necessary for this process realization, should be purified from impurities and have a definite ratio of components. The producing of these ingots is possible, for example, by electron beam remelting of titanium and nickel in vacuum, that provides their refining. As the use of electron beam heating in both processes will cause evaporation of alloy components, a thermodynamic analysis of evaporation of titanium and nickel in the wide interval of temperatures and compositions was made in the present work.

The rate of evaporation of components in vacuum is described by the equation of Langmuir:

$$J = X_i \gamma_i P_i^0 (M_i/2 \pi PT)^{1/2}, \quad (1)$$

where J is the flow of component i from melt, kg/(m²·s); X_i is the concentration of component i in the melt, expressed in atomic fractions; γ_i is the co-

efficient of thermodynamic activity of component i in melt; P_i^0 is the partial pressure of vapours over the pure component i , Pa; M_i is the molecular mass of component i , kg/mol; $R = 8.3143$ J/(mol·K) is the gas constant; T is the absolute temperature of melt, K.

Pressure of vapours over the pure nickel and titanium in molten state can be calculated using the equation of Clausius–Clapeyron:

$$\lg P_i^0 = -A/T + B + C \lg T + 10^{-3}DT. \quad (2)$$

Corresponding values of coefficients of equation (2) are presented in Table 1. Taking into account the values of these coefficients, the expression (1) for calculation of a partial pressure of vapours of nickel and titanium in the international system of units SI takes the form

$$\begin{aligned} P_{\text{Ni}}^0 &= 133 T^{-0.618} \cdot 10^{(-20830/T + 11.617)}, \\ P_{\text{Ti}}^0 &= 133 T^{-0.373} \cdot 10^{(-22946/T + 10.581)}. \end{aligned} \quad (3)$$

Thermodynamic properties of components of Ni–Ti system were optimized from the data of different authors both by the model of ideal associated solution [6] and also in the scope of model of Redlikh–Kister [7]. According to this model, the excessive free energy of formation of a liquid phase in case of a two-component solid solution is described by equation

$$\Delta G^{\text{ex}} = X_A X_B \sum_{n=0}^m L^{(n)} (X_A - X_B)^n, \quad (4)$$

where

Table 1. Constants of equation of Clausius–Clapeyron for nickel and titanium [5]

Melt components	A	B	C	D
Nickel	20830	11.617	–0.618	0
Titanium	22946	10.581	–0.373	0



Table 2. Thermodynamic parameters of excessive free energy of liquid phase of alloys of Ni-Ti system in the scope of model of Redlich-Kister

n	A_n	B_n	C_n	E_n	F_n
0	-206852	95.427	0	$-6.69 \cdot 10^{-6}$	$9.359 \cdot 10^{-10}$
1	-66096.6	23.758	0	0	0

* n — expansion into a power series.

$$L^{(n)} = A_n + B_n T + C_n T \ln T + E_n T^3 + F_n T^4. \quad (5)$$

It is evident that representation of thermodynamic properties of components in the range of model of Redlich-Kister is none other than expansion into a power series of the concentration relationship of excessive free energy of formation of liquid solution $L^{(n)}$ with coefficients, which reflect its temperature relationship.

The values of coefficients describing the optimized thermodynamic properties of liquid phase in alloys of Ti-Ni system are presented in Table 2. Thus, the concentration-temperature relationship of excessive free energy of formation of a liquid phase takes a form

$$\Delta G^{\text{ex}} = X_{\text{Ni}} X_{\text{Ti}} [-206852 + 95.427 T - 6.69 \cdot 10^{-6} T^3 + 9.359 \cdot 10^{-10} T^4 + (-66096 + 23.758 T) (X_{\text{Ni}} - X_{\text{Ti}})]. \quad (6)$$

As is known, the coefficient of activity γ_i is associated with a partial excessive free energy $\Delta \bar{G}_i^{\text{ex}}$ by the following ratio:

$$\gamma_i = \exp (\Delta \bar{G}_i^{\text{ex}} / RT). \quad (7)$$

Values $\Delta \bar{G}_i^{\text{ex}}$ required for substitution into equality (7), were calculated by known ratios between the integral and partial thermodynamic values, which have the following form for the given binary system:

$$\begin{aligned} \Delta \bar{G}_{\text{Ni}}^{\text{ex}} &= \Delta G^{\text{ex}} - X_{\text{Ti}} \partial \Delta G^{\text{ex}} / \partial X_{\text{Ti}}; \\ \Delta \bar{G}_{\text{Ti}}^{\text{ex}} &= \Delta G^{\text{ex}} + (1 - X_{\text{Ti}}) \partial \Delta G^{\text{ex}} / \partial X_{\text{Ti}}. \end{aligned} \quad (8)$$

Substituting relationship (4) into system of equations (8), we shall obtain

$$\begin{aligned} \Delta \bar{G}_{\text{Ni}}^{\text{ex}} &= X_{\text{Ti}}^2 [L^{(0)} + (3X_{\text{Ni}} - X_{\text{Ti}}) L^{(1)}]; \\ \Delta \bar{G}_{\text{Ti}}^{\text{ex}} &= X_{\text{Ni}}^2 [L^{(0)} + (X_{\text{Ni}} - 3X_{\text{Ti}}) L^{(1)}]. \end{aligned} \quad (9)$$

General expressions of relationships of rates of evaporation of nickel and titanium from melt will be obtained by substitution into equation of Langmuir (1) of partial pressures of gases over pure components (3) and activities calculated by expression (6). As a result, the dependence of rates of nickel and titanium evaporation on the composition of melt and temperature will take a form

$$J_{\text{Ni}} = 133 X_{\text{Ni}} \exp (X_{\text{Ti}}^2 (L^{(0)} + (3X_{\text{Ni}} - X_{\text{Ti}}) L^{(1)}) / RT) \times T^{-0.618} \cdot 10^{(-20830/T + 11.617)} (M_{\text{Ni}} / 2\pi RT)^{0.5}; \quad (10)$$

$$J_{\text{Ti}} = 133 X_{\text{Ti}} \exp (X_{\text{Ni}}^2 (L^{(0)} + (X_{\text{Ni}} - 3X_{\text{Ti}}) L^{(1)}) / RT) \times T^{-0.373} \cdot 10^{(-22946/T + 10.581)} (M_{\text{Ti}} / 2\pi RT)^{0.5}. \quad (11)$$

Thus, it is possible to calculate the partial pressures of vapours of nickel and titanium over the pure elements on the basis of relationships (3), while the partial excessive free energies of nickel and titanium in a liquid solution can be calculated by equations (9), that makes it possible to analyze the mass flows of vapours of these components from melt depending on concentration and temperature of the liquid solution.

Figure 1 shows relationships of rates of evaporation of components from melt of equiatomic composition in the 1600–2200 K range of temperatures. It is seen that curves of the temperature relationship of evaporation rates for both components are almost equidistant, and the evaporation rate of titanium is 10 times lower than that of nickel.

Figure 2 gives concentration relationships of evaporation rates of titanium and nickel, calculated at 1600, 1900 and 2200 K temperatures. It is seen that with decrease in nickel concentration the rate of its evaporation is reduced, while the rate of titanium evaporation is increased. Thus, at 1900 K the decrease in nickel concentrations in melt from 70 to 30 at.% causes the decrease in its rate of evaporation from $2.18 \cdot 10^{-3}$ to $1.8 \cdot 10^{-4}$ kg/(m²·s), while the rate of titanium evaporation is increased from $5.19 \cdot 10^{-6}$ to $1.06 \cdot 10^{-4}$ kg/(m²·s).

The change in the alloy composition during holding in a molten state is better characterized by a coefficient of evaporation ER (evaporation ratio). It is

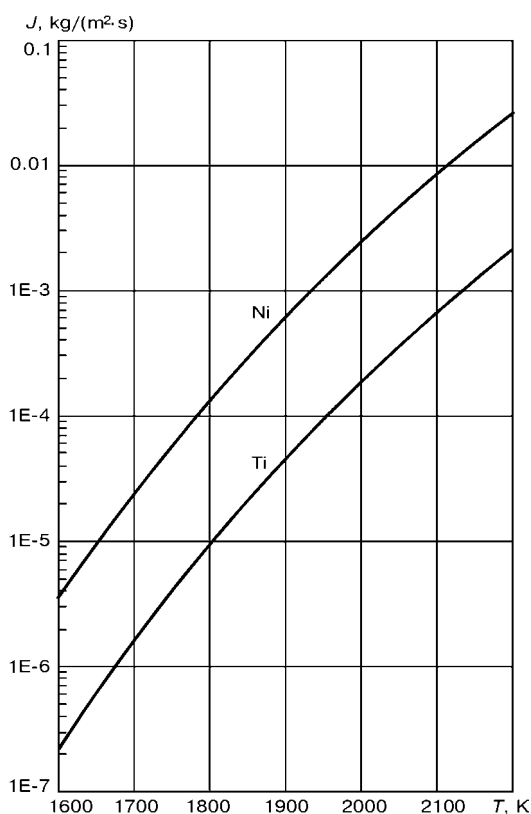


Figure 1. Temperature relationship of rate of evaporation of nickel and titanium from the melt of equiatomic composition

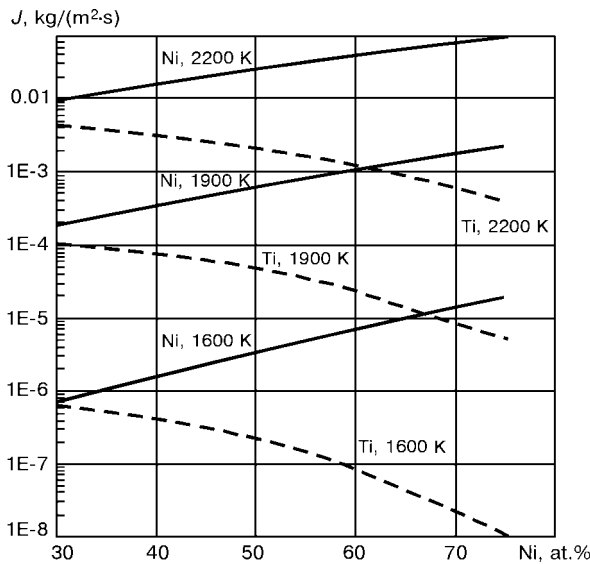


Figure 2. Dependence of evaporation rate of nickel and titanium from melt on nickel concentration in the 1600–2200 K range of temperatures

derived from the condition of a congruent evaporation, when the ratio of molecular flows W of both components is equal to the ratio of atomic particles of components in melt $W_{\text{Ni}}/W_{\text{Ti}} = X_{\text{Ni}}/X_{\text{Ti}}$. Molecular flows are calculated by formulae:

$$W_{\text{Ni}} = J_{\text{Ni}}/M_{\text{Ni}}; \quad (12)$$

$$W_{\text{Ti}} = J_{\text{Ti}}/M_{\text{Ti}}. \quad (13)$$

It is evident, that if

$$ER = (W_{\text{Ni}}/W_{\text{Ti}}) (X_{\text{Ti}}/X_{\text{Ni}}) > 1, \quad (14)$$

the melt is depleted with nickel. As there are simple relationships (12) and (13) between J_i and W_i , then

$$W_i = X_i \gamma_i P_i^0 (2\pi RTM_i)^{-1/2}. \quad (15)$$

It is evident that at the condition of ideal melt ($\gamma_i = 1$) the coefficients of evaporation do not depend on alloy composition, but depend only on the temperature and ratio of molecular mass of components:

$$ER = (P_{\text{Ni}}^0/P_{\text{Ti}}^0) (M_{\text{Ti}}^{1/2}/M_{\text{Ni}}^{1/2}). \quad (16)$$

Deviation of thermodynamic properties of melt from ideality can influence greatly the temperature and concentration relationships ER :

$$ER = [\exp(\Delta G_{\text{Ni}}^{\text{ex}}/RT) P_{\text{Ni}}^0 M_{\text{Ti}}^{1/2}] / [\exp(\Delta G_{\text{Ti}}^{\text{ex}}/RT) P_{\text{Ti}}^0 M_{\text{Ni}}^{1/2}], \quad (17)$$

as the coefficients of activity of nickel and titanium have a complex dependence on temperature and composition (9). Figure 3 gives temperature relationships ER for alloy of equiatomic composition, calculated in approximation of ideal solution and with allowance for deviation of thermodynamic properties of coefficients from ideality. It is seen that the coefficient of evaporation preset by expression (17) has not only

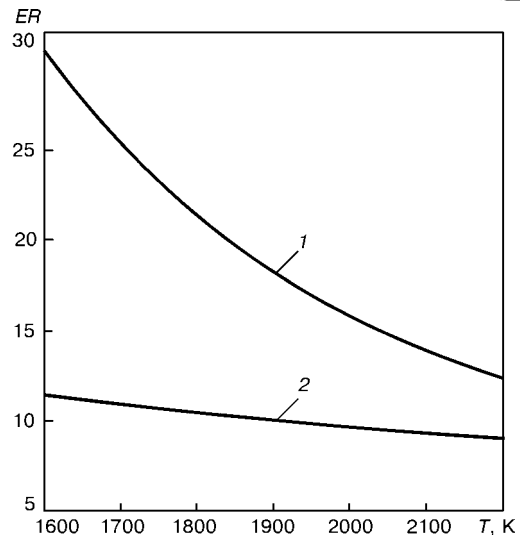


Figure 3. Temperature relationship of coefficient of evaporation from melt of equiatomic composition: 1 — calculated in approximation to ideal solution; 2 — with allowance for deviation of thermodynamic properties from ideality

the quite lower values than in approximation of ideal solution (16), but it also little depends on the temperature.

From the practical point of view, it seems important to establish the concentration relationships ER at different temperatures of the melt (Figure 4). As was noted above, ER in a perfect approximation does not depend on the melt composition. However, it should be noted from the results, obtained with allowance for the deviation of thermodynamic properties of components from the ideality, that with increase in nickel concentration in the melt the coefficient of evaporation is also decreased, moreover, the lower the melt temperature the higher its decrease.

It follows from the relationships given in Figures 3 and 4, that to preserve the preset ratio of components in the process of refining ingots, it is necessary to maintain the melt temperature higher (≈ 2200 K), as in this case ER for alloys with nickel content of higher than 45 at.% is decreased.

Let us consider conditions of formation of condensates on the base of Ti–Ni of equiatomic composition in electron beam evaporation of ingot of the same

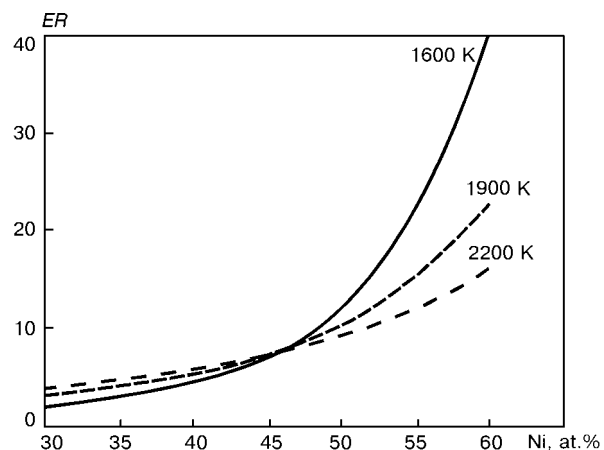


Figure 4. Dependence of coefficient of evaporation on concentration of nickel in alloy in the 1600–2200 K range of temperatures

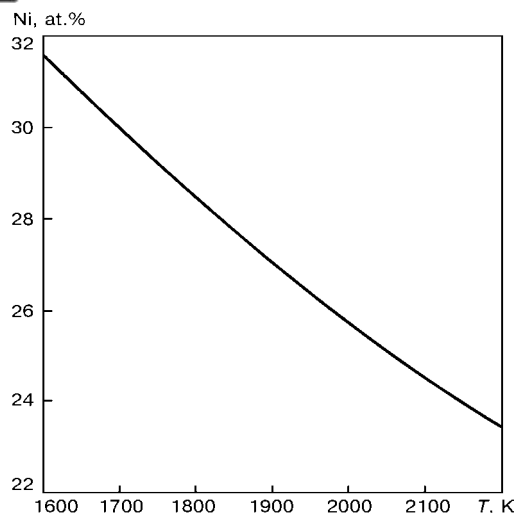


Figure 5. Effect of temperature on concentration of nickel at similar intensity of molecular flows of titanium and nickel

composition, It is clear that at the initial stages of electron beam evaporation of ingot the composition of the molten pool will change due to the fact that the partial pressure of nickel is higher than that of titanium. As a result of pool enrichment with titanium, its rate of evaporation with some time is levelled with a rate of nickel evaporation. Then, the pool composition can be determined from the condition of equality of molecular flows of nickel and titanium:

$$W_{\text{Ni}} = W_{\text{Ti}}, \quad (18)$$

or

$$X_{\text{Ni}} \exp \left(\frac{\Delta G_{\text{Ni}}^{\text{ex}}}{RT} \right) P_{\text{Ni}}^0 (2\pi M_{\text{Ni}} RT)^{-1/2} - X_{\text{Ti}} \exp \left(\frac{\Delta G_{\text{Ti}}^{\text{ex}}}{RT} \right) P_{\text{Ti}}^0 (2\pi M_{\text{Ti}} RT)^{-1/2} = 0. \quad (19)$$

Results of numerical solution of this equation for different temperatures of molten pool are shown in Figure 5. It is seen that to produce condensates, close by composition to the equiatomic composition, the concentration of nickel in the melt in the range of 1600–2200 K temperatures should be lower than 31.55 at.% Ni. Taking into account the results of calculation, presented in Figure 4, it can be concluded that with the change in the melt temperature, the

coefficient of evaporation is changed negligibly for these compositions of the molten pool. This fact will make it possible to preserve the ratio of components in a vapour flow and, as a consequence, to provide a negligible deviation of composition of the vapour phase from the ingot composition in fluctuations of molten pool temperature in the process of ingot evaporation.

CONCLUSIONS

1. The rate of nickel evaporation from Ni–Ti melt of the equiatomic composition exceeds almost by one order the rate of titanium evaporation.

2. The increase in nickel concentration in the melt is accompanied by a rise in its rate of evaporation, moreover, the most intensive growth should be observed at nickel concentration of more than 50 at.%.

3. With increase in melt temperature at nickel concentration of more than 45 at.%, the coefficient of evaporation begin to decrease greatly. Therefore, to preserve nickel concentration of more than 45 at.% in ingots of Ni–Ti alloy, the melt temperature in the process of their refining should be increased.

4. Enrichment of Ti–Ni alloy melt with titanium, close to equiatomic composition, will promote stabilizing of the evaporation process in the conditions of random fluctuations of the pool temperature.

1. Duering, T.W., Melton, K.N., Stockel, D. et al. (1990) *Engineering aspects of shape memory alloys*. London: Butterworth-Heinemann.
2. Mirgazitov, M.Z., Gunter, V.E., Itin, V.I. (1993) *Superelastic implants and structures from shape memory alloys in stomatology*. Berlin: Quintessenz.
3. Ho, K.K., Carman, G.P. (2000) Sputter deposition of NiTi thin film shape memory alloys using a heated target. *Thin Solid Films*, **370**, 18–29.
4. Chu, J.P., Lai, Y.W., Lin, T.N. et al. (2000) Deposition and characterization of TiNi-base thin films by sputtering. *Material Sci. and Eng.*, **A277**, 11–17.
5. Efimov, A.I., Belorukova, L.P., Vasilkova, I.V. et al. (1983) *Properties of inorganic compounds*. Leningrad: Khimiya.
6. Turchanin, M.A., Belokonko, I.V., Turchanin, A.A. (2000) Enthalpies of formation of liquid binary Ni + (Ti, Zr, Hf) alloys. Part 1. *Energy Technology*, **15**, 93–97.
7. Turchanin, M.A., Agraval, P.G., Turchanin, A.A. (2001) Modelling of the temperature-concentration dependence of the thermodynamic properties and metastable phase equilibrium in binary Ni + (Ti, Zr, Hf) systems. In: *Abstr. of 6th Int. School-Conf. on Phase Diagrams in Materials Science*, Kyiv, Oct. 14–20, 2001.



MODELLING OF HYDRODYNAMICS AND MASS EXCHANGE IN ELECTRON BEAM REMELTING OF TITANIUM ALLOYS

A.B. LESNOJ and V.F. DEMCHENKO

E.O. Paton Electric Welding Institute, NASU, Kyiv, Ukraine

Numerical modelling of processes of heat-mass exchange and hydrodynamics in solidification of ingots, produced by electron beam remelting, was made. The model is based on conjugate solution of equations of convective heat-mass transfer and hydrodynamics. The melt motion under the action of thermocapillary and gravitational forces occurring in the presence of gradients of temperatures and concentrations in metal pool is taken into consideration. Factors are analyzed and regularities of formation of chemical non-homogeneity in molten and solidifying metal are established.

Keywords: *electron beam remelting, numerical modelling, thermal, hydrodynamical, mass-exchange processes, evaporation, chemical inhomogeneity, crystallization of EBR ingots*

In the technological processes of melting ingots using the methods of special electrometallurgy, in fusion welding and other allied technologies associated with melting and crystallization of metal, the dynamics of the melt motion exerts a determinative effect on the formation of chemical inhomogeneity in a solidifying metal. Almost for all the above-mentioned cases, the values of mass and temperature number of Peclet exceed greatly the unity, that proves the primary effect of convective flows on heat-mass exchange in the melt.

In spite of understanding the important role of a hydrodynamic factor in attaining of technological results, the investigations of convection of metal pool have at present a rather limiting and, to a certain extent, superficial nature. This status of the problem is connected, first of all, with great experimental difficulties caused by high temperatures, aggressiveness of medium, non-transparency of melt, small volumes of the pool (in welding) and other factors. In this connection, the methods of mathematical modelling of solidification processes have been widely developed, thus minimizing the expensive full-scale experiments, in particular, at the initial stages of technology testing and equipment designing [1].

The existing works on mathematical modelling of mass exchange processes in electron beam remelting (EBR) can be conditionally divided into two groups.

The first group includes models with lumped parameters based on equations of an integral balance of mass [2, 3]. In these works, as a rule, a priori coefficient of mass exchange of near-surface layers of the pool mirror with a perfectly mixed center of the melt is used, which defines actually the diffusion resistance of hydrodynamic boundary layer and intensity of mass exchange processes. The limitative capabilities of these models cannot be used for investigations of non-stationary processes of evaporation at high non-uniform

electron beam heating of the pool mirror surface, which is most typical of many technological diagrams of EBR.

The second group is distinguished by mathematical models with a direct calculation of convective-diffusion mass transfer in the molten metal taking into account the non-uniformity of specific flows of evaporation depending on temperature and concentration of melt components near the surface of the pool mirror. As typical representatives of this group, we shall describe models [4–7], in which calculation of mass exchange processes consists of two parts. In the first part, a thermal model in a transition condition [5] is considered, which is used for determination of the ingot thermal state. In the second part the model of mutual transfer of substance, heat energy and pulse in the metal pool is calculated. The specifics of calculations is such that the modelling of mass-exchange processes is performed in a «fixed» metal pool, whose shape was obtained on the basis of results of the first thermal model. The similar approaches were used for calculation of hydrodynamic processes in ingots produced by the vacuum-arc remelting [6, 7].

The use of this approximation to reduce the volume of calculations is justified to a certain degree by the fact that when the ingot reaches the height comparable with two diameters of the mould, the thermal condition of the ingot is close to the quasi-stationary condition [1] and the pool shape is not almost changed with time. From the other hand, the solution of problems of heat and mass exchange separately from the a hydrodynamic problem leads inevitably to the error in the solution obtained, as the interrelation of processes of transfer of heat, mass and pulse is lost. The most noticeable drawback of a «static» pool is the absence of feasibility to predict the chemical inhomogeneity in a forming solid phase. At the same time the predicting estimations of processes of mass transfer in EBR represent interest by several reasons.

Firstly, the quantitative estimations of kinetics of evaporation of alloying elements, in particular, with a high vapour pressure to compensate their melting

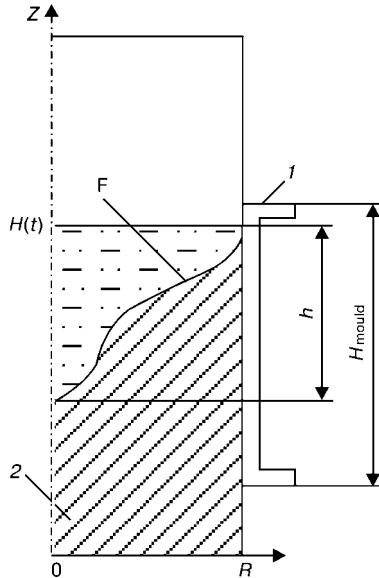


Figure 1. Scheme of mathematical model of formation of round EBR ingot: 1 – mould; 2 – solidified ingot ($H(t)$ – current height of ingot; F – front of solidification; h – pool depth; H_{mould} – mould height)

loss, are necessary. Secondly, it is necessary to have a quantitative representation about on the regularities of formation of chemical inhomogeneity in liquid and solidified metal. Thirdly, it is desirable to be able to have an idea of the nature of distribution of both alloying and impurity elements in an optional section of the ingot to determine the efficient metal yield, corresponding to the technical specifications.

In the present article, unlike the earlier works, a computer model of conjugate processes of heat and mass exchange and hydrodynamics is offered, which makes it possible to follow the kinetics of formation of thermal and concentration state of the ingot in the molten and solidified metal in EBR with an intermediate crucible of titanium alloys with an increased content of aluminium (VT6, VT20), starting from pouring of the first portion of metal up to attaining the quasi-stationary state in the ingot.

The mathematical model of heat exchange and hydrodynamics [8] was added with equations of a convective diffusion. The main statements of a more comprehensive model should be noted. Axial symmetry of thermal, concentration and hydrodynamic fields in the ingot will be assumed. In this connection the three-dimensional problem was reduced to the solution of two-dimensional problem in cylindrical coordinates (Figure 1). Calculation of heat and mass exchange processes takes into account the convective-conductive, convective-diffusion mechanism of transfer of heat energy and mass, and also a turbulent nature of the melt motion. The problem of hydrodynamics is solved on the base of a full system of Navier–Stokes equations in Oberbeck–Boissinesq approximation. The following factors leading to the molten metal motion are taken into account: firstly, the volume gravitational convection occurring in the field of a gravity force in the presence of gradients of temperatures and concentrations in the melt; secondly, the

surface thermocapillary convection of Marangoni, occurring due to change in forces of surface tension at non-uniform heating of a free surface of the pool mirror.

Processes of mass transfer in a multicomponent melt are described by the equation of a convective diffusion:

$$\frac{\partial C_i}{\partial t} + (\vec{V} \nabla) C_i = \text{div} (D_i^{(t)}(T) \nabla C_i); \quad \Omega = \{0 < r < R, 0 < z < H(t)\}, \quad t \in [0, t^*], \quad (1)$$

where C_i is the concentration of i -th component; \vec{V} is the vector of rate; $D_i^{(t)}(T) = D_i + \frac{L}{2} |\vec{V}|$ is the coefficient of diffusion, accounting for turbulent nature of transfer of the i -th substance; L is the mean scale of turbulent vortexes, by which the averaging is made. To calculate the diffusion coefficient D_i the temperature relationship is used:

$$D_i = D_i^{(0)} \exp \left(-\frac{\Delta E}{RT} \right), \quad (2)$$

where ΔE is the energy of activation, J/mol; R is the universal gas constant, J/(mol·K); $D_i^{(0)}$ is the pre-exponential multiplier, cm^2/s .

The change in ingot height in the model can be taken into account by several methods: discretely, i.e. drain of metal by portions from an intermediate crucible, and continuously, i.e. axial remelting and combination of discrete and continuous pouring of metal.

At the front of solidification, the fulfillment of conditions of integration of specific flows of mass of a liquation element is assumed:

$$\begin{cases} D_i^{(L)} \frac{\partial C_i^{(L)}}{\partial n} \Big|_F - D_i^{(S)} \frac{\partial C_i^{(S)}}{\partial n} \Big|_F = v_n (C_i^{(S)} - C_i^{(L)}) \\ C_i^{(S)} \Big|_F = K_i C_i^{(L)} \Big|_F, \end{cases} \quad (3)$$

where v_n is the projection of vector of solidification rate on normal to interphase boundary; K_i is the equilibrium coefficient of distribution of the i -th element; indices S, L correspond to solid and liquid phases.

The boundary conditions were formulated as follows. There is no mass exchange on the axis, lateral and bottom surfaces of the ingot:

$$\frac{\partial C_i}{\partial r} \Big|_{r=0} = 0; \quad \frac{\partial C_i}{\partial r} \Big|_{r=R} = 0; \quad \frac{\partial C_i}{\partial z} \Big|_{z=0} = 0. \quad (4)$$

On the pool mirror the following conditions of a local balance of mass are taken into account enter of metal being remelted into a mould with initial concentration $C_i^{(0)}$; specific flow of mass of alloying element entering from the melt depth due to a convective-diffusion mechanism, and the losses as a result of evaporation:

$$\rho D_i \frac{\partial C_i}{\partial z} \Big|_{z=H(t)} = v_i^{(\text{mass})} + v_i^{(\text{evap})}, \quad (5)$$

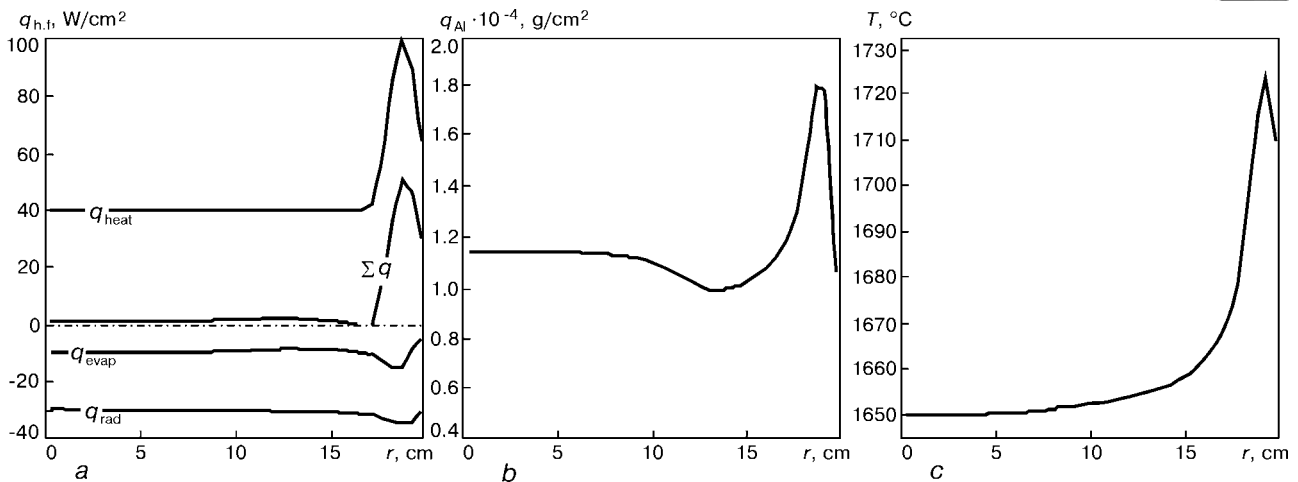


Figure 2. Specific heat flows (a), specific flows of evaporation of aluminium (b) and temperature of pool surface (c)

hence

$$v_i^{(\text{mass})} = m(r) \rho \left(C_i \Big|_{z=H(t)} - C_i^{(0)} \right) v_z(r, t) \Big|_{z=H(t)}, \quad (6)$$

where ρ is the specific density of the melt; $v_i^{(\text{mass})}$ is the specific mass flow associated with enter of metal being remelted into the mould with an initial concentration of the dissolved substance $C_i^{(0)}$ and rate $v_z(r, t) \Big|_{z=H(t)}$; $m(r)$ is the surface density of distribution of drops (depends on specifics of remelting); $v_i^{(\text{evap})}$ is the specific mass flow associated with evaporation of the dissolved substance. Model of evaporation is based on the Langmuir law. It is shown in [9], using the kinetic Boltzmann equation, that in the conditions of technological vacuum of EBR (1.0–0.1 Pa) this ratio makes it possible to calculate adequately the local rates of evaporation:

$$v_i^{(\text{evap})} = \frac{\alpha \gamma_i P_i^0 C_i \Big|_{z=H(t)}}{\sqrt{2\pi R M_i T} \Big|_{z=H(t)}}, \quad (7)$$

where α is the coefficient of accommodation; M_i is the molar mass; γ_i is the coefficient of activity of substance in solution; P_i^0 is the pressure of saturated vapour of a pure component. Here

$$P_i^0 = A_i \exp \left(- \frac{B_i}{T \Big|_{z=H(t)}} \right), \quad (8)$$

where A_i , B_i are the constants.

At the initial moment of time $t = 0$ the existence of priming volume of molten metal of height $H(0)$ with a homogeneous concentration field $C_i(r, z, 0) = C_i^0 = \text{const}$ is assumed.

For a numerical realization of an integrated conjugate model of heat and mass exchange and hydrodynamics a combined Lagrange–Euler method [10] is applied, which uses approximation on local Lagrange networks of convective terms in equations of transfer together with substantial derivatives. This method, due to minimizing the effects of counting dissipation, provides the acceptable precision of numerical solu-

tion [11] on sufficiently rough space and time networks. The problem was calculated in natural variables using schemes of equations splitting by physical subprocesses. Software, developed in medium Compaq Visual Fortran 6.5, allows calculating the full time cycle of formation of the EBR ingot (starting from pouring of the first portion, fade out of shrinkage cavity and cooling the ingot surface to the preset temperature) in the personal computers.

Let us consider factors stipulating formation of chemical inhomogeneity in the metal pool: firstly, the periodic enter of molten metal of initial concentration from the intermediate crucible; secondly, technological specifics of EBR is such that near the mould wall a free surface of melt should be more intensively heated to maintain the molten pool cylindrical part. In these conditions the non-uniformity of heat flow leads to the non-iniformity in evaporation of alloying and impurity components of melt and, consequently, to the formation of chemical inhomogeneity in a liquid phase; thirdly, a complex nature of a directed convective mass transfer in the melt volume under the action of gravitational and thermocapillary forces.

The calculations were performed for melting titanium alloy VT6 using the following technological parameters: mould diameter — 40 cm, mass productivity of remelting — 50 g/s, total capacity of electron beam heating — 65–70 kW, duration of molten metal accumulation in intermediate crucible — 120 s, content of aluminium in melt entered the mould — 7 %, equilibrium coefficient of distribution of aluminium at the solidification front is close to 1. In calculations, the scheme, most widely applied in operating technologies of EBR, of distribution of heat flow of electron beam heating, i. e. uniform for central zone of pool mirror and with a maximum concentration only near the mould wall, was used (Figure 2, a).

Under these conditions an intensive turbulent flow is formed in the molten metal volume, which is localized near the mould wall in the upper part of the metal pool, while the central volumes of the pool are stirring negligibly (Figure 3, b). This circumstance leads to a uniform evaporation of aluminium from the central part of the pool mirror (Figure 2, b).

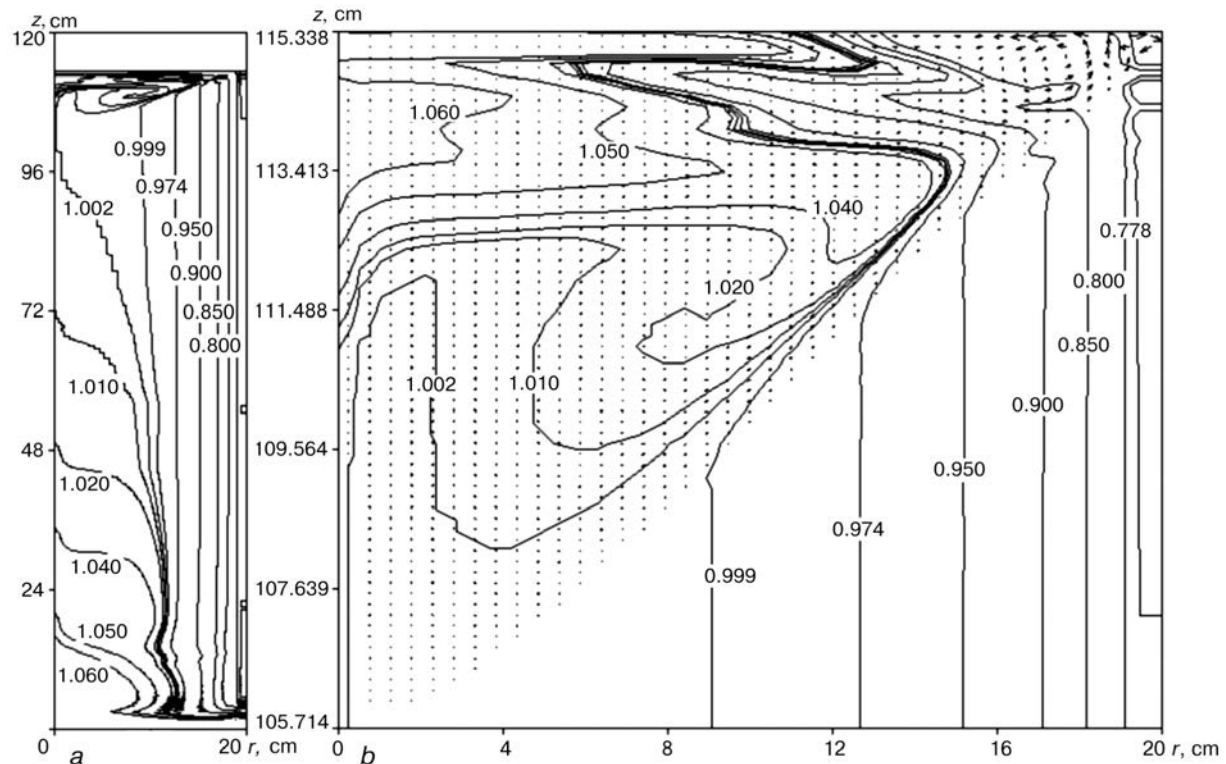


Figure 3. Relative distribution of aluminium (C_{Al}/C_{Al}^x) in solidified ingot (a), metal pool (b) and hydrodynamics of melt at uniform preheating of a central part of melt free surface ($C_{Al}^x = 6.6\%$ is the typical concentration of aluminium in solidified metal)

In the zone of the higher heat input, the highest overheating of metal above the liquidus temperature is formed, i.e. 4 times higher than in the pool central part (Figure 2, c), which stipulates the 1.5 times increase in losses in easily-evaporating components, that causes in its turn the formation of chemical in-

homogeneity in the molten metal near the surface of evaporation. In the zone of the higher heat input ($0.7 < r < 1.0R$) the volumes of metal, depleted with aluminium, are formed in the near-surface part of the pool (Figure 4).

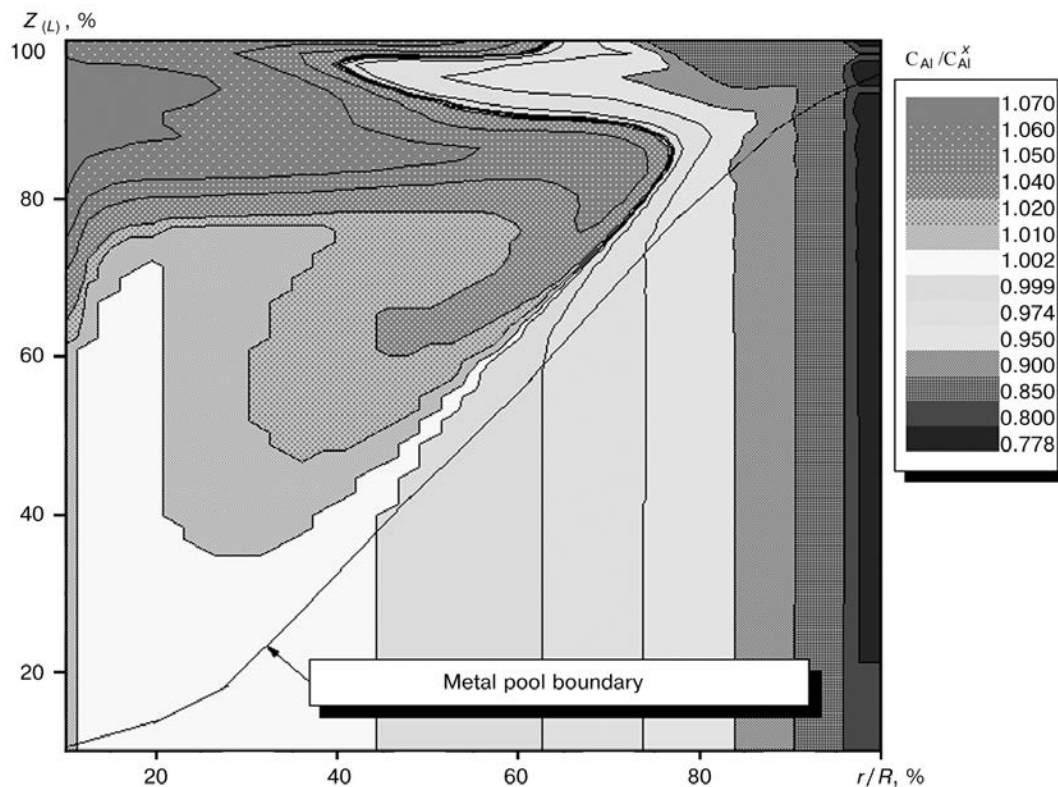


Figure 4. Map of isoconcentrates of relative distribution of aluminium in metal pool at uniform preheating of a central part of melt free surface ($Z_{(L)} = (1 - (H(t) - z)/h) \cdot 100\%$)



The depleted metal is transported by convective flows into two directions: along the free surface from periphery to the ingot axis and also in the form of downward flow along the solidification front, moreover, the metal with higher aluminium content is pushed aside into central volumes of the pool. As a result, the chemical composition of molten metal becomes non-homogeneous both in radial and also in axial directions (Figures 4 and 5). It should be outlined that the downward convective flow along the solidification front (Figures 3, *b* and 4) defines the main mechanism of formation of the chemical inhomogeneity along the radius of the solidifying ingot. At the time when convective flow of melt along a free surface hinders the mass transfer of melt, more enriched with aluminium, from center to the pool mirror, the evaporation of alloying component is decreased, thus causing the curve bending in Figure 2, *b*.

Calculations show (Figure 3, *a*) that the least favourable conditions for appearance of the chemical inhomogeneity along the ingot axis are formed at the transition stages of starting and completion of remelting. Periodic enter of the molten metal from the intermediate crucible with a higher content of aluminium in the solidified metal than that in the metal pool, is manifested in the form of negligible jumps in concentration only near the lateral surface of the ingot ($0.95 < r < 1.0R$). The central part of the ingot is characterized by a sufficiently high homogeneity both in height and also in radius.

CONCLUSIONS

1. The mathematical model for calculation of non-stationary processes of heat and mass transfer and hydrodynamics, proceeding in electron beam remelting titanium alloys with increased content of aluminium has been developed. The model allows investigation of thermal, concentration and hydrodynamic conditions of the ingot depending upon the remelting process parameters.

2. The results obtained make it possible to estimate the specific flows of evaporation and mass losses of aluminium, relative distribution of alloying component across the melted ingot section, degree of evaporation loss and to distinguish the zones of increased chemical inhomogeneity in the ingot.

3. Regularities and mechanisms of formation of a local chemical inhomogeneity in molten and solidify-

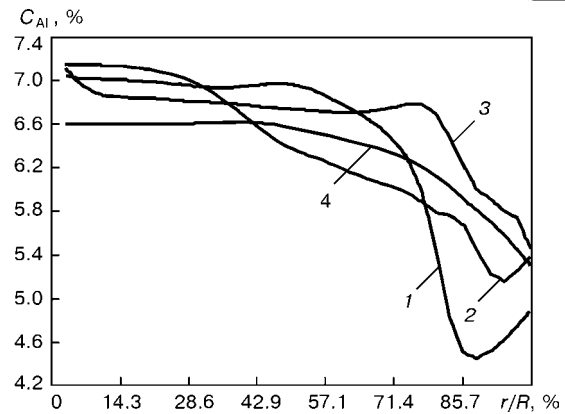


Figure 5. Distribution of aluminium along the ingot radius for horizons of metal pool: 1 – 114; 2 – 113; 3 – 112; 4 – 105 cm

ing metal at uniform heating of the pool mirror central zone with a maximum concentration of heat flow only near the mould wall are established.

1. Paton, B.E. (2000) Current electron beam technologies of the E.O. Paton Electric Welding Institute of the NAS of Ukraine. *Problemy Spets. Elektrometallurgii*, **2**, 22–34.
2. Boronenkov, V.N., Zhadkevich, M.L., Salamatov, A.M. et al. (1995) Mathematical model of calculation of metal composition in electron beam remelting of heat-resistant Ni-base alloys. *Ibid.*, **2**, 24–35.
3. Varich, I.Yu., Akhonin, S.V., Trigub, N.P. et al. (1997) Evaporation of Ti-base aluminium alloys during electron beam melting with intermediate crucible. *Ibid.*, **4**, 15–21.
4. Bellot, J.-P., Jardy, A., Ans, A. et al. (1997) Thermohydrodynamic state of melt in electron beam remelting of titanium ingot. *Ibid.*, **3**, 3–18.
5. Blum, M., Choudhury, A., Romberg, M. et al. (1992) Electron beam remelting of superalloys with low evaporation losses and high cleanliness. In: *Proc. of Conf. on Electron Beam Melting and Refining: State-of-the-Art 1992*, Reno, USA.
6. Jardy, A., Ablitzer, D. (1990) Comportement du puits liquide des lingots VAR. *Memoires et etudes scientifiques de la Revue de Metallurgie*, **7/8**, 421–427.
7. Jardy, A., Ablitzer, D. (1990) On convective and turbulent heat transfer in VAR ingot pools. In: *Proc. of 5th Int. Conf. on Modeling of Casting, Welding and Advanced Solidification Processes*, Davos, Suisse, Sept., 1990.
8. Lesnoj, A.B., Demchenko, V.F., Zhadkevich, M.L. (2001) Modelling of hydrodynamics and heat exchange in solidification of electron beam remelting ingots. *Problemy Spets. Elektrometallurgii*, **2**, 17–21.
9. Bellot, J.-P., Duval, A., Ablitzer, D. (1999) Kinetics of evaporation processes in vacuum metallurgy. *Ibid.*, **4**, 25–39.
10. Demchenko, V.F. (1983) Difference schemes for convective diffusion equation. In: *Proc. of Int. Colloquium*. Sofia: VMEI.
11. Demchenko, V.F., Lesnoj, A.B. (2000) Lagrange–Euler method of numerical calculation of convective diffusion multivariate problem. *Dopovidi Nats. Akad. Nauk Ukrainy*, **11**, 71–75.



THERMAL FIELD OF LARGE-SIZED REFRACTORY SINGLE CRYSTALS AT COMBINED PLASMA-INDUCTION HEATING*

V.A. SHAPOVALOV, V.V. YAKUSHA and A.N. GNIZDYLO

E.O. Paton Electric Welding Institute, NASU, Kyiv, Ukraine

Results of investigations of thermal fields of large single crystals of tungsten in the conditions of plasma-induction zone melting (PIZM) are presented. It is shown that the use of PIZM with fixed plasma-arc heat source allows growing single crystals of tungsten of diameter of not more than 70 mm. Scanning of plasma-arc heat source along the radius of crystal gives an opportunity to increase its diameter. The ratios of capacities of sources of plasma-arc and induction heating in growing large crystals are given.

Keywords: *mathematical model, plasma-induction zone melting, thermal field, internal stresses, large single crystals of refractory metals*

Owing to the use of two independent heat sources [1] and feasibility of a fine adjustment of technological parameters the plasma-induction zone melting (PIZM) opens up the wide opportunities for control of the single crystal growing process. However, the high temperature of melting and complexity of equipment make this method of producing crystals complicated and labour-intensive.

Therefore, the problem of optimizing technological parameters has an actual importance in the development of PIZM technology both for the laboratory investigations and also for its implementation in industry. Rational and effective solution of this type of problems, as the advanced world practice shows, is associated with mathematical modelling of the technological process.

The scientific interest of investigations of growing single crystals of refractory metals is concentrated on the study of temperature state of ingot during its growth. The knowledge obtained about the temperature distribution in the ingot section, about the shape and curvature of surface of phases interface makes it possible to influence effectively the processes of structure formation of single crystals and to optimize the technology for adjustment of the heat source power within the preset ranges.

Earlier in the work [2] we carried out investigations of thermal state of refractory single crystals, forming under the conditions of a combined plasma-induction heating, on the example of a mathematical model. However, the revealed regularities and ranges of power changes were obtained on samples of small sizes (20–30 mm diameter). The problem about the

thermal state of large crystals in this work was not considered.

The aim of the present work is to study the thermal state of refractory metal single crystals of large sizes (up to 100 mm diameter) and to compare the results obtained with earlier revealed relationships on small samples.

The temperature field of single crystals was investigated using a mathematical model on an example of tungsten. Description of the mathematical model of the plasma-induction heating, assumed perfection of heat sources, initial and boundary conditions of equation of heat conductivity are shown in detail in [2, 3]. Diameters of crystals were changed in the range from 20 to 100 mm. Their height, the same as in previous work [2], was not less than three diameters. Effect of inductor height on the pattern of temperature field is higher with the higher specific power of the induction heating. When studying the thermal state of single crystals of 20–30 mm diameter the specific power of the induction heating was changed in the range of 100–400 W/cm². In our investigations we were limited by the most real value 300 W/cm². The effect of inductor height H_{ind} on the metal pool depth h_p at different diameters of single crystal is shown in Figure 1. Curves 1–4 reflect this relationship for the following diameters: 100, 80, 70 and 60 mm. Power of plasmatron was in this case, respectively, as follows: 49, 33, 25.2 and 19 kW.

It was established in [2] that the depth of pool remains constant in that case when the inductor height 3 times exceeds the ingot diameter. It follows from Figure 1 that with increase in single crystal diameter the relationship of effect of inductor height (zone of heating) on pool depth, revealed earlier for small samples, is disturbed. In the investigated range of

*The work was fulfilled under the financing support of Science and Technology Center in Ukraine.

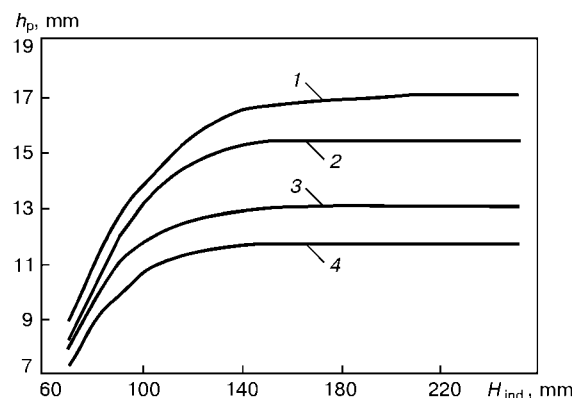


Figure 1. Dependence of pool depth on height of heating zone

diameters of single crystal the inductor height/crystal diameter ratio is decreased from 3 to 1.5.

The mathematical model used for investigation of temperature fields reflects rather precisely, in our opinion, the real pattern of effect of inductor height on pool depth. As to the shape of phases interface the new problems are appeared here, being associated with the perfection of the plasma heat source. The heat flow, entered the pool, is divided conditionally on the model into two zones, in the range of which its power is constant. In practice, when plasma-arc heat sources are used, the length of the zone with a low intensity of flow, as well as the zone of heating with higher intensity (arc spot zone), is not known.

With increase in linear sizes of single crystals (diameter) the investigated scheme of a combined heating does not provide the formation of molten pool of the required sizes. Therefore, the growing of single crystals of diameter of more than 60–70 mm will be problematic. This conclusion is followed indirectly from Figure 1, as the established earlier relation between the critical height of the inductor and diameter of the single crystal is disturbed after increase in the diameter of the latter above the given data. To produce larger single crystals it is rational to move the metal pool of the size, being smaller than crystal diameter, along the entire forming surface. Here, different variants can be suggested, but in each of them the plasmatron is located axisymmetrically with respect to the crystal. The process of crystal formation occurs layer-by-layer with a shifting of the incrementing path or without shifting and with change in the direction of rotation of the crystal after transition to the new layer.

The use of the scheme with a fixed plasmatron (Figure 2, *a*) also puts limitations on limiting values of the single crystal diameter, as the pool diameter should be larger than the single crystal radius. With a large increase in the pool, the problems are appeared, similar to those, which are typical of the axisymmetrical scheme. The process, the diagram of which is shown in Figure 2, *b*, allows growing single crystals of almost any size, however, it can be limited by the capacity of the high-frequency generator, if it is necessary to heat the entire single crystal. If to use another kind of heating to maintain the necessary tem-

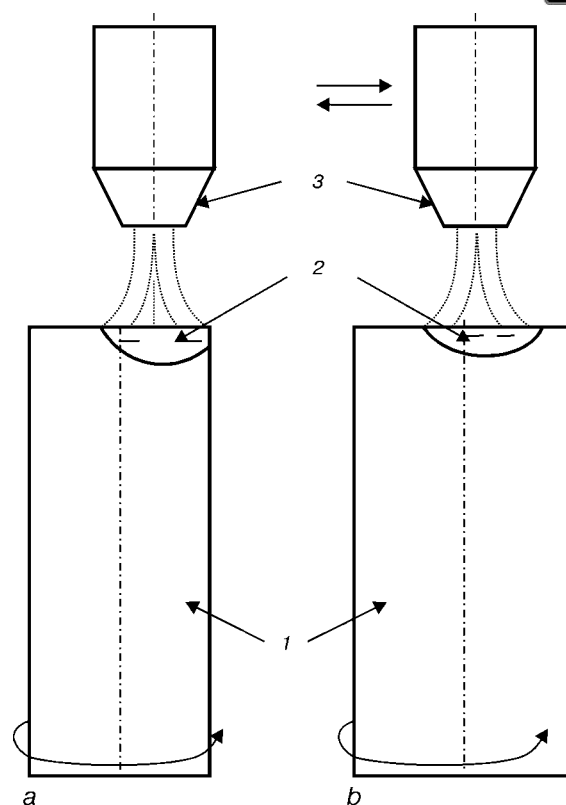


Figure 2. Schemes of PIZM for growing large cylindrical crystals: *a* — fixed plasmatron; *b* — plasmatron is scanning along the single crystal radius; 1 — single crystal; 2 — metal pool; 3 — plasmatron

perature in the lower part of the crystal, for example, radiation heating, then it is possible to grow crystals of a rather large diameter at comparatively low power of the high-frequency generator, required only to maintain metal pool from flowing out and heating of the upper part of the single crystal.

The investigations carried out on modelling of thermal fields allow us to determine the relationships of capacities of plasma-arc and high-frequency heat sources. Figure 3 shows the change in power W of heat flows, taken by the single crystal from each heat source. In experiment conductance the orientation was made to the following. Independently of the single crystal diameter d_{cr} the pool height at its lateral surface was kept constant. The inductor height was minimum, coming from the condition that its further increase does not influence the pool depth in crystal axis. As it follows from the analysis of Figure 3, with increase in diameter of a single crystal the relationship

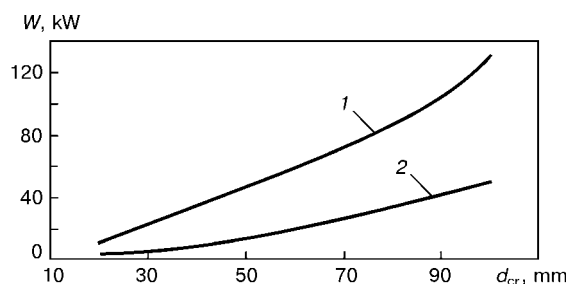


Figure 3. Change in power of heat flows taken by single crystal depending on diameter of the latter at combined heating by plasmatron and inductor: 1 — induction heating; 2 — plasma-arc heating

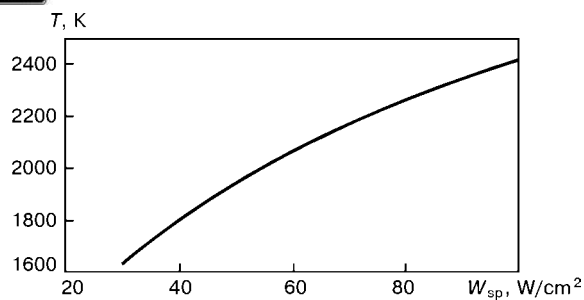


Figure 4. Dependence of temperature of tungsten single crystal on specific power of heating

between the amount of heat, transferred to it by the high-frequency and plasma-arc heating, is reduced from 4.26 to 2.7 with increase in crystal diameter from 20 to 100 mm. The relationship obtained is based on a scale factor.

The relationship is estimating and changed with increase in height of the single crystal, as here it is necessary to increase the specific power of heating W_{sp} to maintain the required temperature in the lower part of the crystal. It was established by us that the specific power of preheating of the crystal lower part in use of the two-sectional mould [2] cannot be lower than 55 W/cm^2 (Figure 4), as for the conditions of relaxation of internal stresses the temperature of preheating of the crystal lower part should be higher than $0.5T_{\text{melt}}$ [4] (for tungsten it is higher than 1880 K).

Thus, when minimizing the capacities of the induction heaters the total value of the power generated by it in reaching the length of crystal equal to 10–40 diameters, can increase 2.5–2.8 times. Therefore, the real ratio of capacities of sources of induction and plasma-arc heating for sufficiently long crystal will change in the range of 7:1–10:1. The lower value is for the larger crystals, while the higher value is for small-diameter crystals.

The conclusion can be made from the investigation results that the great differences in patterns of temperature fields and in ratios of capacities of sources of plasma-arc and induction heating for large single crystals of refractory metals and crystals of small sizes are caused mainly by a scale factor which takes into account the thermophysical characteristics of the material, its volume and geometry of heat-dissipating surface.

When developing the technology of producing large single crystals of refractory metals (of more than 60–70 mm diameter), it is rational to use a plasma heat source of a low single-unit power, required for setting up the molten metal pool of a size, being smaller than the diameter of the growing crystal, and to move it along the forming surface using a preset procedure. Here, it is necessary to use an induction heating along the all height of the forming ingot to grow small-height crystals to maintain the stable heating conditions. In case of growing sufficiently large crystals it is necessary to use a heater composed of two sections. The upper induction section will perform the functions of maintaining the molten metal pool from flowing out, stabilization of geometry of crystallization front, and also removal of the heat shock from the plasma arc flame in the crystal zone adjacent to the region of interface of solid and liquid phases. Functions of the second section of the heater (induction or radiation) will consist in maintaining the required thermal conditions for relaxation of internal stresses in the ingot lower part.

1. Shapovalov, V.A., Zhadkevich, M.L., Torkhov, G.F. et al. (2002) Growing of refractory metal single crystals (Review). *Advances in Electrometallurgy*, **4**, 17–23.
2. Shapovalov, V.A., Yakusha, V.V., Gnizdylo, A.N. (2003) Thermal field of a single crystal at a combined heating. *Ibid.*, **1**, 20–22.
3. Shapovalov, V.A. (2002) Thermal field of tungsten single crystal in plasma-induction zone melting. *Ibid.*, **4**, 24–26.
4. Zolotarevsky, V.S. (1983) *Mechanical properties of metals*. Moscow: Metallurgiya.



EFFECT OF IONIZATION ON VOLTAGE DROP AND FREQUENCY OF DROPLET SHORT-CIRCUITS IN VACUUM-ARC REMELTING OF HIGH-ALLOY STEELS

V.G. LISIENKO, Ya.A. NASYJROV, M.I. KLIMOV, P.S. ALTMAN, A.Yu. TASHKINOV and A.E. GONCHAROV
Verkhnyaya Salda Metallurgical Production Association, Verkhnyaya Salda, Russia

Experiment on vacuum arc remelting of 300 mm diameter electrode of alloy steel into 465 mm diameter mould was performed in the industrial conditions. Statistic model of changing arc voltage drop depending on the duration of relaxation period of ionization has been developed. The offered model can be used for optimum control of process of vacuum-arc remelting.

Keywords: ionization, interelectrode gap, voltage drop, frequency of droplet short-circuits

Ionization in melting is called conditionally a complex of phenomena consisting of ionization and excitation of vapours and gases in a gap between electrode (cathode) and molten metal pool (anode) [1]. Ionization occurs in evaporation and condensation of low-boiling impurities and alloying additions of magnesium, magnesium chloride, manganese, etc. The main part of a luminous cloud has a greenish-blue colour, which is changed for yellow and red being closer to the «crown» of ingot. Luminescence can have a form of a clearly expressed tail and follow the anode spot sliding by trajectory. Luminescence can be short-time (1–5 s), detaching from the arc and illuminating itself the gap between the electrode and mould, and can be also long-time (5–100 s), hiding the mirror of molten metal and electrode lower end under its bright spot.

The main aim of the work is to analyze ionization and to determine its effect on parameters of arc voltage drop and frequency of droplet short-circuits during melting.

Experiment and discussion. During melting the arc voltage drop U_a and frequency of droplet short-circuits F_{DSC} were recorded in industrial computer AWS-800 of company «Advantech» at 1 Hz frequency. All data were averaged from five previous points. Pressure in furnace was maintained at the level of 2 Pa. Interelectrode gap was 15 ± 5 mm within the entire period of melting, arc current was 6 kA. Fi-

gure 1 shows dependencies of arc voltage drop and frequency of droplet short-circuits on time in remelting of 380 mm diameter high-alloy steel electrode in 465 mm diameter mould.

In ionization the arc voltage drop by 1–5 V and decrease in frequency of droplets short-circuits up to its complete absence are occurred [2, 3]. In this connection, it was decided to analyze the most typical processes of ionization during the entire period of melting. 15 different diagrams of ionization were used. Each diagram was differed by an average arc voltage drop before ionization, U_{av} ; minimum voltage drop during ionization, U_{min} ; difference between the arc voltage drop before ionization and its minimum value, U_{diff} ; and also averaged frequency of droplet short-circuits before ionization, F_{av} .

Each ionization is determined by the following parameters: time of voltage drop, t_d ; time of relaxation process of voltage drop, t_r ; time at which the value of frequency of droplet short-circuits is close to zero, t_{DSC} . As a result, a graphical model of ionization behaviour, presented in Figure 2, was suggested. Table gives data for each ionization during melting.

Using package Statistika 5.1, the analysis of dependence of value U_{diff} on duration of relaxation process t_r was made. Relationship is well approximated by the following linear equation:

$$U_{diff} = 0.028t_r + 1.046. \quad (1)$$

Coefficient of regression for the given model is equal to 0.778 which indicates that the model describes well enough the data of experiment. Figure 3 shows distribution U_{diff} depending on duration of

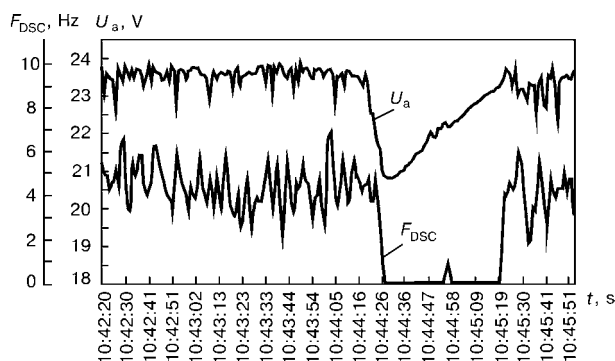


Figure 1. Dependence of arc voltage drop and frequency of droplet short-circuits on time

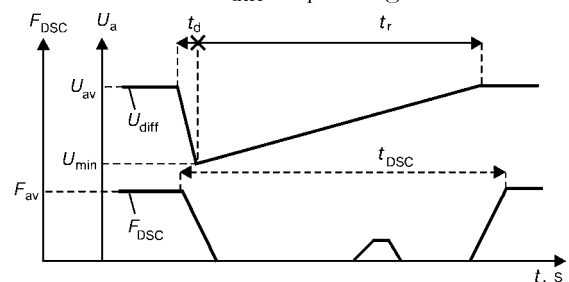


Figure 2. Graphical model of ionization in vacuum arc remelting



Parameters of arc voltage drop and frequency of droplet short-circuits for each ionization

No. of ionization	U_{\min} , V	U_{diff} , V	t_d , s	t_r , s	t_{DSC} , s
1	19.9	3.6	3.0	80	73
2	21.1	2.4	2.0	40	34
3	20.7	2.8	3.0	45	41
4	21.6	1.9	5.0	49	43
5	21.5	2.0	4.5	50	44
6	22.0	1.5	4.0	20	15
7	22.0	1.5	3.0	16	11
8	20.3	3.2	6.0	70	62
9	21.0	2.5	4.0	54	47
10	21.2	2.3	3.0	42	35
11	20.9	2.6	7.0	60	55
12	21.1	2.4	3.0	47	44
13	21.0	2.4	4.0	38	31
14	21.2	2.3	2.0	30	24
15	21.7	1.8	2.0	25	19

Note. U_{av} for all the diagrams of ionization is 23.5 V.

relaxation process t_r , and Figure 4 gives diagram of scattering of dependence of experimental data on predicted values U_{diff} by equation (1).

In addition, the analysis of the rest values was made, i.e. difference of values U_{diff} , predicted by equation (1) and obtained experimentally, was determined. Figure 5 shows graph of rated function of distribution of remnants.

The conclusion can be made from Figures 4 and 5 about the adequacy of suggested regression equation (1). Thus, by changing the parameter U_{diff} it is possible to make assumption with a high share of probability about the duration of ionization and time of its completion. The characteristic feature of ionization is the interruption of droplet short-circuits during relaxation process. During the period of ionization F_{DSC} is equal to zero and only in some cases the so-called «noises» are occurred: the metal droplets from the electrode end lead to short-circuit with a molten metal pool. Frequency of these «noises» is about 1–2 Hz, duration is not more than 3–5 s and it is easy to distinguish it, because the frequency of droplet short-circuits before ionization is 6–8 Hz and more.

Application of model in VAR control. Operation of automated control systems of vacuum-arc remelting is realized, as a rule, either by parameters of voltage drop or by frequency of droplet short-circuits [4]. At long-time ionization, i.e. voltage drop and absence of frequency of droplet short-circuits, the deterioration in operation of automatic controllers is possible, causing the instability in control of the melting process. In accordance with the offered regression model there is a feasibility to identify ionization as a phenomenon and, with allowance for a preset model, to provide the optimum control of the melting process.

CONCLUSIONS

1. Arc voltage drop in vacuum-arc method of remelting is abruptly jumpy decreased, here, the duration of relaxation period is increased slowly to the initial value.

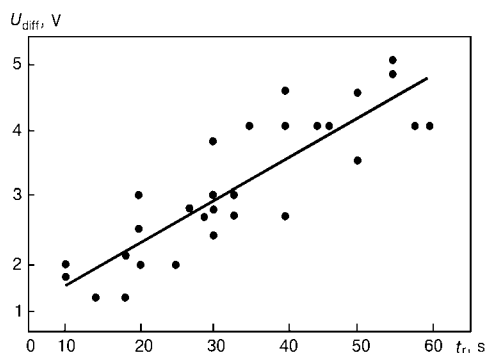


Figure 3. Dependence of U_{diff} on duration of relaxation process of ionization (points — data of experiments; solid line — prediction by equation (1))

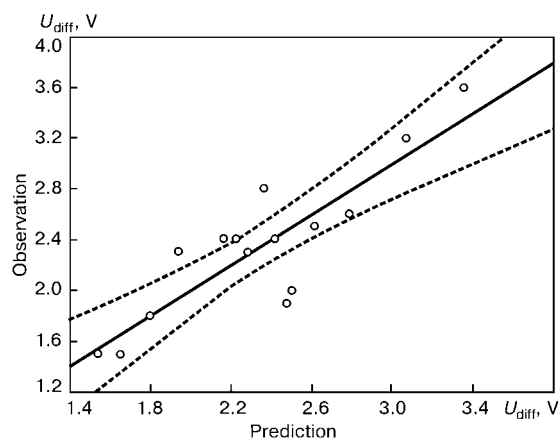


Figure 4. Diagram of scattering of dependence of observed (experimental) data on predicted data by equation (1) (solid line indicates relationship by equation (1), dashed line shows 95 % interval relative to line of regression)

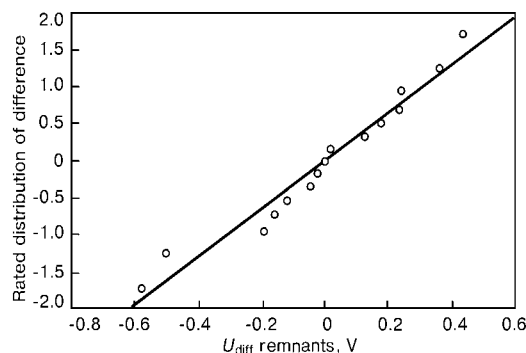


Figure 5. Graph of rated function of distribution of remnants (solid line — function of distribution; points — values of remnants)

2. Dependence of jumpy change in voltage drop on the duration of relaxation period is well described by a linear model.

3. Frequency of droplet short-circuits during relaxation process of ionization is almost interrupted and its level is 0.5–1.5 Hz.

4. The offered regression model can be used in automatic controllers of melting to control the consumable electrode movement.

1. Andreev, A.L., Anoshkin, N.F., Bocharov, G.A. et al. (1994) *Melting and casting of titanium alloys*. Moscow: Metallurgiya.
2. Zanner, F.D., Williamson, R.L., Harrison, R.P. et al. (1997) Vacuum-arc remelting of Inconel 718. *J. Soc. of Specialists on Minerals and Metals*, Series B, 28, 841–853.
3. Zanner, F.D., Skindger, M.E., Highsinger, K.L. et al. (1991) Current strategies of control of vacuum-arc remelting alloys sensitive to liquation. *Ibid.*, 94, 37–46.
4. Alperovich, M.E. (1990) *Automation and optimisation of main processes of special electrometallurgy*. Moscow: Metallurgiya.



INVESTIGATION OF MECHANICAL PROPERTIES OF FORGED SEMI-PRODUCTS OF EXPERIMENTAL TITANIUM ALLOY T-110

S.L. ANTONYUK¹, V.N. KOROL¹, A.G. MOLYAR¹, I.M. ROMASHKO¹, V.N. ZAMKOV² and V.F. TOPOLSKY²

¹O.K. Antonov ANTK Company, Kyiv, Ukraine

²E.O. Paton Electric Welding Institute, NASU, Kyiv, Ukraine

Strength characteristics of forged semi-products of experimental high-strength ($\alpha + \beta$)-titanium alloys of Ti-Al-Mo-V-Nb-Fe-Zr system (T-110) after different conditions of forging and heat treatment are defined. Technological parameters of forging and heat treatment providing the required level of mechanical properties are developed. It is shown that the as-annealed forged alloy T-110 is not inferior by the level of strength to the forgings of industrial alloy VT22.

Keywords: *titanium alloys, heat treatment, forging, microstructure, mechanical properties*

Progress in aircraft engineering is accompanied by a continuous increase in requirements for the quality and level of properties of materials used to provide both maximum service reliability of flying vehicles and also their high weight effectiveness.

To decrease the mass of flying vehicles the high-strength two-phase ($\alpha + \beta$)-titanium alloys are used in structures of their load-carrying elements. Strength of these alloys is determined not only by the degree of alloying, but also by the parameters of pressure treatment, post heat and thermomechanical treatment. However, with increase in alloy strength its ductility is, as a rule, decreased, that is an important drawback of the material of structures, operating under vibration, repeated statics, bending, shock loads. Therefore, during recently the more and more attention is paid to the improvement of ($\alpha + \beta$)-titanium alloys, optimizing of parameters of ingots deformation in manufacture of semi-products from them and conditions of hardening heat treatment.

Physical-chemical and thermophysical peculiarities of titanium and its alloys require comprehensive approach to the processes of their deforming. This is stipulated by the following factors. The reduced heat-conductivity of titanium alloys leads to temperature drops in section of ingots and billets during their heating, occurrence of high internal stresses, and in separate cases to the initiation of cracks. This requires to limit the rate of heating, in particular of ingots and billets of large sizes. Significant temperature drops may also occur in cooling of billets. For example, the rapid chilling of acute angles, thin elements of sections of billets hinders greatly to provide uniform deformation, leads to the formation of cracks and other defects.

Low heat conductivity of titanium and its alloys has a negative effect directly on the process of hot deformation. Due to heat effect of deformation at

high degrees of reduction, a significant metal overheating in zones of intensive deformation, deterioration of its structure and properties are observed. This is clearly manifested under unfavourable conditions of forging (upsetting) of billets, shape rolling of rods and deformational processes. It is possible to prevent the formation of these zones with unfavourable structure only by a proper selection of scheme, degree, rate and initial temperature of metal deformation.

At temperatures of heating, required for hot deformation or heat treatment, titanium alloys interact actively with oxygen, nitrogen, hydrogen and other gases of atmosphere, their diffusion inside the metal is occurred, the surface gas-saturated layers are formed. They are characterized by a high hardness and low ductility, promote the appearance of tears in deformation, deterioration of quality of surface of semi-products. Effective method of prevention of formation of gas-saturated layers is the application of protective coatings, preventing metal from absorption of gases not only in heating, but also in the process of deformation itself and subsequent cooling.

Heating of ($\alpha + \beta$)-alloys of titanium up to the temperatures corresponding to single-phase β -region, is accompanied by a significant increase in ductility, in particular in deformation of cast metal, and by reduction in resistance to deformation. However, the deformation only in β -region does not make it possible to produce the metal structure providing its high service properties. Optimum structure can be produced in deformation in ($\alpha + \beta$)-region, however, the metal ductility, in particular in cast state, in this interval of temperatures is much lower, while the deformation resistance is higher. In practice of industrial production this contradiction is overcome in realization of deformation in two stages: deformation of ingots in β -region and next deformation in ($\alpha + \beta$)-region. Degree of deformation at these stages is selected coming from the required total change in shape of metal in manufacture of semi-product. Minimum value of de-

**Table 1.** Conditions of deformation and heating in forging of experimental titanium alloy T-110

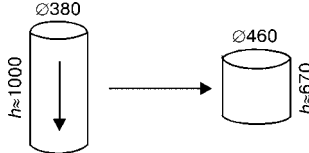

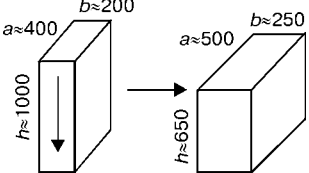
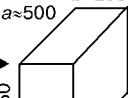
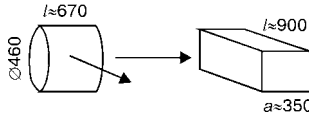
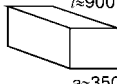
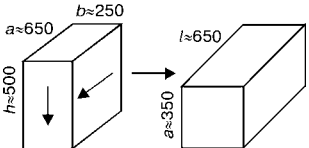

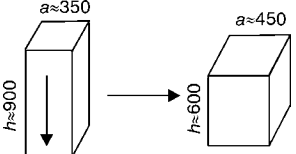
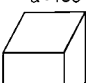
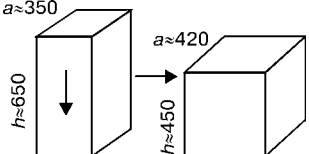
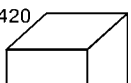
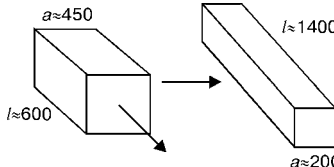
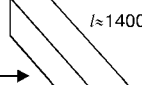
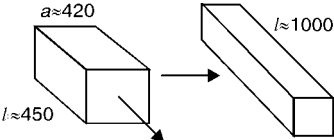
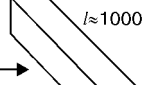
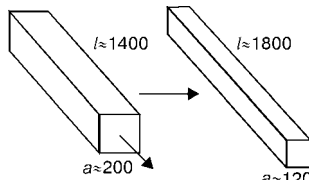
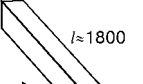
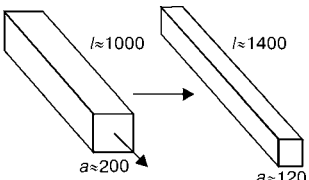
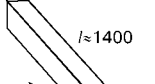
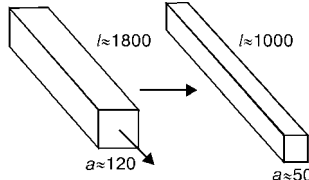
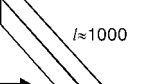
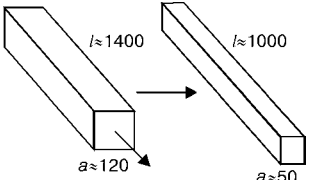
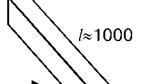
Operation	Ingot		Slab ingot		Duration of operation, h
	Scheme 1		Scheme 2		
	A	B	A	B	
Heating	1180 °C	1050 °C	1180 °C	1050 °C	3
Upsetting for 1/3 of height					0.5
Change in axis and drawing for square					
Change in axis and upsetting for 1/3 of height					
Preheating of billet	920 °C	950 °C	920 °C	950 °C	0.5
Drawing for 200 mm square and cutting for measured billets					0.5
Preheating of billets	900 °C	920 °C	900 °C	920 °C	0.5
Drawing for 120 mm square and cutting for measured billets					0.5
Preheating of billets	850 °C	860 °C	850 °C	860 °C	1
Drawing for 50 mm square and cutting for measured billets					0.5

Table 2. Mechanical properties of alloy T-110 after forging

Scheme of forging	Type of semi-product	σ_t , MPa	δ , %	ψ , %	KCU_2 , J/cm ²
1-A	Rod	1131–1162	11.6–16.0	40.8–50.4	39–44
	Forging	1119–1153	14.0–18.0	47.3–53.0	38–49
1-B	Forging	1063–1083	14.0–16.0	34.4–47.3	35–50

formation degree at the first stage is defined by the need in producing fine-grain macrostructure, at the second stage — in producing optimum microstructure. As regards to different types of semi-products this principle is realized in various variants of values of degree and temperature of deformation [1].

The aim of the present work was to establish the parameters of deformation in forging and conditions of post heat treatment, providing the required level of mechanical properties of titanium alloy T-110.

**Table 3.** Mechanical properties of forged rods after heat treatment

Condition of heat treatment	σ_t , MPa	δ , %	ψ , %	KCU, J/cm ²
1	1100–1150	9.6–13.5	34.4–49.8	40–44
2	1180–1240	9.6–16.9	41.6–53.7	40–56
3	1130–1195	13.1–20.8	48.0–58.2	49–57

Table 4. Mechanical properties of semi-products of alloy VT22

Type of semi-product	σ_t , MPa	δ , %	ψ , %	KCU, J/cm ²
Rod of 42 mm diameter	1180	16.5–17.0	56.0–58.9	40
Rod of 70 mm diameter	1196–1198	12.0–16.0	35.2–40.9	48–53
Rod of 120 mm diameter	1200–1210	4.6–5.4	16.0–17.1	28–29
	1240	10.0–12.0	28.6–32.2	21–28

Procedure of experiment. As initial cast billets of alloy T-110, the ingots-slabs of 400×200×1000 mm size, and also round ingots of 380 mm diameter and 1000 mm length were used. Ingot were melted (double remelting) in electron beam installation with an intermediate crucible of the UE-121 type at R&P Center «Titan» of the E. O. Paton Electric Welding Institute. Temperature of polymorphous $\beta \leftrightarrow (\alpha + \beta)$ transformation of cast metal was determined to make a proper selection of temperature conditions of deforming and conditions of post heat treatment by the method of hardening. It was 905 °C for both ingots. As an example, we shall give the chemical composition of a round ingot of alloy T-110, wt. %: Ti — base, Al — 5.35, Mo — 1.10, V — 1.37, Nb — 5.04, Fe — 1.60, Zr — 0.35, O₂ — 0.009, N₂ — 0.02, H₂ — 0.003.

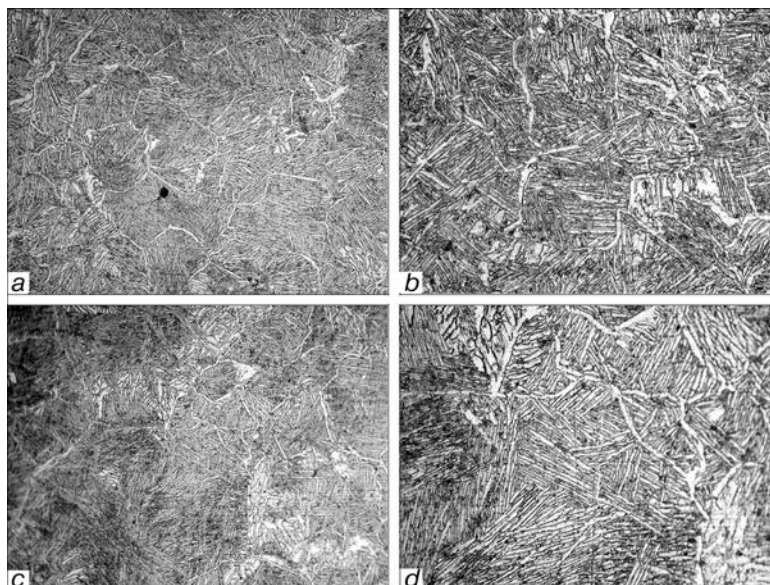
The round ingot and ingot-slab were subjected to forging for 120 mm diameter rod. Then this rod was forged again for square rod with 50 mm side and subjected to heat treatment.

It was required in the conditions of this work to produce the following mechanical properties: $\sigma_t \geq 1100$ MPa, KCU ≥ 40 J/cm², i.e. it was necessary to provide high ductility at simultaneous preserving of high level of strength. These boundary conditions are typical in the selection of materials for highly-loaded elements of aircraft structures, in particular chassis.

Deformation by forging was performed by two schemes (Table 1) for ingot and slab. Parameter, which was changed in the process of forging, was temperature. Here, the obligatory condition was to perform deformation at next for the last intermediate and final sizes at temperature below the temperature of $\beta \rightarrow (\alpha + \beta)$ transformation for not less than by 50 °C.

To define the optimum temperature conditions of forging the pre-forging of small templets of 20 kg mass was made using all operations given in Table 1. Templets were reformed for a rod and forgings and then subjected to heat treatment using one common condition: annealing at temperature 780 °C, 2 h holding, air cooling at 5–8 °C/min rate. Results of testing these forgings and rod for static tension and impact strength are given in Table 2.

It is seen from Table data that scheme of forging 1-A gives more stable results and provides better combination of mechanical characteristics than forging by scheme 1-B. This is, probably, stipulated by the fact that in the first layer at the first transition of forging the better processing of initial cast structure takes place in the process of deformation at the higher temperature. Analysis of microstructure of forged metal confirms this assumption (Figure 1). Type of grain of microstructure corresponds to 4–6 type of 9-type scale of VIAM. However, after forging by scheme

**Figure 1.** Microstructure of alloy T-110 after forging by schemes 1-A (a, b) and 1-B (c, d): a, c — ×200; b, d — ×400

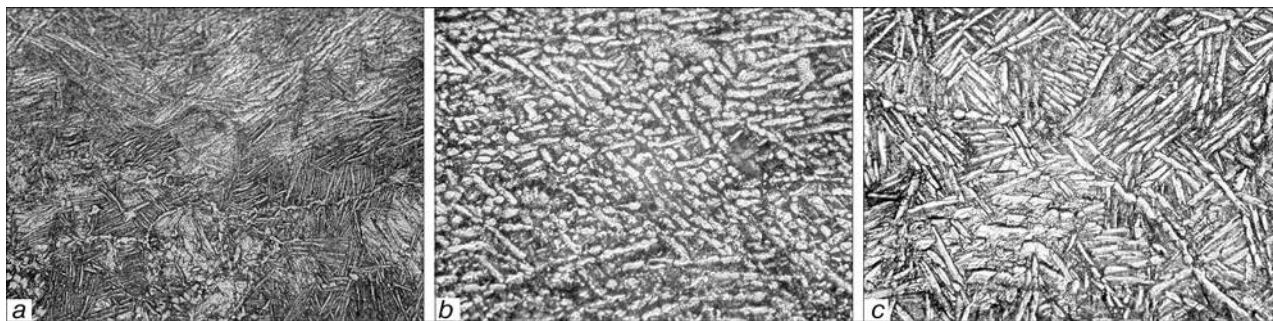


Figure 2. Microstructure of forged rods of alloy T-110 after heat treatment according to conditions 1 (a), 2 (b) and 3 (c) ($\times 500$)

1-B, due to insufficient processing of structure of cast metal, the great difference in grains is observed in its microstructure.

From results of these preliminary experiments the forging of a round ingot and ingot-slag was made by scheme 1-A. Forged rods were subjected to heat treatment using following conditions:

1. Heating up to 750 °C, 1 h holding, air cooling;
2. Heating up to 870 °C, 0.5 h holding, furnace cooling to 800 °C, 0.5 h holding, furnace cooling to 750 °C, 1 h holding, air cooling; heating up to 380 °C, 8 h holding, air cooling; heating up to 570 °C, 2 h holding, air cooling;

3. Vacuum annealing at 850 °C, 1 h holding.

Conditions of heat treatment of alloy T-110 were selected earlier [2]. Mechanical properties of forged rods after heat treatment are given in Table 3. For comparison, Table 4 gives typical properties of semi-products of alloy VT22 after heat treatment.

Microstructure of rods after heat treatment is presented in Figure 2.

Examinations of structure showed that macrostructure of rods corresponds to 4–5 marks in 10-mark scale of macrostructures, while the type of grain of microstructure corresponds to 3–4 type in 9-type scale of microstructures. Microstructure of metal of rods after heat treatment according to conditions 2 and 3 has a globular morphology of α -precipitations inside the grains. Moreover, the globularization of precipitations of α -phase occurs in more complete volume in the process of treatment by stages. In parallel with globular precipitations the laminar precipitations are also present in structure. This type of structure is referred to bimodal. In vacuum treatment (condition 3) the amount of the globular precipitations is

smaller, and the laminar precipitations form the structure in the form of a basket weaving.

CONCLUSIONS

1. Parameters of forging of experimental titanium alloy T-110 have been selected. It was established that the preliminary forging in β -region should be performed at temperature of not lower than 1100 °C to provide the more complete processing of cast structure in the process of deformation.

2. Forged rods of as-annealed alloy T-110 have the level of strength of not less than 1100 MPa, being not inferior by this characteristic to alloy VT22, and superior to it by the level of ductility and impact strength.

3. Vacuum annealing (condition 3) makes it possible to produce the highest ductility and impact strength of alloy T-110. Multi-stage heat treatment (condition 2) of alloy T-110 provides the best combination of characteristics of strength and ductility. Annealing at temperature 750 °C (condition 1) is simplest by a type of heat treatment and provides also minimum required level of mechanical properties.

4. Macro- and microstructures of produced forged rods correspond to 4–5 marks of 10-mark scale of macrostructures and 3–4 type of 9-type scale of microstructures, i.e. correspond to the requirements specified to the parameters of structure of this type of semi-products.

1. Aleksandrov, V.K., Anoshkin, N.F., Bocharov, A.G. et al. (1979) *Semi-finished products from titanium alloys*. Moscow: Metallurgiya.
2. Antonyuk, S.L., Molyar, A.G., Kalinyuk, A.N. et al. (2003) Titanium alloys for aircraft industry of Ukraine. *Advances in Electrometallurgy*, 1, 10–14.



DISTRIBUTION OF NITROGEN BETWEEN METAL AND SLAG

B.P. BURYLYOV and L.P. MOJSOV

NIIMontazh Company, Krasnodar, Russia

Calculation equations are given for determination of nitrogen solubility in metal and slag melts. Thermodynamic properties of slag melts of $\text{CaO-SiO}_2\text{-Al}_2\text{O}_3$ system are considered. Using the given equations the values of nitrogen solubility in metal and slag, and also the coefficient of nitrogen distribution between the slag and metal are established.

Keywords: nitrogen solubility, coefficient of distribution, activity of components, composition of metal and slag

At present, there are many experimental data about the solubility of nitrogen in metal phase and little data about its solubility in slags. However, it is necessary to have data about its solubility in both phases to determine the coefficients of nitrogen distribution.

In the present works calculation equations of nitrogen solubility in metal and slag are given and the effect of different factors on change in content of nitrogen in these melts is defined.

Nitrogen solubility in Fe-base metal was studied earlier in [1]. The nitrogen content in different compositions of Fe-C-Si-P melt can be determined from equation

$$\lg [\% \text{ N}] = -\frac{700}{T} - 0.98 + \frac{1}{2} \lg P_{\text{N}_2} - \frac{2.0x_{\text{Si}}}{x_{\text{Fe}}} - \frac{1.75x_{\text{C}}}{x_{\text{Fe}}} - \frac{1.6x_{\text{P}}}{x_{\text{Fe}}} + \lg (2x_{\text{Fe}} - 1), \quad (1)$$

where P_{N_2} is the partial pressure of nitrogen in gas phase; x is the atomic fraction of components; T is the absolute temperature.

To have a complete characteristic of nitrogen behaviour in metal, it is important to know its solubility in slags. Equations are derived on the basis of theory of non-metals, dissolved in mixed solvents [2]. With account for the concentration relationship of energy of interaction the coefficient of activity f_3 of substance 3 in the solution of components 1 and 2 is determined by equation

$$RT \ln f_3 = \frac{2x_3}{x_1 + x_2} \varphi_{33}^{(01)} + \frac{2x_2}{x_1 + x_2} \varphi_{33}^{(2)} - \frac{x_1 x_2}{x_1 + x_2} \varphi_{33}^{(1)} - RT \ln (x_1 + x_2 - x_3), \quad (2)$$

where $\varphi_{33}^{(01)}$, $\varphi_{33}^{(2)}$ and $\varphi_{33}^{(1)}$ is the energy of interaction between particles of the substance being dissolved, in a pure solvent 1 and at adding of component 2, respectively;

tively; $\frac{x_1 x_2}{x_1 + x_2} \varphi_{33}^{(1)} = \Delta G^{\text{exc}}$ is the excessive molar energy of Gibbs for the solution of components 1 and 2.

If the solution is saturated by a component 3 and is in the equilibrium with a pure substance 3, having activity, equal to unity, then

$$\ln x_3 = -\ln f_3, \quad (3)$$

and from expressions (2) and (3) we shall find solubility:

$$RT \ln x_3 = -\frac{2x_3}{x_1 + x_2} \varphi_{33}^{(01)} - \frac{2x_2}{x_1 + x_2} \varphi_{33}^{(2)} + \frac{\Delta G^{\text{exc}}}{x_1 + x_2} + RT \ln (x_1 + x_2 - x_3). \quad (4)$$

Substituting $x_2 = 0$ or $x_1 = 0$, we shall obtain solubility of substance 3 in pure components 1 and 2:

$$x_3^{(1)} = (1 - 2x_3) \exp \left(-\frac{2x_3}{1 - x_3} \frac{\varphi_{33}^{(01)}}{RT} \right); \quad (5)$$

$$x_3^{(2)} = (1 - 2x_3) \exp \left(-\frac{2x_3}{1 - x_3} \frac{\varphi_{33}^{(01)}}{RT} - \frac{2\varphi_{33}^{(2)}}{RT} \right). \quad (6)$$

Then it follows from expressions (4)–(6) that

$$RT \ln x_3 = \frac{x_1}{1 - x_3} RT \ln x_3^{(1)} + \frac{x_2}{1 - x_3} RT \ln x_3^{(2)} + \frac{\Delta G^{\text{exc}}}{1 - x_3}. \quad (7)$$

At a small amount of dissolved substance 3 the value of a molar fraction in denominator can be neglected as compared with unity. The derived equations are easily summarized for systems, containing n components of solvent i , in which the substance j is dissolved:

$$RT \ln x_i = \sum_{i=1}^n x_i RT \ln x_j^{(i)} + \Delta G. \quad (8)$$

Thus, to calculate the nitrogen solubility in complex systems, it is necessary to know its solubility in



pure components, and also the thermodynamic properties of the solution formed by these components.

The excessive Gibbs energy of ternary solution is determined by the equation

$$\begin{aligned}\Delta G^{\text{exc}} &= RT (x_1 \ln f_1 + x_2 \ln f_2 + x_3 \ln f_3) = \\ &= RT \sum_{i=1}^n x_i \ln f_i,\end{aligned}\quad (9)$$

where f_i is the coefficient of activity of components i ; n is the number of solvent components.

It follows from expression (9) that it is necessary to know coefficients of activity of components for slags of CaO–SiO₂–Al₂O₃ system. Results of calculation for CaO–SiO₂ system are given in [3]. Activities in CaO–Al₂O₃ melts and in ternary CaO–SiO₂–Al₂O₃ system are determined experimentally by different methods, the review of which is given in [4].

To obtain interpolation formulae of concentration relationship of coefficients of activity of components in binary melts CaO–Al₂O₃ and SiO₂–Al₂O₃ the following expression is used:

$$RT \ln f_i = (1 - x_i)^{(2)} Q_{ij} + K, \quad (10)$$

where x_i is the ion fraction of component i ; Q_{ij} is the energy of shifting of components i and j ; K is the constant which depends on selection of standard state of component i .

Values Q_{ij} are given in [3–5]. From different experimental data, we shall obtain $Q_{13} = -200$ kJ/mol, $Q_{12} = -240$ kJ/mol and $Q_{23} = -160$ kJ/mol. In further calculations we shall use mean value $Q_{13} = -200$ kJ/mol.

Molar energy of Gibbs of ternary solution can be determined according to [3] by equation

$$\begin{aligned}G &= x_1 G_1 + x_2 G_2 + x_3 G_3 + \\ &+ RT (x_1 \ln x_1 + x_2 \ln x_2 + x_3 \ln x_3) + \\ &+ x_1 x_2 Q_{12} + x_1 x_3 Q_{13} + x_2 x_3 Q_{23} + q x_1 (3x_2 - 1)^2.\end{aligned}\quad (11)$$

From this expression, it is possible to obtain values of chemical potentials of solvent components

$$\mu_i = \frac{\partial G (x_1 + x_2 + x_3)}{\partial x_i}, \quad (12)$$

and as

$$\mu_i = G_i + RT \ln x_i + RT \ln f_i, \quad (13)$$

then the coefficients of activity of oxides of silicon (IV) and aluminium (III) are determined by equations:

$$\begin{aligned}RT \ln f_2 &= [Q_{11} + 6q (3x_2 - 1)] x_1 (1 - x_2) - \\ &- x_1 x_3 Q_{13} + x_3 (1 - x_2) Q_{23};\end{aligned}\quad (14)$$

$$\begin{aligned}RT \ln f_3 &= [-Q_{12} - 6q (3x_2 - 1)] x_1 x_2 + \\ &+ x_1 (1 - x_3) Q_{13} + x_2 (1 - x_3) Q_{23}.\end{aligned}\quad (15)$$

Value $Q_{23} = -70$ kJ/mol was determined from expression (14) with allowance for values $Q_{12} = -113$ kJ/mol, $q = 26.4$ kJ/mol and $Q_{13} = -200$ kJ/mol from experimental data of activity of silica in slags with a content of alumina up to 20 wt.% in the 1723–1823 K range of temperatures.

The obtained data Q_{ij} were checked by comparison of results of calculation by equations (14) and (15) with experimental data of measurements of activity of silicon oxide (IV) and aluminium oxide (III) in ternary solutions CaO–SiO₂–Al₂O₃ by EDS method at 1903 K.

Taking into account expressions (9) and (11) for excessive energy of Gibbs of ternary solution CaO–SiO₂–Al₂O₃ we shall obtain

$$\begin{aligned}\Delta G^{\text{exc}} &= -113x_1 x_2 - 200x_1 x_3 - \\ &- 70x_2 x_3 + 26.4x_1 (3x_2 - 1)^2.\end{aligned}\quad (16)$$

It was found from equations (8) and (16) with account for experimental data [6], that logarithm of solubility of nitrogen in hypothetic pure CaO, SiO₂ and Al₂O₃ is about 1.4, –0.3 and 1.7. These values are confirmed by experimental data about the nitrogen solubility in basic and acid slags. Usually, the nitrogen content in white slags of reduction period exceeds that of slags of oxidizing period in production of steel in arc electric furnaces.

The calculation equation (8) of nitrogen solubility in slags at 1773 K and $P_{N_2} = 0.92$ atm (93220 Pa) will take a form

$$\begin{aligned}\lg [\% N] &= 1.4_{\text{CaO}} - 0.5_{\text{SiO}_2} + \\ &+ 1.7_{\text{Al}_2\text{O}_3} + \frac{\Delta G^{\text{exc}}}{19.15 T}.\end{aligned}\quad (17)$$

The comparison of results of calculation with experimental data [6] is shown in the Table. Error in determination of nitrogen solubility in slags of different compositions is on average about 20 % from a measured value, that is somewhat higher than limits of accuracy of experimental determinations. A large scattering in the next to the last values of experimental and calculated content of nitrogen is, probably, explained by the presence of a large number of calcium carbide in this slag, which increases nitrogen solubility. In addition, it follows from the Table that the calculated values of nitrogen solubility are lower for highly-basic slags, having CaC₂, which was not taken into account in experiments [6] and calculation formula (17). It makes grounds to consider that expression (17) will give good results in calculation of nitrogen solubility in different slags of welding production.

The calculations of coefficients of nitrogen distribution between the slag and metal phases showed that nitrogen solubility in slags does not depend on metal grade, but depends on slag basicity. The limiting content of nitrogen in a metal phase does not depend on slag composition, but differs significantly depending



Nitrogen solubility in slags of CaO–SiO₂–Al₂O₃ system ($P_{N_2} = 0.92$ atm (93220 Pa), $T = 1773$ K)

Chemical composition						Nitrogen content, wt. %	
Mass percents			Ion fractions			Experimental	Calculated
CaO	SiO ₂	Al ₂ O ₃	x_{Ca}	x_{Si}	x_{Al}		
23	57	20	0.244	0.542	0.224	0.234	0.303
30	50	20	0.304	0.473	0.223	0.153	0.208
40	40	20	0.403	0.376	0.221	0.187	0.175
50	30	20	0.500	0.280	0.220	0.210	0.366
60	20	20	0.597	0.185	0.118	0.250	0.232
40	60	–	0.417	0.583	–	0.407	0.460
40	50	5	0.435	0.505	0.060	0.312	0.345
40	50	10	0.410	0.477	0.113	0.266	0.234
40	35	25	0.400	0.326	0.274	0.442	0.159
55	40	5	0.562	0.382	0.056	0.544	0.427
50	40	10	0.508	0.380	0.112	0.435	0.277
48	40	12	0.488	0.378	0.134	0.324	0.246
30	40	30	0.269	0.335	0.296	0.203	0.305
35	39	36	0.315	0.329	0.356	0.306	0.174
50	–	50	0.476	–	0.524	1.460	0.004
50	50	–	0.518	0.482	–	0.462	0.509

on metal composition, that is caused by different effect of alloying elements on nitrogen solubility. It is known [1] that manganese and chromium increase solubility, while carbon, silicon, phosphorus and nickel decrease it. Therefore, the final content of nitrogen is determined by amount of alloying elements, temperature and partial pressure of nitrogen in gas phase.

Coefficient of nitrogen distribution between slag and metal

$$L = \frac{(\% N)}{[\% N]} \quad (18)$$

is determined, first of all, by the composition of contacting metal and slag phases.

Coefficient of distribution can be determined by knowing the value of coefficients of activity of nitrogen in slag and metal:

$$L = \frac{a_N^{sl}}{a_N^{met}} = \frac{(\% N) f_N^{sl}}{[\% N] f_N^{met}} \quad (19)$$

Coefficient of activity of nitrogen in metal phase can be calculated by equations, similar to those given in [1], and coefficient of nitrogen activity of nitrogen of a wide range of compositions at $P_{N_2} = 1$ atm (101325 Pa) can be determined by expression

$$f_N = 0.48 - \lg \frac{x_{Ca} + x_{Mg}}{x_{Si}} - \lg K_N. \quad (20)$$

If to assume the nitrogen state in slag with basicity, equal to unity, as a standard state, then in this case $f_N^{sl} = 1$ and $\lg K = 0.48$.

Taking into account these expressions the coefficient of nitrogen distribution between slag and metal from equation (19) will be $L = 8$. It depends only on temperature and is not changed with a change in composition of metal and slag in the wide range of concentrations. The mentioned problem of saturation of deposited metal with nitrogen from a slag melt is actual and its solution will make it possible to control the nitrogen amount in metal by changing the slag melt composition.

1. Burylyov, B.P. (1964) On gas saturation of cast iron. *Izv. AN SSSR, Metallurgiya i Gornoe Delo*, **3**, 118–121.
2. Burylyov, B.P. (1965) To theory of non-metallic solutions in mixed solvents. *Zhurnal Fiz. Khimii*, **5**, 1157–1163.
3. Kozheurov, V.A. (1955) *Thermodynamics of metallurgical slags*. Sverdlovsk: Metallurgizdat.
4. Burylyov, B.P., Sryvalin, I.T., Korpachyov, V.G. (1986) *Application of approximated methods for calculation of thermodynamical properties of oxide and metallic systems*. Krasnodar.
5. Mojsov, L.P., Burylyov, B.P. (1993) *Physical-chemical bases of creation of new welding consumables*. Rostov-on-Don: RGU.
6. Kamyshov, V.M., Esin, O.A., Chuchmaryov, S.N. (1964) Solubility of nitrogen in iron-free slags. *Izv. Vuzov, Chyorn. Metallurgiya*, **7**, 24–28.



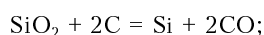
THERMODYNAMIC MODEL OF PROCESS OF MELTING FERROSILICIUM IN HIGH-CAPACITY ORE THERMAL ELECTRIC FURNACES

M.I. GASIK, M.M. GASIK, O.I. POLYAKOV and V.L. ZUBOV
National Metallurgical Academy of Ukraine, Dnepropetrovsk, Ukraine

Thermodynamic model of process of producing ferrosilicium (silicon alloys) has been offered from the results of computer modelling equilibriums in Si-O-C-(H₂, H₂O) system, taking into account the effect of hydrogen and moisture in gas phase of high-temperature reaction zone of ore thermal electric furnace on thermodynamic stability of gas and condensed phases in carbon reduction of quartzite.

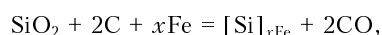
Keywords: computer modelling, thermodynamic equilibrium, silicon, reduction, quartzite, hydrogen, moisture, oxidation-reduction potential, stability of gas phase, non-efficient consumption of carbon, moisture of carbon reduction

Thermodynamic models allowing prediction of parameters of processes of high-temperature carbon thermal reduction of silicon from quartzite in ore thermal electric furnaces in production of crystalline silicon of Kr00–Kr3 grades with Si ≥ 99–96 % mass fraction and ferrosilicium of the widest assortment of FS20–FS92 grades with 19 ≤ Si ≤ 94 % mass fraction, are a modern physical-chemical basis for the development of industrial technologies for production of silicon alloys (including production of ferrosilicochromium, silicoaluminium, etc.) [1]. These models are based on the analysis of equilibrium of reactions in Si-O-C (crystalline silicon) and Fe-Si-O-C (ferrosilicium) and, in more general case, Me-Si-O-C (Cr-Si-O-C – ferrosilicochromium; Al-Si-O-C – silicoaluminium, etc.) systems. Schematically, the process of producing crystalline silicon can be described by reaction



$$K_{\text{Si}} = P_{\text{CO}}^2 \text{ and } \Delta G_{\text{Si}}^0 = 697390 - 359.07T \text{ [J/mol]},$$

where K is the constant of equilibrium; ΔG_{Si}^0 is the standard change in Gibbs energy; and the process of producing ferrosilicium by reaction



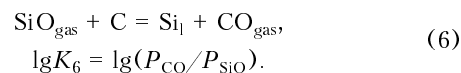
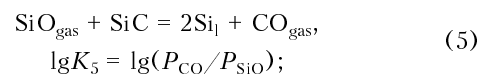
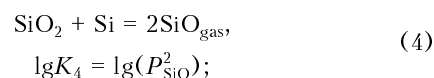
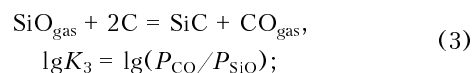
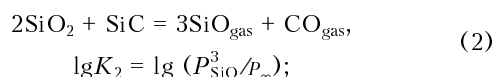
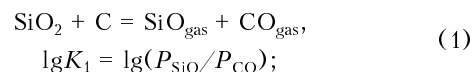
where x is the stoichiometric coefficient;

$$K_{\text{Si}} = a_{\text{Si}} P_{\text{CO}}^2,$$

where a_{Si} is the activity of silicon in solution Fe-Si-C_{sat}, saturated with carbon. The change in Gibbs energy of the last reaction at constant temperature and pressure is determined by the activity of silicon in alloy, which is in its term, is the function of silicon concentration in ferrosilicium.

Processes of carbon reduction of silica are proceeding with participation of two intermediate compounds, such as gaseous monoxide of silicon SiO_{gas} and hard silicon carbide SiC, which is thermally stable up to temperature (2818 ± 40) K, and at the higher temperature it is decomposed into gaseous silicon Si_{gas} and hard graphite.

In accordance with a rule of Gibbs phases the Si-O-C system with two external parameters (variable temperature and constant pressure), in the presence of four condensed phases (SiO₂, C, SiC and Si) and two-component (SiO_{gas}, CO) of gas phase is described by the system of six chemical reactions:



Originally, in works of I. Ryabchikov [2] and N. Tolstoguzov [3] the phase diagram of condensed phases in coordinates $\lg(P_{\text{SiO}}/P_{\text{CO}}) - 1/T$ was plotted on the basis of a thermodynamic analysis of the mentioned reactions. In later publications of some authors, including new thermodynamic data and algorithms of calculations, its separate structural elements were clarified (diagram in Figure 1 was plotted by us using data of [4]).



V. Mindin and S. Mazmishvili [5] analyzed the Si–O–C system on the basis of minimizing the Gibbs energy of closed system:

$$\Delta G_{\text{total}} = \sum_1^n x_j \left[\Delta G_j^0 + RT \ln \frac{P_{x_j}}{\sum_1^n x_j} \right] + \sum_{n+1}^{n+k} \Delta G_j^0 x_j,$$

where n is the number of gaseous components; k is the number of condensed phases which are taken into account at this stage of calculation; R is the universal gas constant; P is the pressure of gas phase; x_j is the amount of moles of the j -th component; ΔG_j^0 is the standard change in Gibbs energy of the j -th component. For the system, closed by mass (amount of moles), the following condition is kept:

$$\sum_{j=1}^{n+k} a_{ij} x_j = b_i, \quad i = 1-m,$$

where a_{ij} is the number of atoms of i sort in the j -th component; b_i is the total amount of atoms of i sort in the system; m is the amount of sorts of atoms in the system.

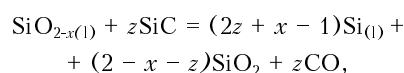
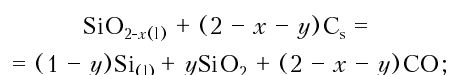
In calculations the following components were taken into account: gaseous (condition of ideal gas) — O_1 ; O_2 ; O_3 ; C_1 ; C_2 ; C_3 ; CO ; CO_2 ; Si ; Si_2 ; SiO ; SiO_2 ; SiC_2 ; Si_2C ; and condensed (individual pure substances, not forming solutions) — C ; Si ; SiO_2 ; SiC . The calculations in [5] were made in the interval of temperatures 1700–2900 K at pressure 10.1 MPa and molar ratio $N_C/N_{Si} = 1.0, 1.5, 2.0, 2.5$ and 3.0 . Results are given as change in amount of components of gas phase and condensed phases in coordinates x_j-N_C/N_{Si} at different temperatures (with 200 K pitch), and also in the form of diagram of regions of stability of condensed phases in coordinates $N_C/N_{Si}-T$.

Similar method was used by authors of [6] for calculation of silica interaction with carbon at temperatures 2000–3000 K, pressure 0.1 MPa and molar ratio C/SiO_2 from 0.8 to 2.4. In this work the effect of temperature on equilibrium of content of compounds (gaseous and condensed) is shown and regions of stability of condensed phases in coordinates $N_C/N_{SiO_2}-T$ are presented.

I. Kulikov [7] has developed the method of thermodynamic analysis of Si–O–C system, which is based on reactions of atomization (dissociation of individual substances into constituents of their atoms being in the condition of ideal gas). According to this method, the partial pressure of gas phase constituents at different temperatures is determined by values of energy of atomization. As a condition of a condensed phase stability, the exceeding of a partial pressure of vaporous component P_i over the pressure of its saturated vapour $P_{i \text{ sat}}$ at the preset temperature $T_i \geq T_{i \text{ sat}}$ is taken.

In the course of thermodynamic investigations the probable mechanisms of silica reduction with carbon in melting of ferrosilicium and crystalline silicon were studied in separate works. The balance method of thermodynamic analysis, directed to the study of a supposed mechanism of carbon thermal reduction processes at separate stages of producing ferrosilicium and silicon in ore thermal electric furnaces was developed by V. Berdnikov [8]. Model, suggested by Yu. Ponomarenko [9], is based on the analysis of the most energy-consuming so-called chemical boiling of possible processes proceeding in the pool of ferrosilicium (or silicon) electric furnace. It is supposed that this process stabilizes the temperature of the thermodynamic system at the level defined by an equality of pressure formed in a local volume of gas (vapour) and the external pressure.

N. Yakushevich and G. Galevsky generalized and analyzed in [10] the thermochemical and thermokinetic models of carbon reduction of silica (quartzite). According to [10], one of major features of interaction of elements in Si–O–C and Fe–Si–O–C systems is the «removal» of oxygen from the lattice of quartz or cristobalite, i.e. polymorphous modifications of silica, with the formation of non-stoichiometric phase SiO_{2-x} , scarce in oxygen (here x — index of non-stoichiometry, i.e. number of vacancies for two atoms of oxygen), the temperature of this phase transition into liquid state is ≈ 1743 K. In accordance with this hypothesis, the liquid silica (ferrosilicium) is formed in local zones of silica–coke contact in the presence of SiC and Si_{vap} as a result of interaction of melt $SiO_{2-x(l)}$ with carbon of a reducing agent and silicon carbide by reactions



where y is the share of forming SiO_2 ; z is the share of SiC , coming into reaction.

In all the considered models and schemes the equilibrium gas phase is presented by two components, such as gaseous monoxide of silicon SiO_{gas} and monoxide of carbon CO . The validity of this representation was convincingly proved in [1–11]. At the same time, in our publication [12] the idea, suggested by M.I. Gasik, about the effect of hydrogen (and nitrogen) of gas phase of ore thermal furnace, melting crystalline silicon and ferrosilicium with different content of silicon, that is also applicable for silicon alloys of the wide range, was widely spread. To forestall events, it should be noted that the account for hydrogen contained in gas phase of Si–O–C–(H) system leads to shifting of equilibrium so that the temperature of stable existence of silicon melt (or Fe–Si) is noticeably reduced. This can explain the available practical (industrial) data (temperature at tapping



and silicon content in alloy) and also the relatively high concentration of hydrogen in alloys leading to porosity of ferrosilicium ingots. The recent observation, which was, unfortunately, not taken into attention by the former developers of thermodynamic models of carbon thermal reduction of silica in the conditions of a real process of production of silicon and ferrosilicium (silicon alloys), became the basis of the suggested working hypothesis.

At the same time, a number of experimental works, devoted to the determination of solubility of molecular hydrogen in Fe-Si alloys, containing 0–100 % Si, is known. Temperature relationships of hydrogen solubility in liquid and solid silicon at 1523–1683 K, from data of T. Kostina and B. Baum [13], are described by equations

$$\lg K_{\text{H}}^{\text{Si}} = -5780/T - 0.726; \quad \lg K_{\text{H}}^{\text{Si}} = -12700/T + 3.97.$$

In [14] the temperature relationship of solubility of molecular hydrogen in pure silicon is presented by equation

$$\lg [\% \text{H}]_{\text{Si}} = 0.0447 - 5312/T.$$

We did not manage to find the published experimental data about the hydrogen solubility in crystalline silicon of industrial melting.

Solubility of hydrogen in melts Fe-Si has an extremal nature with minimum of $\approx 10\text{--}15 \text{ cm}^3/100 \text{ g}$ at 50–55 at.% Si [13]. Authors of [14] give the equation describing the temperature relationship of hydrogen solubility in model alloys Fe-Si containing 75 wt.% Si:

$$\lg [\% \text{H}]_{75\% \text{ Si}} = -0.6638 - 4526/T.$$

Works [11–19] are devoted to the determination of hydrogen content in commercial ferrosilicium. Hydrogen concentration in quick-hardened samples of 75 % melt of ferrosilicium was, from the data of P. Geld and V. Yavojsky [15], 26.54, 22.40 and $21.20 \text{ cm}^3/100 \text{ g}$ at the tap-hole, in ladle and ingots, respectively.

It is noted in work of Ya. Shchedrovitsky [11] (with reference to data of B. Baum) that hydrogen concentration in melt of ferrosilicium at tapping from furnace reaches $30\text{--}40 \text{ cm}^3/100 \text{ g}$ for ferrosilicium of FS65 grade and $70 \text{ cm}^3/100 \text{ g}$ for FS75 grade, that 3–6 times exceeds its concentration in ingots. In [16] the content of hydrogen in 75 % melt of ferrosilicium was determined. Results showed that at the beginning, middle and end of tapping from the furnace (on jet) the hydrogen concentration in ferrosilicium alloy was 22.5, 5.0 and $32.5 \text{ cm}^3/100 \text{ g}$, respectively, and at the beginning, middle and end of pouring (after holding in ladle) it was 17.5, 16.0 and $15.2 \text{ cm}^3/100 \text{ g}$, respectively.

The given data, in spite, sometimes, of significant difference in numerical values, showed that hydrogen content in commercial ferrosilicium exceeds its solu-

bility in alloys Fe-Si at $P_{\text{H}_2} = 0.1 \text{ MPa}$ and $T = 1800\text{--}2100 \text{ K}$. This can be caused by the fact that hydrogen in the zone of arc of the ore thermal furnace exists not only in a molecular, but also in atomic form. The probability of formation of gaseous ions of hydrogen in electric arc plasma is also high. Thus, in plasma-arc melting a zone of absorption, in which the chemical potential of gas should be higher than chemical potential of gas dissolved in metal, is formed at the surface of metal pool contacting the arc (plasma flame), as the gas absorption by metal is occurred. At temperature of $\approx 6000 \text{ K}$ the hydrogen plasma is almost completely atomized, unlike the nitrogen plasma, for which at the same conditions $P_{\text{N}_2} \geq 50 \text{ kPa}$ and $P_{\text{N}_2} > P_{\text{N}}$ [17]. The pool surface, not covered with a plasma flame, represents a zone of desorption, in which a partial metal degassing is occurred. Ratio of areas of surfaces of zones of desorption and absorption defines, finally, the exceeding of concentration of dissolved gases over the solubility calculated in assumption of satisfiability of Sieverts law.

As the practice showed, the hydrogen content in plasma-arc melting of metals can several times exceed its standard solubility $[\text{H}] = K_{\text{H}_2} P_{\text{H}_2}^{1/2}$, that is outlined, for example, in [18], the authors of which associate it with increase in activity of gas particles in electric arc column. Similar phenomena should take place, undoubtedly, in furnaces for melting crystalline silicon and ferrosilicium (silicon alloys), all the more that area of zone of metal contact with electric arc is 30–80 % of the metal pool area depending on silicon content (lower boundary corresponds to ferrosilicium of FS25 grade, the upper boundary — to FS90 grade).

Calculations of equilibrium in the widened system Si-O-C-(H) were performed taking into account the data of P. Geld and O. Esin [19], who analyzed the thermodynamics of reaction $\text{SiO}_2 + 2\text{H}_2 = \text{Si} + 2\text{H}_2\text{O}$ and showed that molecular hydrogen is much weaker reducing agent relative to SiO_2 than even CO. Calculations of equilibrium in systems Si-O-C-(H₂O) and Si-O-C-(H) at temperature 1500–3000 K, made by us using software HSL Chemistry 5.0 (ESM Software, Outokumpu, Finland), and new thermodynamic data of [4] showed that ratio $\lg (P_{\text{H}_2\text{O}}/P_{\text{H}_2})$ is within the ranges of $-3.46\text{--}-4.46$ for the first system and $-2.86\text{--}-4.39$ for the second system. These data confirm the conclusions of work [9] about the fact that hydrogen in system Si-O-C-H can be considered as a reducing agent of silicon. Therefore, it was accepted that in a widened system Si-O-C-(H) hydrogen is an inert solvent, whose partial pressure is included as item into expression for total pressure of gas phase $P_{\Sigma} = P_{\text{SiO}} + P_{\text{CO}} + P_{\text{H}_2}$, though the hydrogen shows also a definite effect on electric resistance of gas phase in under-electrode space (arc discharge gap). Atomic hydrogen was not taken into account in calculations, as at the temperature $T \leq 3500 \text{ K}$, unlike the zone of effect of electric arcs, the ratio



$P_{\text{H}}/P_{\text{H}_2} \geq 1$, and it is such temperature at which the processes of reduction in the system considered are proceeding.

Thermodynamic data of [4], which are seemed to us as most reliable from all available data, are included into recommendations IUPAC and CODATA and used in national and foreign banks of thermodynamic data. Results of calculations $\Delta G_T^0 = \Delta H_T^0 - \Delta S_T^0 T$ of reactions (1)–(6) are approximated by linear equations $\Delta G_T^0 = \Delta H_T^0 - \Delta S_T^0 T$, that made it possible to simplify the mathematical model by linearizing the temperature relationships of logarithms of constants of equilibrium of reactions $\lg K = A/T + B$:

$$\lg K_{P(1)} = -33505/T + 16.45;$$

$$\lg K_{P(2)} = -70897/T + 32.86;$$

$$\lg K_{P(3)} = 3886/T + 0.089;$$

$$\lg K_{P(4)} = -31389/T + 14.57;$$

$$\lg K_{P(5)} = -8119/T + 3.656;$$

$$\lg K_{P(6)} = -2116/T + 1.88.$$

The same as in [2, 3], the results of calculations of equilibrium are presented in the form of a diagram of stability of condensed phases in coordinates $\lg(P_{\text{SiO}}/P_{\text{CO}}) - 1/T$. Ratio $P_{\text{SiO}}/P_{\text{CO}}$ for reactions (3), (5) and (6) is determined directly from constants of equilibrium and for reaction (4) — from the equation

$$P_{\text{SiO}}/P_{\text{CO}} = \sqrt{K_4} / (P_{\Sigma} - P_{\text{H}_2} - K_4).$$

For reaction (1) $P_{\text{SiO}}/P_{\text{CO}}$ is determined by the solution of system of equations

$$K_1 = P_{\text{SiO}}/P_{\text{CO}};$$

$$P_{\text{Si}} + P_{\text{CO}} = P_{\Sigma} - P_{\text{H}_2},$$

which are reduced in a trivial way to a quadratic equation.

For reaction (2) the ratio $P_{\text{SiO}}/P_{\text{CO}}$ can be obtained from the system of equations

$$K_2 = P_{\text{SiO}}^3 P_{\text{CO}};$$

$$P_{\text{SiO}} + P_{\text{CO}} = P_{\Sigma} - P_{\text{H}_2},$$

i.e. as the solution of equation of the fourth degree.

In calculations, the partial pressure of gas-solvent of furnace gas atmosphere (H_2) was taken equal to $P_{\text{H}_2} = 0.3 \cdot 10^5$ Pa and $P_{\Sigma} = P_{\text{SiO}} + P_{\text{CO}} + P_{\text{H}_2} = 1.01325 \cdot 10^5$ Pa.

The obtained diagram of stability of condensed phases of system Si–O–C–(H) is presented in Figure 1 (solid lines). To make the degree of hydrogen effect in gas phase on position of lines and points (their shifting), corresponding to mono- and non-variant equilibriums of co-existing condensed phases, more descriptive and visualized, the diagram Si–O–C–(H) is combined with a diagram of «ideal» system Si–O–C (bold dashed lines), calculated using the

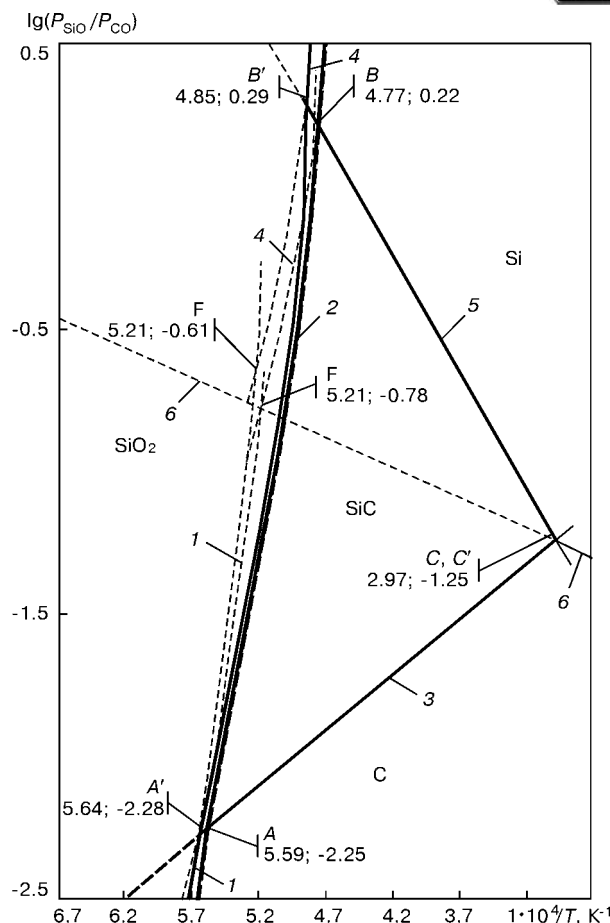


Figure 1. Diagram of stability of condensed phases in SiO–O–C–(H) system (designation of lines and points see in text; figures on curves are numbers of chemical reactions)

same thermodynamic data [4] (dashed lines for equations (1), (2) and (4), whose coordinates are shifted in hydrogen adding to the system). Solid lines in Figure 1 correspond to monovariant equilibrium: 1 — (SiO_2 ; C); 2 — (SiO_2 ; SiC); 3 — (C; SiC); 4 — (SiO_2 ; Si); 5 — (Si; SiC) and 6 — (Si; C). The mentioned points refer to non-variant equilibrium (designations with hatching are referred to system Si–O–C–(H), without hatching — to system Si–O–C); figures in points are their coordinates.

Points of non-variant equilibrium	A; A'	B; B'	C; C'
Co-existing components	(SiO ₂ ; C; SiC)	(SiO ₂ ; SiC; Si)	(SiC; C; Si)

Bivariant equilibrium, i.e. the regions of stability of condensed phases SiO_2 , Si, SiC, C, is designated with corresponding chemical formulae.

The data obtained prove that the presence of hydrogen in under-electrode gas cavities of pool of ore thermal furnace leads to widening the region of thermodynamic stability of silicon and silicon carbide. This is clearly manifested in construction of diagram in Figure 1: coordinates of point B — $T = 2096$ K and $P_{\text{SiO}}/P_{\text{CO}} = 1.66$; point B' — $T = 2062$ K and $P_{\text{SiO}}/P_{\text{CO}} = 1.95$. Coordinates of points A and A' are



also significantly differed. Coordinates of point *A* correspond to $T = 1790$ K and $P_{\text{SiO}}/P_{\text{CO}} = 0.0056$; point *A'* — $T = 1773$ K and $P_{\text{SiO}}/P_{\text{CO}} = 0.0052$.

Thus, it is shown that the observed high content of hydrogen in ferrosilicium is the consequence of significant partial pressure of hydrogen in under-electrode cavities, and this should be obligatory taken into account in thermodynamic analysis of reactions of carbon thermal reduction of silicon from silica. Though the molecular hydrogen does not participate directly in reduction reactions, its presence in system Si–O–C–(H) shifts the boundaries of region of thermodynamic stability of condensed phase of a purposeful component (silicon) in real conditions of ore thermal furnace in melting of silicon and ferrosilicium (or other silicon alloys) to the region of lower temperatures that improves thermodynamic conditions of their melting.

It should be noted that the high hydrogen content, observed in practice, in melt of ferrosilicium at tapping from furnace, which exceeds greatly its solubility, determined in accordance with Sieverts law, causes the need in physical-chemical grounding of the process of interaction of hydrogen from gas phase of high-temperature under-electrode cavity of electric arc discharge with a melt of ferrosilicium (silicon).

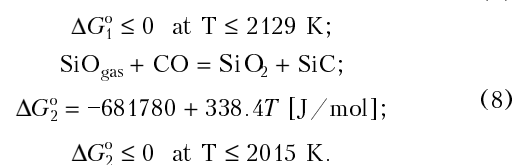
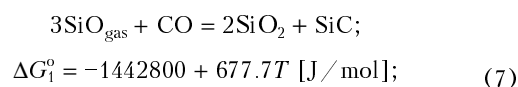
Another important factor, discussed in the present work, consists in the fact that, as will be shown below, the moisture, entered together with charge materials, plays a rather essential role in processes of electrothermal production of silicon ferroalloys based on carbon thermal reduction of silicon from silica. In this part of article we shall consider first the thermodynamic aspects of effect of water drops on equilibrium composition of gas and condensed phases of Si–O–C–H₂O system, and then we shall express our considerations concerning the sources of water enter into the electric furnace pool, moreover, into high-temperature ($T \geq 1773$ K) zones of reduction processes. This sequence of interpretation seems to us rational by the following reasons:

- high content of hydrogen in ferrosilicium is stipulated by the presence of hydrogen in gas phase with a significant partial pressure (see above);
- it is improbable that all hydrogen was entered by heavy hydrocarbons of reducing agent (from coke, coals, etc.), in spite of the fact from data of E. Tajts [20], that its content in hard coal is from 3.5 to 6.0 wt.%, and in coke — about 1–2 wt.%;
- the most probable source of water is the moisture of natural minerals [21] of ore constituent of charge, and to the larger extent, moisture of coke (wet extinguishing), whose threshold structure by its origin is fractal [22, 23], that allows this material to maintain water to temperature ≈ 1773 K and higher. So, the moisture is, undoubtedly, introduced into the pool of the ore thermal electric furnace. It would be correctly, if we define, firstly, the degree of its effect on reduction process, and then, in case of positive answer

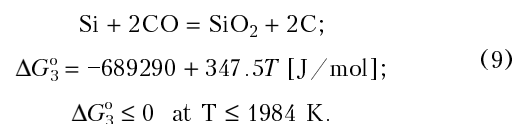
on the first question, we shall consider the source of enter.

In previous publication [24] we considered the causes of non-efficient consumption of reducing agents in ferroalloy processes. It was shown that the leading role is played by oxidation-reduction potential of gas phase of furnace atmosphere, in particular, the presence of components-oxidizers, such as vapours of water and carbon dioxide in the production of silicon alloys (ferrosilicium mainly). Moreover, it is H₂O_{vap} that is the oxidizing component of gas phase which provides recycling of SiO₂ in the electric furnace pool and, thus, leads to non-efficient consumption of carbon of the reducing agent. The above-said can be confirmed on examples of the scheme, including the reactions of disproportion of gaseous monoxide of carbon $2\text{SiO}_{\text{gas}} = \text{SiO}_2 + \text{Si}$ and oxidation of the forming silicon by water vapours $\text{Si} + 2\text{H}_2\text{O} = \text{SiO}_2 + 2\text{H}_2$, or a summed reaction $\text{SiO}_{\text{gas}} + \text{H}_2\text{O} = \text{SiO}_2 + \text{H}_2$.

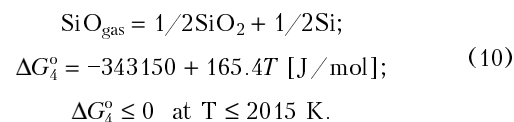
It should be noted that carbon monoxide can also play role of an oxidizer with respect to SiO_{gas}, as in the conditions of ore thermal electric furnace the following reactions are realized:



In addition, silicon, forming as a result of reaction of disproportion of gaseous monoxide of carbon, can be also oxidized by carbon monoxide:



Thus, the gas phase CO–SiO_{gas}, typical of the process of producing ferrosilicium (silicon alloys), is instable at temperatures, lower than 2130 K, due to proceeding of reactions (7)–(9), and at $T < 2075$ K — due to reaction of disproportion:



It should be noted that scheme, including reactions (7)–(10), cannot serve the grounding of need in excess of carbon against its stoichiometric content in production of ferrosilicium (silicon alloys), as some authors suppose, for example, of work [25]. Actually, alongside with the formation of oxidized component SiO₂ the reduced components are formed simultaneously during proceeding the mentioned reactions: SiC — by (7); Si — by (10); free carbon — by (8) and (9). In other words, the balance of carbon and



oxygen is closed, and with increase in temperature as a result of transfer of products of these reactions, with a charge lowering into the lower horizons of the pool, the direction of processes in accordance with change in Gibbs energy is changed for opposite.

Surely, it is necessary also to take into account that the transfer of amorphous SiO_2 , product of reactions (7)–(10), from the furnace pool exceeds greatly the total losses of carbon, produced as a result of reactions (8)–(9) with a dust, and SiC , product of reaction (7) with slags. In practice, this is taken always into account when calculating the charge [1, 11, 25].

The role and importance of gas phase in reduction processes in producing ferrosilicium (silicon alloys), and especially gaseous monoxide of silicon, were confirmed by many investigations [1–11]. Comprehensive review of suggested thermodynamic models was made by us in work [12]. In spite of somewhat different initial premises and different interpretation of results in details, all the mentioned works are similar in one point, i.e. the equilibrium ratio $\text{CO}:\text{SiO}_{\text{gas}}$ defines in many ways the proceeding and results of SiO_2 carbon reduction. Most part of considered thermodynamic models in [1–11] (except [5, 6]) is based on the analysis of change in Gibbs energy in reactions, proceeding in system Si-O-C in standard conditions (ΔG_i^0), that is not always correct, as it is necessary to take into account also the mass fraction of components in initial mixture, this idea belonged even to J.V. Gibbs [26].

In this connection, in the present work we have studied the stability, in the sense of possibility of realizing reactions (7)–(10), of two-component gas phase $\text{CO-SiO}_{\text{gas}}$ with decrease in temperature. In other words, the conditions are modelled, occurring in filtering gas through the layer of charge materials to the top of the ore thermal furnace.

Calculations of equilibrium in gas phase $\text{CO-SiO}_{\text{gas}}$ are made using software HSC Chemistry 5.0 (ESM Software, Outokumpu, Finland), realizing the algorithm of minimizing Gibbs energy, whose main equation is written in the following form with allowance for mass balance:

$$\Phi = \sum_i n_i \left(\mu_i^0 + RT \ln \frac{n_i}{\sum_i n_i} \right) + \sum_j \lambda_j \left(n_j^0 - \sum_i \nu_{ij} n_i \right) \quad (11)$$

where n_i is the amount of moles of the i -th substance; μ_i^0 is the standard value of chemical potential ($T, P = \text{const}$); n_j^0 is the total amount of moles of particles of basis (elementary chemical forms, chemical elements in our case); λ_i is the Lagrange multipliers; ν_{ij} is the stoichiometric coefficient for j -th particle of basis in the i -th reaction and new thermodynamic data [4].

Figure 2 presents data only about those substances, whose amount of moles is in equilibrium $n_i \geq 0.01$. Composition of gas phase is presented by amount of

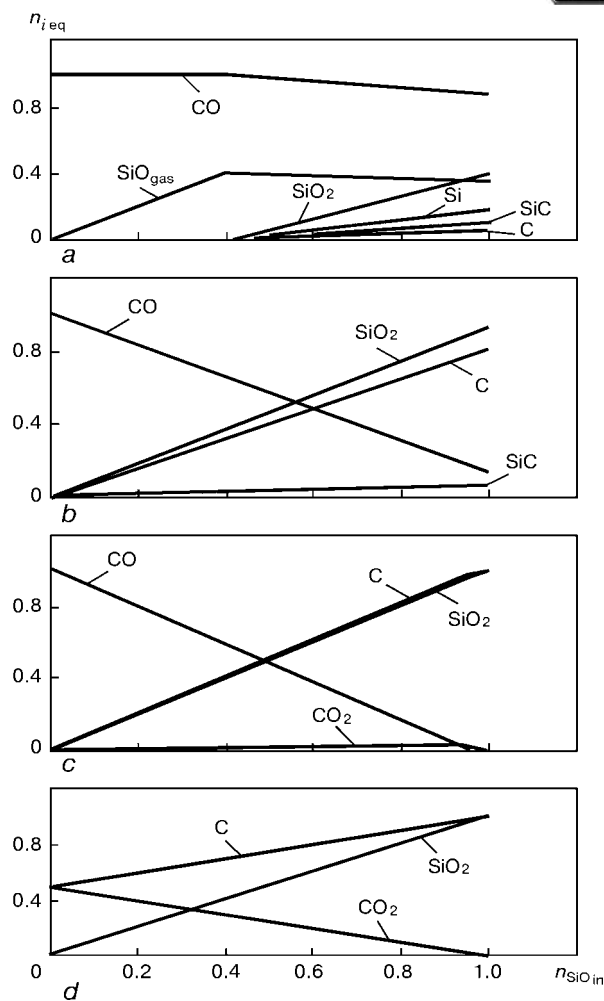


Figure 2. Computer modelling of stability of two-component gas phase at different ratio $\text{CO}:\text{SiO}_{\text{gas}}$ in initial mixture at 2123 (a), 1773 (b), 1273 (c) and 773 (d) K ($n_{i,\text{eq}}$ — amount of moles of component in equilibrium)

moles of n_i components but not partial pressure, so as to observe its change easier. Thus, $n_{\text{CO}} = 1$ mol was taken in calculations and n_{SiO} was varied within 0–1 mol, and the deviation from composition of initial mixture was interpreted, for example, as a result of proceeding of chemical reactions (7)–(10).

The following conclusions can be made on the basis of analysis of data obtained. At temperature 2123 K (Figure 2, a), when composition of gas phase $\text{CO-SiO}_{\text{gas}}$ should not undergo changes as compared with initial mixture according to equations for standard energy of Gibbs of reactions (7)–(10), the system remains stable only at $n_{\text{SiO}} \leq 0.4$ mol. The further increase in n_{SiO} in initial mixture leads to change in equilibrium composition, moreover, not only high-temperature reactions $3\text{SiO}_{\text{gas}} + \text{CO} = 2\text{SiO}_2 + \text{SiC}$ (7) (appearance of condensed SiC) and $\text{SiO}_{\text{gas}} = 1/2\text{SiO}_2 + 1/2\text{Si}$ (10) (the presence of condensed silicon, getting ahead of growth in SiO_2 amount) are realized, but also the low-temperature reactions $\text{SiO}_{\text{gas}} + \text{CO} = \text{SiO}_2 + \text{C}$ (8) and $\text{Si} + 2\text{CO} = \text{SiO}_2 + 2\text{C}$ (9), leading to the formation of a free carbon. Here, it is worthy to note once again, that it is not enough to use the data about standard energy of Gibbs of chemical reactions in thermodynamic investiga-

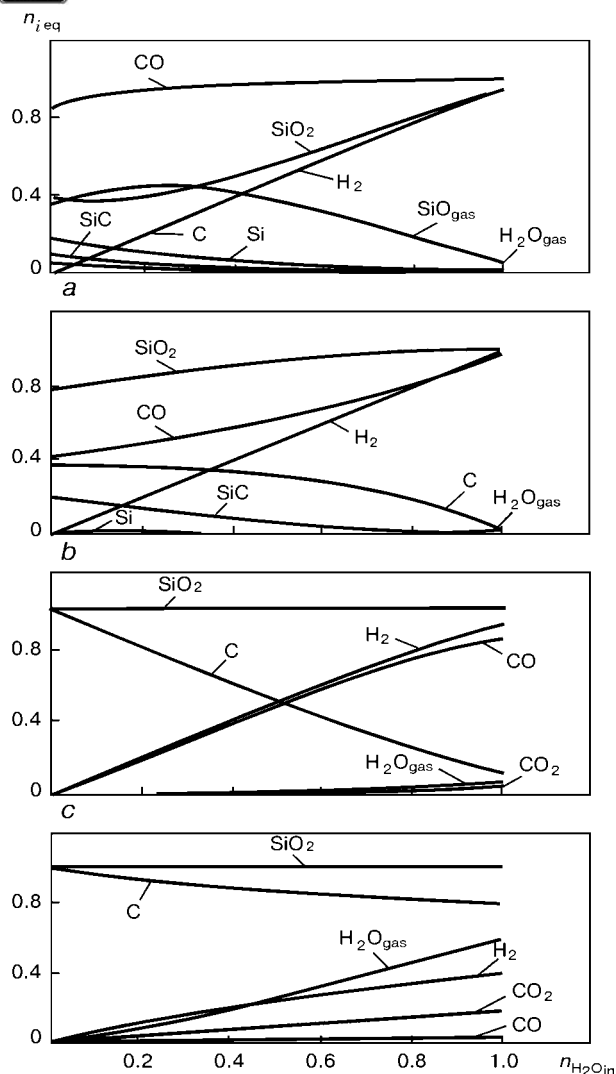


Figure 3. Computer modelling of stability of gas phase of CO-SiO₂-H₂O gas system depending on H₂O content in initial mixture at ratio CO:SiO₂ = 1 (a-d — see Figure 2)

tions, but it is necessary also to take into account the amount of substances, composing the initial system. In other words, the definite equilibria from constants according to the second or third law of thermodynamics ΔG_T^0 for individual chemical reactions characterize rather specific standard conditions of their proceeding. Calculations for any real system require another approach, for example, the use of method of thermodynamic potentials of Gibbs [26] which is reduced finally to minimizing of suitable (depending on thermodynamic conditions of system mating with environment) characteristic (derivative) function. For conditions $T, P = \text{const}$, it is equation (11). We did not consider here the theory of chemical affinity [27, 28], allowing for producing entropy in system with chemical reactions and considering chemical processes as non-equilibrium. Results of the present work were obtained completely in the scope of the equilibrium thermodynamics.

With decrease in temperature of gas phase CO-SiO₂ (Figure 2, b-d) both quantitative (change in amount of moles of co-existing phases), and also qualitative (reduction of number of co-existing chemical

substances, especially of condensed phases) changes in equilibrium system are observed. Thus, at 1773 K (Figure 2, b) silicon disappears almost completely, content of SiO₂ and carbon is abruptly increased, content of SiC is decreased by one third; monoxide of silicon SiO_{gas} in the entire interval of changing its content in initial mixture is not observed in gas phase. It is consumed completely by reactions $3\text{SiO}_{\text{gas}} + \text{CO} = 2\text{SiO}_2 + \text{SiO}$ (7) and $\text{SiO}_{\text{gas}} + \text{CO} = \text{SiO}_2 + \text{C}$ (8) (that is manifested in decrease of amount of CO moles as compared with initial mixture), and also consumed partially by reaction of disproportionation of SiO_{gas} $= 1/2\text{SiO}_2 + 1/2\text{Si}$ (10), where some amount (though small, due to developing reaction (9) $\text{Si} + 2\text{CO} = \text{SiO}_2 + 2\text{C}$) of a free silicon is yet present. The further decrease in temperature leads to the growth of oxidizing potential of gas phase. Even at 1273 K (Figure 2, c) the equilibrium CO₂ begins to appear, while condensed phases are presented only by carbon and SiO₂.

At 773 K (Figure 2, d) the gas equilibrium phase is reduced to single-component phase and consists of only CO₂, and the condensed phases are presented only by SiO₂ and carbon. In case of $n_{\text{SiO}} = 0$ the composition of equilibrium gas phase is controlled completely by reaction

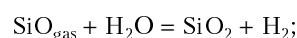


$$\Delta G_{12}^0 = -84480 + 86.9T \text{ [J/mol]};$$

$$\Delta G_T^0 \leq 0 \text{ at } T \leq 972 \text{ K},$$

and, at adding of silicon monoxide into initial mixture, it is also controlled by reaction $\text{SiO} + 1/2\text{CO}_2 = \text{SiO}_2 + 1/2\text{C}$. Data, obtained at such relatively low temperature should be considered taking into account kinetic factors, as the reaching of thermodynamic equilibrium by the system can require much time.

Equilibrium in widened system SiO-CO-H₂O was studied at ratio CO:SiO = 1 (that corresponds to the conditions of formation of melt of ferrosilicium in ore thermal electric furnaces under the appropriate temperature conditions, such as $T \geq 2123 \text{ K}$), by varying amount of H₂O in initial mixture in the range of 0-1 mol (Figure 3). It is clear, the upper limit of interval of H₂O changing seems to be much increased. It is made for the purpose to follow the changes occurring in adding of moisture into initial mixture SiO-CO. At $T = 2123 \text{ K}$ (Figure 3, a) a noticeable growth in CO content in equilibrium gas phase is observed, that is a result of suppression of reactions $3\text{SiO}_{\text{gas}} + \text{CO} = 3\text{SiO}_2 + \text{SiC}$ (7) and $\text{SiO}_{\text{gas}} + \text{CO} = \text{SiO}_2 + \text{C}$ (8) by a competing process



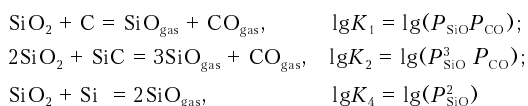
$$\Delta G_{12}^0 = -546460 + 195.4T \text{ [J/mol]}; \quad (12)$$

$$\Delta G_T^0 \leq 0 \text{ at } T \leq 2797 \text{ K}.$$

The same reaction leads to a significant increase in SiO₂ content in equilibrium system, and also sili-



con, silicon carbide and carbon (compare with Figure 2, *a*). This is a result of the hydrogen presence in equilibrium gas phase, forming by reaction (12) and widening the regions of stability of silicon and SiC (see Figure 1). Content of SiO_{gas} is decreased significantly, and, here, the relationship acquires an extremal nature with maximum corresponding to $n_{\text{H}_2\text{O}} \approx 0.21$ mol. Water vapours in the equilibrium system are appeared at $n_{\text{H}_2\text{O}} \geq 0.91$ mol. Thus, situation is appeared, which, from the first glance, may seem to be paradoxical: the presence of oxidizer (water vapours) in the system causes the increase in content of a reduced component, i.e. silicon. Actually, if to pay attention to the fact that moisture, entered the system at the stage of preparation of initial mixture, is completely consumed by reactions $\text{SiO}_{\text{gas}} + \text{H}_2\text{O}_{\text{gas}} = \text{SiO}_2 + \text{H}_2$ (12), and the forming hydrogen shifts the equilibrium of reactions (1), (2) and (4)



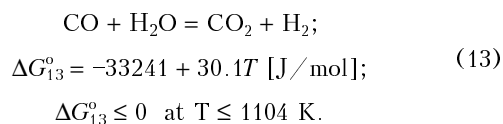
so, that the boundaries of regions of stability silicon and SiC in widened system $\text{Si-O-C-(H}_2\text{O, H}_2\text{)}$, as was shown above, are shifted in the direction of lower temperatures, as compared with the system Si-O-C , the situation looks quite naturally.

One more important moment, directly associated with a non-efficient consumption of carbon (excess of reducing agent against stoichiometric agent in production of ferrosilicium), looks as follows from the point of view of results obtained. In practice of production of silicon alloys (crystalline silicon, ferrosilicium, ferrosilicochromium and others), the calculation of required amount of carbon of the reducing agent is based on making material balances of melting. Here, the following items of consumption are taken into account: for reduction of silicon from silica (quartzite, ash of coke fines) by stoichiometric reaction $\text{SiO}_2 + 2\text{C} = \text{Si} + 2\text{CO}$; for reactions of formation of silicon monoxide with a loss of SiO_{gas} part together with a top gas; for reactions of reduction of impurity metals (aluminium, calcium, barium and others) in their transition into ferrosilicium; for oxidation of carbon of reducing agent at the top (loss); for losses of a negligible part of SiC with furnace slags, containing from 10 to 25 wt.% SiC; losses of a negligible part of alloy in the form of biscuits of ferrosilicium with slag. It is supposed here that moisture, entered the furnace with charge materials, is evaporated at the top (or in upper horizons of electric furnace), and the excess of reduced silicon (in comparison with thermodynamic calculations by any model) is referred either to non-equilibrium of system, or it is corrected by the correction of silicon activity in the alloy. The peculiar feature of the model, suggested by us, in the aspect of the effect being discussed, is the accounting for effect of hydrogen of gas phase on the equilibrium of process of carbon thermal reduction of silicon from

silica in production of silicon alloys. Moreover, it is not important whether the hydrogen enters the gas medium in a molecular form in the composition of hydrocarbons or formed in high-temperature zones in interaction of moisture of charge with silicon monoxide, for example, from reaction (12): $\text{SiO}_{\text{gas}} + \text{H}_2\text{O}_{\text{gas}} = \text{SiO}_2 + \text{H}_2$ (it follows from results of investigations of systems Si-O-C-(H) , described in [12], and also above in the present work, and $\text{Si-O-C-(H}_2\text{O)}$ (Figure 3, *a*)). From the other hand, to interpret and explain the mechanism of occurrence of effect of «reducing agent excess», the reaction (12) itself is decisive for reduction of SiO_2 forming from oxidation of monoxide of silicon SiO_{gas} with water vapours, an additional amount of carbon which, in the known sense, can be considered non-efficient (see [24]).

Decrease of temperature in $\text{SiO-CO-H}_2\text{O}$ system leads, the same as in SiO-CO system, to the reduction in amount of co-existing chemical substances, accompanied by change in amount of preserved compounds. Thus, at 1773 K (Figure 3, *b*) SiO_{gas} is disappeared completely both at the expense of proceeding reactions $3\text{SiO}_{\text{gas}} + \text{CO} = 2\text{SiO}_2 + \text{SiC}$ (7) and $\text{SiO}_{\text{gas}} + \text{CO} = \text{SiO}_2 + \text{C}$ (8), and also owing to reaction $\text{SiO}_{\text{gas}} + \text{H}_2\text{O}_{\text{gas}} = \text{SiO}_2 + \text{H}_2$ (12), finding the wider development (with growth of H_2O in initial mixture). Moreover, reaction (8) prevails over (7), that is reflected in significantly passing ahead growth of carbon content, as compared with SiC medium, though the content of the latter is also increased with decrease in temperature from 2123 to 1723 K. Content of SiO_2 is noticeably increased, that reflects the effect of joint action of processes described by reactions $3\text{SiO}_{\text{gas}} + \text{CO} = 2\text{SiO}_2 + \text{SiC}$ (7), $\text{SiO}_{\text{gas}} + \text{CO} = \text{SiO}_2 + \text{C}$ (8) and $\text{SiO}_{\text{gas}} + \text{H}_2\text{O}_{\text{gas}} = \text{SiO}_2 + \text{H}_2$ (12). Content of CO of gas phase is lower than at 2123 K, but it is increased with growth of H_2O in initial mixture, moreover, the same as at 2123 K to the level of 1 mol due to suppression of reactions (7) and (8) by reaction (12).

At 1273 K the water vapours in equilibrium system are appeared even at $n_{\text{H}_2\text{O}} \approx 0.4$ mol in initial mixture, CO_2 is appeared at $n_{\text{H}_2\text{O}} \approx 0.6$ mol, that is a result of proceeding reaction of water gas:



Here, the reaction (13) is realized by the conditions of temperature relationship ΔG_{13}^0 , as was expected, at a significant excess of H_2O in initial mixture. The abrupt decrease in carbon content indicates the feasibility of its oxidation by water vapours: $\text{C} + \text{H}_2\text{O} = \text{CO} + \text{H}_2$ or (that is hardly probable at this temperature) $1/2\text{C} + \text{H}_2\text{O} = 1/2\text{CO}_2 + \text{H}_2$. Amount of SiO_2 , reaching the level $n_{\text{SiO}} = 1$ mol, is not changed with increase in $n_{\text{H}_2\text{O}}$ even at $n_{\text{H}_2\text{O}} = 0$.



At 773 K temperature the presence of water vapour is observed (starting from $n_{\text{H}_2\text{O}} \approx 0.005$ mol its amount in initial mixture is increased up to 0.6 mol at $n_{\text{H}_2\text{O}} = 1$ mol in initial mixture). Here, the content of H_2 and CO in gas phase is abruptly decreased; the CO_2 content is increased, probably, as a result of reaction $\text{CO} = 1/2\text{CO}_2 + 1/2\text{C}$, that is proved by decrease in carbon content in equilibrium system as compared with $T = 1273$ K, in spite of more intensive proceeding of reaction $\text{C} + \text{H}_2\text{O} = \text{CO} + \text{H}_2$ ($1/2\text{C} + \text{H}_2\text{O} = 1/2\text{CO}_2 + \text{H}_2$ is also possible). Ultralow content of CO in thermodynamically equilibrium system (0.01–0.03 mol) attracts attention. Here, the same as for CO-SiO system, the results should be considered also in a kinetic aspect of reaching equilibrium by system.

Let us discuss the possible sources of moisture enter into reaction zones of the furnace. Actually, all charge materials, used in melting of ferrosilicium (quartzite, iron chips, coke fines) are the sources of moisture enter the pool of the ore thermal electric furnace. Moisture in quartzite may be contained both in microcracks and also in gas-liquid (fluid) inclusions. The latter contain volatile components (first of all water), participating in magmatic processes both in the form of substances dissolved in melt, and also in the form of an independent fluid phase. The fluid inclusions are usually multiphase. Their main components are as follows: water, salts (NaCl , CaCl_2 , KCl), carbonates and sulphates of iron and magnesium in small amounts); gases (mainly CO_2 , which can be available in the form of liquid, in addition, CO , CH_4 , H_2 , H_2S , N_2 , HCl , HF , SO_2 , NH_4 , Ar and other in subordinate amounts). Gas-liquid inclusions at room temperature are divided into single-phase (which contain only gas or only liquid), two-phase (gas and liquid are present in inclusion), three-phase (consisting of two gases and liquid or of two liquids and gas) and multiphase inclusions (with daughter phases, containing gas, liquid and daughter minerals). Content of water in quartzites can reach 0.5 % (typical value amounts to about 0.3 %). Water, bound in quartzites, leads to a thermal cracking of the latter. These quartzites are not used in ore thermal process as the cracking of quartzite at the top or at a small depth of the pool leads to the formation of a large amount of fines and, finally, to the decrease in gas permeability of charge column and disturbance in electric furnace operation.

Moisture of iron chips (hydroxides of iron, mainly as products of atmospheric corrosion) cannot, probably, play a significant role, as its amount is negligible, and, besides, the thermal resistance of iron hydroxides is quite insufficient to transfer moisture into high-temperature zones of the pool.

The most probable source of moisture enter can be carbon reducing agent, in particular coke fines. This conclusion can be confirmed by the following arguments. Thus, from the data of investigations given by foreign scientists, the network of pores (diameter

of the least of them is about 2 nm) in coals and coke, used as reducing agent in ferroalloy processes, has a fractal structure with a fractal dimension $D_s \approx 3$. Samples for investigations were obtained in processing of hard coal at 1023 K by water. From the estimates of foreign researchers, the surface of pore structure is not less than $1000 \text{ m}^2/\text{g}$. Moisture, absorbed on it, is associated with a material surface with induced dipole moment of water molecules by Van der Waals forces with binding energy equal to energy of ideal gas at pressure 2000 MPa. This estimate of adsorption energy is well coincided with data of [21], where values of energy 40–120 kJ/mol are given for water of monomolecular adsorption, and not less than 40 kJ/mol for the water of polymolecular adsorption. Temperature up to 1850 K is required for thermal activation of desorption and water evaporation at these values of energy of adsorption in accordance with Trouton rule $\Delta H_{\text{vap}} = 10.4RT$ [29].

Fractal dimension of network of pores of coal $D_p = 2.8$ –3.0, treated with nitrogen and water vapour at high temperature, was revealed by the nature of a low-angle scattering of X-rays on the sample by its capability to absorb the nitrogen, and also using the scanning tunnel microscope. In oxidation with water vapour the walls between microscopic cavities were fractured and chaotic system of interrelated channels of diameters from 1.5–2.0 up to 300–340 nm was occurred. Total porosity of samples investigated was 0.3–0.6, that corresponds to porosity of most carbon reducing agents. At the mentioned parameters and 0.38 nm^2 , area for one molecule of water, up to 7 % of moisture can absorb at the surface of nanopores, this moisture is not determined by technical analysis of carbon reducing agent by the reasons considered above.

Movement of water molecules in channels of nanoporous structure of carbon reducing agent cannot be already considered as gas movement in approximation of a continuous medium. E. Kalashnikov and B. Pevzner [30] suggested to coincide this movement as dislocation-dynamic diffusion in model of Frenkel–Kantorova, which accounts for a local preservation of a pulse in interaction with a periodic potential field created by atoms forming the channel walls. Except the modulus of material shear, forming the channel, energy of activation in the scope of the suggested model, depends on polarizability of molecules (particles) of a diffusant. As the polarizability of inert gas atom is by one order lower than polarizability of dipole molecules of water, the dielectric permeability of which in thin films is also decreased greatly (from 81 in volume up to 3–40 nm in thin films, in films of 0.5–0.6 nm thickness the values of dielectric permeability do not exceed 3–4 [21]), the noticeable mass transfer, associated with overcoming of activation barrier of 1.25 eV height (120 kJ/mol) at each single diffusion shear will be observed at temperature, reaching not less than 1390 K. In the conditions of two-dimensional diffusion on the surface of pores, the time



required for removal moisture from the material will exceed greatly the time of reducing agent duration in the electric furnace pool.

Mass transfer of moisture by channels of micrometric size is hindered due to increase in viscosity of bound water by 1.1 times in films of 200–300 nm thickness and by 1.6 times in films of 10 nm thickness [21].

In other words, carbon reducing agent serves not only as supplier of moisture to the ore thermal furnace, but is also a means of its transport to the reaction zone. In the course of consumption of coke lumps for reduction processes, the bound water contained in them is released and has an active participation, as was shown above, in physical-chemical processes of high-temperature reaction zones of electric furnace.

1. Gasik, M.I., Lyakishev, N.P. (1999) *Theory and technology of ferroalloy electrometallurgy*. Moscow: Internet-Engineering.
2. Ryabchikov, I.S. (1966) Thermodynamic investigation of Si–O–C system at high temperatures. *Izv. AN SSSR, Metallurgy*, **2**, 11–19.
3. Tolstoguzov, N.V. (1992) *Theoretical principles and technology of melting of silicon and manganese alloys*. Moscow: Metallurgiya.
4. Gurvich, L.V., Vejts, I.V., Medvedev, V.A. et al. (1979) *Thermodynamic properties of individual substances*. Refer. Book. Ed. by V.P. Glushko. Moscow: Nauka.
5. Mindin, V.Yu., Mazmishvili, S.M. (1984) Thermodynamic analysis of interaction in silicon-carbon dioxide system. *Zhurnal Prikl. Khimii*, **5**, 1204–1206.
6. Hatchison, S.G., Richardson, L.S., Wal, S.M. (1988) Carbothermic reduction of silicon dioxide: a thermodynamic investigation. *Metallurgical Transact.*, **19B**, 249–253.
7. Kulikov, I.S. (1969) *Thermodynamic dissociation of compounds*. Moscow: Metallurgiya.
8. Berdnikov, V.I. (1991) Application of balance thermodynamic analysis for investigation of silicon reduction mechanism in ferroalloy furnace. *Stal*, **2**, 42–45.
9. Ponomarenko, Yu.G. (1991) Calculations for model of carbothermic reduction of silicon in electric furnace. *Ibid.*, **4**, 35–37.
10. Yakushevich, N.F., Galevsky, G.V. (1995) *Interaction of carbon with calcium, silicon and aluminium oxides*. Novokuznetsk: Sibir. GPU.
11. Shchedrovitsky, Ya.S. (1961) *High-silicon ferroalloys*. Sverdlovsk: Metallurgizdat.
12. Gasik, M.I., Gasik, M.M., Zubov, V.L. et al. (2002) Influence of hydrogen of furnace gas phase on thermodynamic stability of condensed phase components in Si–O–C–(H). *Stal*, **12**, 30–35.
13. Kostina, T.B., Baum, B.A. (1971) Solubility of hydrogen in liquid alloys of iron with silicon. *Zhurnal Fiz. Khimii*, **4**, 813–815.
14. Klean, O.S., Engh, T.A. (1995) Dissolved impurities in FeSi development of a filter sampler. In: *INFACON-7*, Trondheim.
15. Geld, P.V., Yavojsky, V.I. (1950) *Study of causes of gas dissolution in ferroalloys*. Sverdlovsk: UPI.
16. Lichman, V.S., Kravchenko, V.A., Serebrennikov, A.A. (1970) Improvement of quality of 75 % ferrosilicium of machine pouring. *Stal*, **4**, 322.
17. Grigorenko, G.M., Pomarin, Yu.M. (1989) *Hydrogen and nitrogen in metals during plasma melting*. Ed. by B.E. Paton. Kyiv: Naukova Dumka.
18. Houden, D., Milner, D. (1963) Hydrogen absorption in arc melting. *British Welding*, **6**, 304–316.
19. Geld, P.V., Esin, O.A. (1950) *Physical chemistry of pyrometallurgical processes*. Part 1. Sverdlovsk: Metallurgizdat.
20. Tajts, E.M. (1961) *Properties of coals and process of coke generation*. Moscow: Metallurgizdat.
21. Korolyov, V.A. (1996) Bound water in rocks: new cases and problems. *Sorosov. Obrazovat. Zhurnal*, **9**, 79–85.
22. Shreder, M. (2001) *Fractals, chaos, power laws*. Izhevsk: Reg. i Khaotich. Dinamika.
23. Bale, H.D., Smith, P.W. (1984) Small-angle X-ray scattering investigation of submicroscopic porosity with fractal properties. *Phys. Rev. Lett.*, **53**, 596–599.
24. Gasik, M.I., Zubov, V.L., Polyakov, O.I. (2002) Problem of non-productive use of reducing agents in melting of ferroalloys. *Stal*, **3**, 81–84.
25. Tolstoguzov, N.V., Elkin, K.S., Tolstoguzov, V.N. (1995) Study of laws of carbon consumption in melting of silicon alloys. *Ibid.*, **10**, 40–42.
26. Gibbs, J.V. (1982) *Thermodynamics. Statistical mechanics*. Moscow: Nauka.
27. de Donde, T., van Risselberg, P. (1984) *Thermodynamic theory of affinity (Book of principles)*. Ed. by V.M. Glazov. Moscow: Metallurgiya.
28. Prigozhin, I., Kondepudi, D. (2002) *Current thermodynamics*. Moscow: Mir.
29. Girschfelder, J., Kertis, C., Berd, R. (1961) *Molecular theory of gases and liquids*. Moscow: Inostr. Literatura.
30. Kalashnikov, E.V., Pevzner, B.Z. (2002) Helium atom motion along the channel of proportional diameter in the context of Frenkel–Kantorova model. *Fizika Teyord. Tela*, **44**, 283–288.

MATHEMATICAL MODEL OF CALCULATION OF SPECIFIC ELECTRICAL RESISTANCE OF GRAINED THERMOANTHRACITE DEPENDING ON ITS FRACTIONAL COMPOSITION

V.I. LAKOMSKY

E.O. Paton Electric Welding Institute, NASU, Kyiv, Ukraine

It is shown how it is possible to obtain analytical dependence of specific electrical resistance of bulk mass on internal specific resistance of material of solid body and fractional composition of bulk mixture by using conception of R. Holm about a real contact of two fragments of solid body.

Keywords: *bulk materials, electrical resistance of bulk mixture, fractional composition of grained material*

At the industrial enterprise of Company «Ukrainian graphite» several powerful electrical furnaces-calcinators for the production of thermoanthracite are operating. Due to some drawbacks in their design, the extra consumption of energy is observed. The present article is the first work of the E.O. Paton Electric Welding Institute for the improvement of technology and design of these furnaces.

The major characteristic of quality in furnaces-calcinators of electrothermoanthracite is the specific electrical resistance (SER). Quantitative determination of SER is made by the method, specified by GOST 4668-75, if to speak about the factory consumption or export to CIS countries. If the thermoanthracite is exported abroad, then SER should be estimated by the international standard ISO 10143.

According to the first standard, to determine SER of thermoanthracite it is necessary to crush it to 0.400–0.315 mm fractions and to measure electrical resistance of pressing under $6 \text{ MPa} \pm 0.1 \%$ pressure. If the SER is determined by the international standard, then the thermoanthracite is crushed to the sizes of 1.0–0.5 mm particles and the pressure is reduced to $3 \text{ MPa} \pm 1 \%$.

It is generally known, that electrical current is passed through bulk electroconductive material both on the particles of this materials and also on points of electrical contact between them. It is also known, that contact electrical resistance exceeds always the resistance of mass of the material itself. Consequently, the smaller particles, the larger amount of places of current transition from particles of one elementary layer to particles of another layer, the lower electric resistance of the grained material. In other words, the better crushing of bulk material, the higher its electric conductivity.

Further, it can be said a priori, that with increase of pressure on bulk material mass the resistance of

the latter will decrease due to the fact that material is packed, and the number of points of the electrical contact is increased. Moreover, the volume of pores, filled with air, not participating in electric conductivity of pressing, is decreased. In addition, with increase in pressure the electrical resistance of contacting particles is decreased due to increase in area of a real contact between the particles, and also closer pressing of contacting surfaces against each other.

Taking into account the above-said, it is easy to understand that values of SER, measured by two standards, will not coincide obligatory, and the more so they will not represent SER of anthracite as a massive material, and also in the form of a charge of the furnace-calcinator.

At the same time, to have a skilled analysis of processes of electrical heating of anthracite in the furnace shaft and to control these processes, it is necessary to know SER of anthracite itself of different fractional composition, which can be used for calcination.

Thus, the problem is to find the analytical dependence of SER of bulk material of different fractional composition on SER of the same material but as a monolith and degree of crushing of this monolith. In other words, it is necessary to show the change in SER of electroconductive material in the course of its crushing.

To obtain the analytical relationship between SER of bulk material and size of its particles, let us imagine the following model of the electroconductive grained material. Let us assume, as it is made in modelling of dispersed media [1], that the bulk material represents a system of spherical particles of radius r , homogeneous in chemical composition and structure. Then, we shall consider a row packing of the grained material first on a definite length, and then multirow packing on a definite area and, at last, we shall decide how many similar particles can be packed in the unity of volume at the same scheme of packing.

It is not difficult to imagine that at the length unity in this case the amount of particles equal to $1/2r$ is packed in row n_l , and $n_s = 1/4r^2$ is arranged at the area unity. As to the unit volume, then the latter will contain $n_v = 1/8r^3$ particles. This packing is called cubic in the crystallography. If to join the centres of neighboring spheres, then we shall obtain cube, whose side is equal to $2r$. In this case all eight spherical segments with centres in cube angles are equal between themselves, and the sum of their volumes is equal to the full volume of one sphere. Then the volume, occupied by pores in each cell, consisting of eight spheres, is equal to $\frac{8r^3 - 4/3\pi r^3}{8r^3}$. As is seen

from this formula, the volume of pores does not depend on radius of sphere and is 47.67 % of the total volume of cell. Roughly speaking, only a half of volume of bulk material at such arrangement is filled with spherical particles, while the second half of the volume is pores. This scheme of packing is «porous», it is instable under the mechanical action on bulk material mass and can be packed at intensive shaking of the material, and its bulk mass can increase.

In cubic packing each particle of a spherical shape has 6 points of contact with neighboring spheres: one contact with lower, second — with upper and 4 — with lateral spheres. As the electrical current is a vector value, then in this case only 2 contacts of each sphere will conduct electrical current.

In nature, beside the above-mentioned packing, there is also dense, the so-called tetrahedral packing. This packing, unlike the cubic packing, is stable, because at any shaking the bulk material will never be packed. At such packing the lines connecting centers of neighboring spheres will form an equilateral triangle. In this system each sphere has already not 6, but 12 points of contact: 4 with upper spheres, 4 with lower and the same amount with lateral spheres. Volume of voids between the spheres in this case is only 25.95 %.

According to the theory of contact heat transfer in dispersion media [1], the phenomenon similar to electrical conductivity of bulk materials, the scheme of cubic packing of spheres is close to real structures, free from external load of bulk masses. This structure

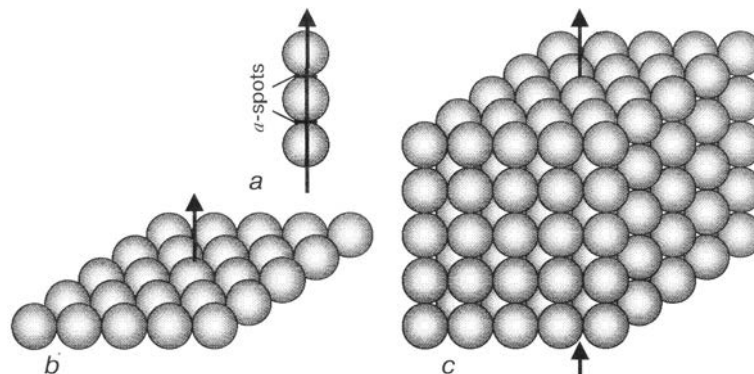
is formed in pouring out of any dispersed material from a hopper without any subsequent packing. Analysis of this structure has not only the theoretical, but also practical importance.

Taking into account the scheme of loading of crushed anthracite into furnace and conditions of formation of charge column in the furnace shaft, let us take cubic scheme of packing of elementary spheres for analysis of processes of electric current transmission in a layer of bulk material and try to establish the analytical relationship between electrical resistance of bulk material and its fractional composition.

Following the classical theory of electrical contacts [2], let us assume that transition of electrical current from one particle of solid material into another particle is realized through so-called a -spot by terminology of R. Holm, the author of this theory. The mentioned a -spots are rather small as compared with a visible geometric area of the contact. In this connection, the electrical current, passing through them, undergoes significant compression before entering a -spot and expansion after coming out from it already in another particle of the electroconductive material. Researchers, studied the contact thermal resistance [3], consider that the shape of contact a -spot approaches circle, if we are dealing with collision of two bodies with a rough surface, as that of anthracite.

A certain energy is consumed for compression in one and expansion is another grain of anthracite of electrical power lines, which is proportional to the resistance, equal, according to [2], to $\rho_0/2a$, where ρ_0 is the SER of the anthracite itself, a is the radius of elementary a -spot. The given expression is referred to one a -spot of radius a , it takes into account both the compression resistance at current input to a -spot, and also the expansion resistance at current output from a -spot. In real contacts numerous contact spots are usually available. As the electrical current is passed simultaneously along all the available spots, then the resistance of compression as a whole will be n times lower and equal to $\rho_0/2na$.

In mathematical calculations the first expression of contact resistance is used, as it is impossible to count the number of separate a -spots. In particular, when analyzing the scheme of current passing from one piece of coal to another piece in a layer of an-



Scheme of arrangement of grains of hard material: a — in one row; b — in one plane; c — in the form of cube (arrows show the directions of electric current)

thracite of cubic packing, we shall consider one given spot, as was above-agreed.

To calculate the electrical resistance in current passing in volume of a spherical particle, we shall use the known procedure in mathematics, i.e. instead of sphere we shall imagine an equivolume cylinder, whose height is equal to the sphere radius, and the cylinder radius is $2/\sqrt{3}$ of the sphere radius. Then, the electrical resistance in current passing in volume of the anthracite particle of an imagined cylindrical shape will be $\frac{3\rho_0}{4\pi r}$, where r is a radius of the spherical anthracite particle accepted by us.

As the electrical current, passing through each particle at its row packing, is overcoming successively both contact resistance, and the resistance of volume of the particle itself, then the impedance of each elementary particle of the bulk material (Figure, *a*) is the sum of these resistances $R_\Sigma = \frac{\rho_0}{2a} + \frac{3\rho_0}{4\pi r}$ or after transformation $R_\Sigma = \frac{\rho_0}{2} \left(\frac{1}{a} + \frac{3}{2\pi r} \right)$

Now, let us estimate electrical resistance of unity of volume of the bulk material, either it is cubic centimeter or cubic meter, that is SER, in principle, of the grained material considered in different units of measurement. The electrical resistance of one layer of particles of a row packing at the area unity will be equal to the impedance of each elementary particle, divided by the number of particles in this layer, that is followed from the rule of parallel switching on of resistance (Figure, *b*). In volume unity, let be cube (Figure, *c*), as much layers of particles will be arranged as their quantity could be arranged in length of this cube edge. Consequently, the obtained quotient should be multiplied by the number of layers in this cube. Thus, the electrical resistance of volume unity of grained material or the same as SER of this bulk material, will be equal to $\rho_{BM} = \frac{R_\Sigma^4 r^2}{2r}$.

If to substitute the value of electrical impedance of the elementary particle of the material considered, then, after the appropriate transformations, we shall obtain the unknown analytical expression

$$\rho_{BM} = \rho_0 \left(\frac{r}{a} + \frac{3}{2\pi} \right) \quad (1)$$

This equation can be simplified, taken away the term in brackets, representing the inner resistance of the sphere material, as it is low as compared with contact resistance, and then we shall obtain

$$\rho_{BM} = \rho_0 \frac{r}{a} \quad (2)$$

Let us analyze the given analytical dependence SER of bulk material on size of its composed particles.

It follows from the dependences:

- SER of crushed electroconductive material is always higher than SER of monolithic material, be-

cause value a can never reach and, moreover, exceed the value r , that is followed from the above-given determination of a value;

- the larger particles of bulk material mixture, i.e. the higher value r , the higher SER of fractional materials and, surely, the higher its difference from SER of monolith;

- SER of bulk material is differed from SER monolith because of a significant role played by a size of a -spot of a real electrical contact, that is followed from mathematical and physical considerations;

- with a growth of pressing force of contacting particles to each other the diameter of a given a -spot is increased, consequently, the SER of bulk material should decrease, that is observed in practice (the resistance is always lower, and the current density is higher in a thick layer of bulk material, through which the electric current is passing, in the lower monolayer, undergoing the pressure of superadjacent layers). In general, the radius of the real contact is determined by an external force applied to a contact pair and the hardness of its material, if we are speaking about similar material, or hardness of softer material in case of dissimilar materials.

Let consider the field of adaptability of the relation obtained with respect to radius of particles of separate fractions of anthracite. As to the maximum value r , then there is no limitations from the physical point of view, while from the point of view of heat treatment of «green» anthracite it is hardly rational to use the fraction of larger than 25 mm. Otherwise, the non-homogeneity of properties of separate pieces of thermoanthracite, produced in furnace, is increased greatly. The value r should be recognized hypothetically minimum when it is equal to the radius of a given a -spot.

As is known, the value a is increased with a growth of pressure. What are the maximum pressures at which the obtained dependence can be used? Special investigations showed [4] that to equalize the resistance of powders of carbon materials with that of monolith, it is necessary to increase pressure up to 150 MPa.

To use the obtained analytical relationships in practical calculations, it is necessary to know SER of the material itself as a monolith and its temperature relationship, as well as a radius of a -spot for anthracite at different pressures and temperature. The SER of the material itself at room temperature can be determined by the method of ammeter-voltmeter by cutting from the largest particles of thermoanthracite of sample in the form of a parallelepiped with a high possible ratio of the latter to the side of its cross section. Taking into account the non-homogeneity and anisotropy of anthracites it is necessary to analyze a large amount of samples to obtain the valid data.

Recently, we have determined the SER of the anthracite produced in gas heating furnace, because only in this furnace the anthracite of large fractions suitable for cutting out of samples from it of 40 mm length and 7x7 or 8x8 mm section is calcinated. The SER of



eight samples was measured. As was expected, it was different and amount from 74.8 up to 134.1 $\mu\text{Ohm}\cdot\text{m}$. The reproducibility of results of measurements on each sample was excellent: on six samples the error of determinations was not beyond $\pm 1\%$, on two samples — beyond $\pm 2.8\%$.

Results of determination of SER (according to GOST 4668–75) of the same thermoanthracite, but in a crushed sample, showed on average 900 $\mu\text{Ohm}\cdot\text{m}$. If to use now the equation (2), then it is possible to determine that radius of given a -spot in accordance with GOST measurement (fraction composition of coal 0.315–0.400 mm, 60 MPa pressure for pressing) will be from 15–27 μm .

It is possible to show how important is the effect of pressure on electrical resistance of layer of crushed coal if to measure SER of this coal in the layer of 210–250 mm thickness without external pressure. Thus, SER of the anthracite of 4–6 mm fraction is 41460 $\mu\text{Ohm}\cdot\text{m}$. Radius of given a -spot equal to 6 μm for this value of SER, while for fraction 8–10 mm it is 10 μm .

This example proves that in electric calcinator, in which the column of coal charge reaches 2 m, the SER of bulk material is changed in the process of anthracite calcination from tens of thousands of $\mu\text{Ohm}\cdot\text{m}$ in upper layers of charge column (but not in the uppermost layers, where «green» anthracite enters) up to several thousands of $\mu\text{Ohm}\cdot\text{m}$ in the lower layers before the unloading from the furnace, and this is associated with an effect of pressure, not even speaking about other factors, for example temperature.

Knowing the dependence of SER of bulk material on its fractional composition and that SER of mixture is additive with respect to its fractions [5, 6], it is possible to obtain the estimated value of electrical resistance of mixture of crushed anthracite at room temperature and absence of pressure on coal. For this, only the value of radius of a -spot should be preset.

Let us assume that the fractional composition of coal (by mass), entered for calcination, is the following: fractions of 6–10 mm — 40 %, fractions of 10–15 mm — 30 %, fractions of 15–20 mm — 20 %, and fractions of 20–25 mm — 10 %. Assume also that the mean radius of the given a -spot is 20 μm (this is the most daring assumption). Now, using the above-obtained dependence, we shall determine SER of each

fraction at room temperature and absence of pressure on the coal layer, using a mean arithmetic radius of fraction particles in calculation. SER of coal fraction of 6–10 mm will be 20000, fraction of 10–15 mm — 31250, fraction of 15–20 mm — 43750 and, at last, fraction of 20–25 mm — 56250 $\mu\text{Ohm}\cdot\text{m}$. The weighted mean value of SER of mixture in these conditions is 31750 $\mu\text{Ohm}\cdot\text{m}$.

Naturally, the SER of thermoanthracite in furnace will be different (lower), as the latter will be located under the pressure and temperature, changing in height of the charge column. In addition, it would be outlined that the mentioned SER of lumpy anthracite is the true value, but not conditional, determined by GOST.

It is seen from the above-mentioned that radius of a -spot is important for calculations of SER of electrothermoanthracite, especially its dependence on pressure on contact spot and properties of anthracite as a contact material. In literature, as is known to us, there are no these data. By the way, there are no also conception about structure of a -spot on anthracite. It is possible only to suppose by the similarity with the process of measurement of microhardness of anthracite that the real contact spot for determination of electric resistance in electric current passing will be like indentation of a indenter in microhardness measurement. As to the latter, then the authorities in the field of carbon materials recognize [7] that the «microhardness of anthracite can be measured only on very small areas of the sample investigated, and only at a complete absence of plastic deformations». In this connection it can be assumed that a -spot on the anthracite will represent very small local zone of brittle fracture in sizes, in which not-removed micro-products of fracture are present.

1. Chudnovsky, A.F. (1954) *Heat exchange in dispersed media*. Moscow: Gostekhizdat.
2. Holm, R. (1961) *Electrical contacts*. Moscow: Inostr. Literatura.
3. Shlykov, Yu.P., Ganin, E.A., Tsarevsky, S.N. (1977) *Contact thermal resistance*. Moscow: Energiya.
4. Agroskin, A.A. (1965) *Physics of coal*. Moscow: Nedra.
5. Agroskin, A.A. (1959) *Thermal and electric properties of coals*. Moscow: Metallurgizdat.
6. Ariakos, G.Ya. (1934) Electric conductivity of mixture of powder carbonaceous materials. *ZhTF*, 4, 307–312.
7. Fialkov, A.S. (1997) *Carbon, interlayer compounds and composites on its base*. Moscow: Aspect Press.

INFORMATION FOR CONTRIBUTORS TO JOURNAL ADVANCES IN ELECTROMETALLURGY

ADVANCES IN ELECTROMETALLURGY is a scientific journal publishing fundamental and applied papers and short notes in the area of

- *electroslag welding and cladding*
- *electroslag remelting, casting, hot topping, heating*
- *plasma-arc melting and remelting*
- *vacuum-arc remelting*
- *induction melting*
- *electrometallurgy of steel and ferroalloys*
- *electron beam remelting*
- *electron beam evaporation and condensation of metallic materials in vacuum*
- *ladle steel treatment*
- *metal dispersion and producing condensates*
- *designing of electrometallurgical equipment*
- *technologies of producing ingots, high-quality castings from different materials*
- *technologies of producing titanium alloy ingots*
- *deposition of coatings, including those of composite materials*
- *energy- and resources-saving technologies*
- *physical and chemical fundamentals of steel production*
- *theories of metallurgical processes*
- *investigations in gas-slag-metal system*
- *systems of automation of remelting processes*
- *mathematical modelling of processes*

The journal accepts also advertisements and announcements of conferences and publications on related topics.

ADVANCES IN ELECTROMETALLURGY is published four times per year. Subscription requests should be sent to the Editorial Office.

Manuscripts should be submitted in duplicate in English, and supplemented with a text file and figures on a diskette. An electronic copy may be submitted by e-mail.

The rules for submission of electronic copies are as follows:

- an electronic copy should be submitted on a diskette or by e-mail simultaneously with sending a hard copy of the manuscript;
- acceptable text formats: MultiEdit (*.txt), MS Word 97 (*.rtf, *.doc);
- acceptable graphic formats for figures: EPS, TIFF, CDR. Figures created using software for mathematical and statistical calculations should be converted to one of these formats.

Manuscripts should be sent to

Aleksander T. Zelnichenko
Executive Director of Project
PWI, International Association «Welding»
11, Bozhenko Str.,
03680, Kyiv, Ukraine
Tel.: (38044) 227 67 57, Fax: 268 04 86
E-mail: journal@paton.kiev.ua

Manuscripts should be supplemented with

- official letter signed by a chief manager of the institution where the work was performed. This rule does not apply to papers submitted by international groups of authors;
- publication permission: conclusion of a commission authorized to permit open publication of the paper (only for authors from Ukraine).

Title Page:

- title of the paper and name(s) of the author(s);
- name of affiliated institution, full address, telephone and fax numbers, e-mail addresses (if available) for each author.

Abstract: up to 100 words, must be presented in English. Before the abstract text one should indicate in the same language: the paper title, surnames and initials of all authors.

Key words: their amount must not exceed eight word units. In the specific cases it is acceptable to use two- or three-word terms. These words must be placed under the abstract and written in the same language.

Text should be printed double-spaced on white paper (A4 format) with a 12-point font. Titles of the paper and sections should be typed with bold capitals.

Tables should be submitted on separate pages in the format of appropriate text processors, or in the text format (with columns separated by periods, commas, semicolons, or tabulation characters). Use of pseudo-graphic characters is not allowed.

List of references should be double-spaced, with references numbered in order of their appearance in the text.

Captions for figures and tables should be printed in the manuscript double-spaced after the list of references.

Pictures will be scanned for digital reproduction. Only high-quality pictures can be accepted. Inscriptions and symbols should be printed inside. Negatives, slides and transparencies are accepted.

Figures: each figure should be printed on a separate page of the manuscript and have a size not exceeding 160 × 200 mm. For text in figures, use 10-point fonts. All figures are to be numbered in order of their appearance in the text, with sections denoted as (a), (b), etc. Placing figure numbers and captions inside figures is not allowed. On the back side, write with a pencil the paper title, author(s) name(s) and figure number, and mark the top side with an arrow.

Photographs should be submitted as original prints. Color printing is possible if its cost is covered by the authors or their sponsors. For information about the rules and costs, contact the Executive Director of Project.

No author's fee is provided for.

Publication in ADVANCES IN ELECTROMETALLURGY is free of charge.